THE
PHYSICAL REVIEW
A Journal of Experimental and Theoretical Physics Established by E. L. Nichols in 1893
VOL. 50, NO. 2 JULY 15, 1936 SECOND SERIES

Theory of the Effect of Temperature on the Reflection of X-Rays by Crystals

III. High Temperatures. Allotropic Crystals

CLARENCE ZENER* AND S. BILINSKY, *Wayman Crow Hall of Physics, Washington University, St. Louis*
(Received May 22, 1936)

In previous comparisons of the theoretical and experimental temperature effect for the reflection of x-rays, a marked discrepancy was found at high temperatures. It is here shown that this discrepancy disappears when proper account is taken of the variation of the characteristic temperature with temperature. Further, a relationship is found between the temperature factors for two allotropic modifications of the same element.

§1. INTRODUCTION

THE effect of temperature in decreasing the intensity of reflected x-rays has been surprisingly well interpreted at ordinary temperatures by the simple Debye model of a solid.[1] In this model the observed structure factor F is given by fe^{-M}, where f is the structure factor for a perfect lattice, and[1, 2]

$$M=\frac{6h^2T}{m_a k\Theta^2}\frac{\sin^2\theta}{\lambda^2}\phi\left(\frac{\Theta}{T}\right). \qquad (1)$$

Here m_a is the mean mass of the atoms, θ is the glancing angle of incidence of the x-rays on the reflecting plane, and ϕ is a factor which deviates appreciably from unity only when $\Theta/T>1$. If Θ is regarded as independent of temperature, as it has always been in the literature on x-rays, log F becomes a linear function of temperature in the region $T>\Theta$. The only experimental values of F at high temperatures are for NaCl[3] and for KCl.[4] The observed values of log F for these two crystals deviates radically from a linear function above 400°C. The purpose of the first part of this paper is to show that the temperature factor e^{-M} calculated by the simple Debye model is in agreement with the observed temperature factor even at high temperatures when proper account is taken of the variation of Θ with temperature.

While in §2 the continuous variation of M for a single crystal phase is discussed for the entire temperature range of that phase, in §3 the discontinuous variation of M is examined when the crystal undergoes an allotropic transformation.

* The senior author was aided in part by a grant from the Rockefeller Foundation to Washington University for research in science.

[1] See Compton and Allison, *X-Rays in Theory and Experiment*, pp. 435–445.

[2] For a simple derivation, see Zener and Jauncey, Phys. Rev. **49**, 17 (1936).

[3] James and Firth, Proc. Roy. Soc. **A117**, 62 (1928).

[4] James and Brindley, Proc. Roy. Soc. **A121**, 155 (1928).

§2. Temperature Factor at High Temperatures

The Debye model of a solid can make definite predictions about the temperature dependence of its properties only when the volume of the solid is kept constant. Thus in order to compare the observed specific heat with that predicted by the Debye model, C_p is always first reduced to C_V. In order fairly to compare with experiment the prediction of the Debye model as to the influence of temperature upon the intensity of reflected x-rays, proper account must be taken of the fact that the observations are made at constant pressure and not at constant volume.

Two methods of approach are available. In the first method, Eq. (1) is written in the form[1, 2]

$$M=8\pi^2\mu \sin^2\theta/\lambda^2, \tag{2}$$

where μ is the mean-square displacement of an atom. One then constructs a molecular model of the solid, including third- and fourth-order terms in the expression for the potential energy, which expands with temperature. Both C_p-C_V and the mean-square displacement μ are then directly calculated. This approach has already been investigated,[5] but has not given any quantitative predictions on the variation from the linear dependence of M with T at high temperatures.

In the second method of approach one starts from the phenomenological Debye model, and determines that dependence of Θ upon temperature which is necessary to fit the specific heat data. This function $\Theta(T)$ is then substituted into Eq. (1). This second method is the one adopted in this paper.

Two methods may be used to determine the function $\Theta(T)$ from specified heat data. The simpler one is to find that Θ which gives the observed C_V.[6] Thus $\Theta(T)$ is defined by the equation

$$C_V(T)=C_D\{\Theta(T)/T\}. \tag{3}$$

The second method[7] is to determine that function $\Theta(T)$ which makes the observed entropy equal to the entropy calculated from the Debye model. The observed entropy (per atom) at a temperature T_0 is

$$S_{\text{obs.}}(T_0)=k\int_0^{T_0}\frac{C_p}{T}dT.$$

In order to calculate the entropy by the Debye model, one must pass from the absolute zero to the temperature T_0 in two steps. First one changes the volume of the solid, keeping it at the absolute zero, from its value at $p=0$, $T=0$, to its value at $p=0$, $T=T_0$. According to the Nernst heat theorem,[8] the entropy change is zero in this change of volume at the absolute zero. The solid is now heated, at constant volume, from $T=0$ to $T=T_0$. Throughout this second process the characteristic temperature remains constant. Hence the entropy change is given by

$$S_D(T_0)=k\int_0^{T_0}\frac{C_D\{\Theta(T_0)/T\}}{T}dT.$$

If we now equate these two expressions for the entropy, and differentiate with respect to T_0, we obtain

$$(d\ln\Theta)/dT=-(C_p-C_D(\Theta/T))/TC_D(\Theta/T). \tag{4}$$

If the Debye model gave an exact representation of the specific heat, and if the empirical C_p and C_V were known precisely, Eqs. (3) and (4) would give the same function $\Theta(T)$. However, since $C_D(\Theta/T)$ becomes very insensitive to Θ when T becomes comparable with and larger than Θ, either a small error in the empirical values of C_V or a slight deviation of the true C_V from C_D produces a relatively large change in $\Theta(T)$. This is illustrated in Table I. The function $\Theta(T)$ obtained from Eq. (4) is not sensitive to these errors. The second method is thus used in this paper.

The integration of Eq. (4) only gives the ratio $\Theta(T)/\Theta(0)$. $\Theta(0)$ must be determined by using Eq. (3) at low temperatures. The function $\Theta(T)$ thus determined, when substituted into Eq. (1), gives the temperature factor at all temperatures

Table I. The second row gives the percent error in Θ due to a 1 percent error in C_V, when $\Theta(T)$ is determined from Eq. (3).

Θ/T	0.25	0.5	1	2	4
$\delta\ln\Theta/\delta\ln C_V$	240	35	9.5	2.7	0.8

[5] I. Waller, Ann. d. Physik **83**, 153 (1927).
[6] Jauncey and Deming, Phys. Rev. **48**, 481 (1935).
[7] This method is in principle identical to that used by Fowler, *Statistical Mechanics*. The derivation here given is, however, simpler than that given by Fowler.
[8] M. Plank, *Treatise on Thermodynamics*, 5th edition, p. 274.

TABLE II. *Log of ratio $\Theta(T)/\Theta(0)$ for KCl and NaCl at various temperatures as given by Eq. (5).*

T (°C)		−200	−100	0	100	200	300	400	500	600
$-\ln\{\Theta(T)/\Theta(0)\}$	KCl	0.00346	0.0176	0.0341	0.0513	0.0690	0.0870	0.106	0.123	0.141
	NaCl	0.00266	0.0160	0.0330	0.0519	0.0717	0.0911	0.111	0.132	0.153

with constant pressure as predicted by the Debye model.

According to the Debye model C_D and C_V are identical. Hence in Eq. (4) C_D may be replaced by C_V. Now it is well known that the ratio[9] $(C_p-C_V)/(TC_VC_p)$ is very nearly a constant over the entire temperature range of those solids with a simple structure, the only solids to which the Debye model is applicable. The constant K may be calculated from the known values of C_p and C_V at one temperature T_0, say at room temperature. When this relationship is used, the integration of Eq. (4) gives

$$\Theta(T)=\Theta(0)e^{-KH(T)}, \tag{5}$$

where $$H(T)=\int_0^T C_p dT$$

and $K=[C_p(T_0)-C_V(T_0)]/TC_p(T_0)C_V(T_0)$.

The only experiments over a wide range of temperatures are for NaCl[3] and KCl.[4] The ratio $\Theta(T)/\Theta(0)$ obtained from Eq. (5) for these two crystals is given in Table II. The accepted values of $\Theta(0)$, which are obtained from Eq. (3), are 281°K for NaCl and 230°K for KCl. The comparison between the calculated and experimental values of $\log F(T)/F(290°)$ is given in Figs. 1 and 2. A better fit with the experimental data is obtained by taking slightly larger values for $\Theta(0)$ than given by Eq. (3). The experimental points at the two highest temperatures for KCl fall considerably below the best theoretical curve. In view of the excellent fit with the other points, and in view of the increasing spread of the experimental points with temperature, these two isolated experimental points are probably too low.

It is to be expected that the $\Theta(0)$ which gives the best fit to the x-ray reflection data will always be somewhat larger than the $\Theta(0)$ determined from the specific heat data via Eq. (3). This is because on the Debye model the solid is strictly not specified by a single Θ. The Θ used in C_D and in Eq. (1) refers to an average Θ, but not to the same average. In the first case Θ refers to an average of the type $(\overline{\theta^{-3}})^{-\frac{1}{3}}$, in the second case to an average of the type $(\overline{\theta^{-2}})^{-\frac{1}{2}}$. Now it may readily be proved, by using Schwarz' inequality,[10] that

$$(\overline{\theta^{-3}})^2 \geqslant (\overline{\theta^{-2}})^3.$$

The application of this inequality to an elastically isotropic solid will now be considered. Here Θ as defined by the first average, say Θ_{C_V} is given by

$$\Theta_{C_V}{}^{-3}=(2\theta_t{}^{-3}+\theta_l{}^{-3})/3,$$

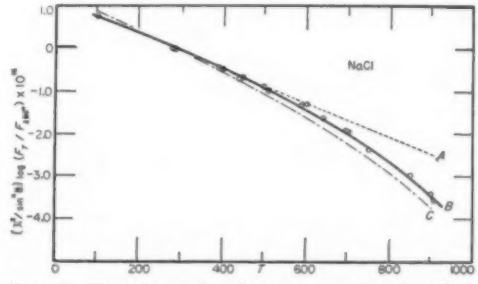

FIG. 1. Experimental points are marked by circles. Curve A, theoretical curve with constant Θ. Curves C and B, theoretical curves with Θ calculated by Eq. (5), with $\Theta(0)=281$, $\Theta(0)=298$, respectively.

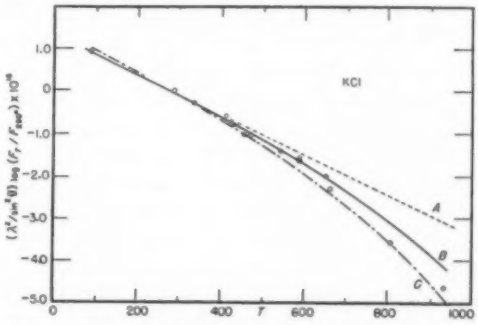

FIG. 2. Experimental points are marked by circles. Curve A, theoretical curve with constant Θ. Curves C and B, theoretical curves with Θ calculated by Eq. (5), with $\Theta(0)=230$, $\Theta(0)=240$, respectively.

[9] Eucken, *Handbuch der Experimentalphysik*, Vol. VIII/1 (1929), p. 204.

[10] Courant and Hilbert, *Methoden der Mathematischen Physik* Vol. I (1924), pp. 2, 33.

TABLE III. The second row gives for various values of Poisson's ratio the ratio for an elastically isotropic solid of the Θ which must be used in the Debye factor, Eq. (1), for the intensity of x-ray reflection to the Θ which must be used in the Debye expression for the specific heat.

σ	0.25	0.3	0.35	0.4	0.45	0.5
Θ_μ/Θ_{C_V}	1.025	1.027	1.032	1.040	1.051	1.070

where θ_t, θ_l refer to the characteristic temperatures associated with the transverse and longitudinal vibrations, respectively. The Θ defined by the second average, say Θ_μ, is given by

$$\Theta_\mu^{-2}=(2\theta_t^{-2}+\theta_l^{-2})/3.$$

The ratio Θ_μ/Θ_{C_V} will in this case be a function only of Poisson's ratio σ, and is given in Table III. The elastic anisotropy of all actual crystals will still further increase the ratio of the two types of average.

§3. Relationship Between the Temperature Factors of Allotropic Forms of the Same Element

According to the Debye model of a solid, each crystal phase is associated with a definite characteristic temperature (which according to §2 must, however, be regarded as a function of temperature). The value of the characteristic temperature Θ_1 of the low temperature modification at the transition temperature T_0 may be calculated as described in §2. The value of the characteristic temperature Θ_2 of the high temperature modification at T_0 may at once be obtained from the entropy equation

$$S_D\{\Theta_2/T_0\}-S_D\{\Theta_1/T_0\}=L/T. \qquad (6)$$

Here L is the latent heat of the transition (in calories per gram atom when S is the entropy per gram atom). The solution of this equation for Θ_2 may be affected either by use of tables[12] of $S_D(\Theta/T)$ or, when $T>\Theta$, by the analytical expression[11] for S_D. When $T>1.25\Theta$, the following equation gives S with an error of less than 1 percent:

$$S_D=R\{4+3\ln T/\Theta\}.$$

Substitution of this equation into (6) gives

$$\Theta_1/\Theta_2=e^{L/(3RT_0)}.$$

Using Eq. (1), we obtain

[11] An analytical expression for $S(x)$ is given by Gruniesen, *Handbuch der Physik*, Vol. X (1926), 22.

[12] Extensive tables of $S_D(x)$ are given by Simon, *Handbuch der Physik*, Vol. X (1926), pp. 369–370.

TABLE IV.

ELEMENT	TRANSITION TEMPERATURE (°K)	HEAT OF TRANSFORMATION (calories per gram atom)	$\frac{M_2}{M_1}$
Tin[1]	298	564	1.54
Arsenic[2]	1017	525	1.19
Selenium[3]	423	174	1.15
Zinc[4]	618	190	1.11
Manganese[5]	1108	158	1.05
	1317	249	1.06
Calcium[6]	673	100	1.05
Thallium[7]	498	51	1.03

[1] Lewis and Randel, *Thermodynamics* (1923), p. 464.
[2] Laschtschenko, J. Chem. Soc. **121**, 972 (1922).
[3] Mellor, *A Comprehensive Treatise on Inorganic and Theoretical Chemistry*, Vol. X, p. 715.
[4] Reference 3, Vol. IV, p. 430.
[5] Umino Science Reports, Tohoku University **16**, 775 (1927).
[6] *International Critical Tables*, Vol. VII, p. 293.
[7] Werner, Zeits. f. anorg. Chemie **83**, 275 (1913).

$$M_2/M_1=e^{2L/(3RT_0)} \qquad (7)$$

for the ratio of the two M's at the transition temperature.

When a crystal phase is anisotropic, the Debye function M will vary with the orientation of the reflecting plane.[13] In this case Eq. (7) can only be valid when M_1 and M_2 refer to some sort of average. The correct type of average may be uniquely obtained when $T>\Theta$. In this case the Einstein model of a solid may be used to describe the vibrations of the atoms. In this model each atom is considered as bound elastically to a fixed lattice point. Let μ_{1x}, μ_{1y}, μ_{1z} and μ_{2x}, μ_{2y}, μ_{2z} be the mean squares of the displacement of the atoms along the three principal axes, for the low and high temperature phase, respectively. The change of entropy may then be written in terms of the ratio of two phase integrals.[14]

$$\frac{L}{T_0}=-R\ln\frac{\int\int\int_{-\infty}^{\infty}e^{-\frac{1}{2}(x^2/\mu_{1x}+y^2/\mu_{1y}+z^2/\mu_{1z})}dxdydz}{\int\int\int_{-\infty}^{\infty}e^{-\frac{1}{2}(x^2/\mu_{2x}+y^2/\mu_{2y}+z^2/\mu_{2z}}dxdydz}.$$

The reduction of this integral gives

$$\mu_{2x}\mu_{2y}\mu_{2z}/\mu_{1x}\mu_{1y}\mu_{1z}=e^{2L/RT_0}.$$

Using Eq. (2), we see that this equation is equivalent to Eq. (7) where now M stands for the geometrical mean $(M'\,M''\,M''')^{\frac{1}{3}}$. Here M', M'', M''' are the three M's in which the reflecting plane is normal to a principal axis. Table IV gives a list of the ratios M_2/M_1 which are predicted by Eq. (7).

[13] Zener, Phys. Rev. **49**, 122 (1936).

[14] Herzfeld, *Kinetische Theorie der Warme* (1925), p. 161.

The Absorption of X-Rays of Wave-Length $50 \leq \lambda < 150$ X.U. by Elements of Low Atomic Number

TREVOR R. CUYKENDALL, *Cornell University, Ithaca, N. Y.*

(Received May 11, 1936)

With a 600 kv x-ray source and a two-crystal spectrometer especially designed for short wave-length x-rays, the mass absorption coefficients for C(6), Na(11), Al(13), S(16), K(19), Ni(28), Cu(29) were determined for wave-lengths from 50 to 209 X.U. A small $\delta\lambda$ interval was used. The results are estimated to be in error by no more than two percent. The present results are compared with the few overlapping measurements of other observers. The values of the electronic scattering coefficient predicted by the Klein-Nishina formula are in excellent agreement with the experimental values of the scattering by carbon in the region $40 \leq \lambda \leq 100$ X.U., which confirms the Klein-Nishina formula for this wave-length region. The photoelectric absorption in copper was found to be proportional to $\lambda^{2.83}$.

INTRODUCTION

THE determination of the absorption coefficients of monochromatic x-rays in the region of wave-lengths shorter than 150 X.U. is of importance (1) in testing the Klein-Nishina formula[1] for the intensity lost by scattering, and (2) in providing additional information which may be used to check the validity of recent formulae for the photoelectric absorption. Furthermore, absorption measurements for monochromatic radiation are of value to the medical profession in the use of high voltage x-rays for therapeutic purposes.

No systematic study of absorption coefficients has been made for the present wave-length region. Absorption measurements at wave-lengths less than 120 X.U. require a powerful, high voltage, x-ray source of constant intensity, and an analyzing spectrometer or other device which effects a satisfactory compromise between intensity and monochromaticity of the emergent beam. It is to be noted that there exists no *practical* target material, except possibly uranium, whose characteristic x-radiation is shorter than 120 X.U., and therefore the continuous spectrum must be used.

Early determinations[2–5] of absorption coefficients include a few measurements in the present wave-length region. However the low intensity of the continuous spectrum produced by the x-ray sources then available, combined with the difficulties encountered in measuring very small ionization currents with the electrometer as compared with the FP-54 vacuum tube, favored intensity at the expense of resolving power. Thus, although a single crystal spectrometer was used as monochromator, the $\delta\lambda$ interval (as calculated from the spectrometrical geometry) was a large fraction of λ, which means that the uncertainty in the effective wave-length was large. A further disadvantage of the single crystal spectrometer, resulting from the small Bragg angles encountered at short wave-lengths, is the problem of adequately shielding the ionization chamber from scattered radiation.

The filtered end-radiation from a heterogeneous beam has been used recently in the determination of absorption coefficients.[6] The results obtained with this method are discussed elsewhere.[7]

In consideration of the low resolving power used in previous work, and the small number of elements studied, the present investigation in the wave-length region $50 \leq \lambda < 150$ X.U. was undertaken with a 600 kv, 2000-watt, x-ray source, and with a two-crystal spectrometer especially designed for this wave-length region. The results of the absorption measurements for a series of elements of low atomic number are given herein, and for elements of high atomic number are given in the following paper by M. T. Jones.[7]

[1] Klein and Nishina, Zeits. f. Physik **52**, 853 (1928).
[2] Compton and Allison, *X-Rays in Theory and Experiment*, p. 534.
[3] Richtmyer, Phys. Rev. **18**, 13 (1921).
[4] Richtmyer and Warburton, Phys. Rev. **22**, 539 (1923).
[5] Allen, Phys. Rev. **27**, 266 (1926).
[6] Alichanjan and Kosman, Zeits. f. Physik **90**, 799 (1934).
[7] Jones, Phys. Rev. **50**, 110 (1936).

Apparatus and Method of Observation

The apparatus used in this investigation has been previously described.[8] Because of the greater practical resolving power without undue sacrifice of intensity, a two-crystal, rather than a single-crystal, spectrometer was used as monochromator. The particular design of the present instrument, which utilizes internal reflection of the x-rays as they are transmitted through the body of the crystals, permitted adequate shielding of the ionization chamber from scattered radiation. The vertical limiting slits were so adjusted that the geometrical resolving power was many times greater than that due to the crystals. The horizontal divergence was limited by the size of the focal spot. The $\delta\lambda$ interval, as determined from considerations previously discussed,[8] was $1.8<\delta\lambda<1.0$ X.U. for $50<\lambda<215$ X.U., respectively.

The absorbers, placed between the x-ray tube and the first crystal, were mounted as described in reference 8. Lead shields having holes $3/4\times1/2$ inches in the path of the x-ray beam protected the absorbers from radiation scattered by other objects in the vicinity. It was thought possible that an error might be introduced in the observations taken at wave-length λ_1, due to radiation of $\lambda<\lambda_1$, present in the beam, undergoing a wave-length shift by multiple Compton scattering within the absorber in such a way as to be reflected by the crystals as radiation of wave-length λ_1. The error due to this effect was calculated and found to be entirely negligible.

Each measurement of an absorption coefficient consisted of 9 to 12 values of $(I+I_s)$ and of (I_0+I_s), where I and I_0 represent, respectively, the ionization current with the absorber in the path of the beam, and removed, and where I_s represents the background or residual ion current. At intervals during the recording of the other ion currents, 4 or 5 values of I_s were determined by stopping the x-ray beam with a lead shutter, 3/4 inch thick, placed between the target and the first crystal. That this method gave the true residual current is shown by the fact that for the shutter open or closed no difference was observed in the residual ion current (I_s) when one crystal had been turned a few degrees (about 5°) from its position previously determined by the setting of the wave-length screw (see reference 8) for a given value of λ. This test was made for several wave-lengths, including 50 X.U.

At each wave-length λ the x-ray tube was operated at a voltage such that there was not present in the beam second-order energy of wave-length $\lambda/2$. Especial care was taken to keep the tube voltage constant, but due to the type of voltage source employed it is probable that occasionally there were random fluctuations of as much as 3 percent. It is believed that this fluctuation was the greatest source of error. In order to reduce errors due to this cause, a large number of observations were taken.

The Absorbers Investigated

Particular care was taken to obtain absorbers of high purity. The effect of such impurities as were present in the samples is less than the experimental error of the results. The carbon absorbers (99.9 percent pure) were regraphitized graphite made especially for spectroscopic purposes. The aluminum used was 99.97 percent pure and contained 0.008 percent copper and 0.008 percent iron as the principal impurities. Chile copper, 99.96 percent pure, was used. The nickel absorbers were the same high purity absorbers used in a previous investigation.[4] The sulfur absorbers were carefully cast from the highest grade C.P. sulfur obtainable.

The sodium and potassium absorbers were prepared by the R. and H. Chemicals Department of the E. I. duPont de Nemours & Company. The metals were cast in blocks of suitable dimensions and each block was wrapped in sheet of aluminum foil whose edges were sealed with adhesive tape and paraffine. The purity of the samples was reported to be as follows: The sodium was 99.7 percent pure and contained no heavy metals and not over 0.04 percent calcium. The potassium was 99.0 percent pure with sodium as the other main constituent. Samples of both metals contained as other impurities traces of the oxide, hydroxide, and carbonate.

Results

The atomic absorption coefficient, μ_A, is defined by the relation

$$\mu_A=\tau_A-Z\sigma_e, \qquad (1)$$

[8] Cuykendall and Jones, Rev. Sci. Inst. **6**, 356 (1935).

where τ_A is the photoelectric absorption coefficient, Z the atomic number, and σ_e the total scattering per electron. As discussed presently, for elements of low atomic number and for the present wave-length region, the scattering, $Z\sigma_e$, is the greater part of the observed absorption. Several theoretical formulae have been proposed which express the variation of σ_e with wave-length. Of these the Klein-Nishina formula[1] predicts values of σ_e which differ considerably from those of the earlier theories, and the Klein-Nishina values have been shown to agree with the observed scattering at wave-lengths from 20 to 50 X.U.[9] The present report is largely concerned with the comparison of $Z\sigma_e$ as predicted by theory and as experimentally observed in the wave-length region $40<\lambda<100$ X.U.

The variation of τ_A with Z and λ may be written as

$$\tau_A = KZ^p\lambda^q, \qquad (2)$$

where K is a constant for $\lambda<\lambda_{K\ \text{limit}}$, and p and q are constants, approximately 4 and 3, respectively. [More precisely, as discussed elsewhere,[7] p and q may be functions of Z and λ.] It has been shown that for gamma-rays the photoelectric absorption in elements $Z=1$ to $Z=16$ is less than experimental error.[10] Hence, because of the relation in Eq. (2), it may be expected that the photoelectric absorption in carbon, $Z=6$, is less than the experimental error of μ_A at wave-lengths considerably greater than those of gamma-rays. Therefore, the absorption measurements for carbon provide a test of the validity of the Klein-Nishina formula.

The experimental results for carbon are given in Table I. In Fig. 1 are plotted the experimental values of μ_A/Z and also the theoretical values of the total scattering per electron, σ_e, as calculated from the Klein-Nishina formula. The values of μ_A/Z and σ_e are in excellent agreement from 40 X.U. to the wave-length at which the photoelectric absorption becomes appreciable, about 100 X.U., which confirms within experimental error the Klein-Nishina formula for this wave-length region.

The absorption coefficients determined for Na, Al, K, Ni, and Cu are given in Table II, and for S are given in Table III. The mass absorption curves are shown in Fig. 2. The values of τ_A were calculated from the absorption Eq. (1) in which were used the values of σ_e given in Table I. The variation of τ_A with λ is shown in Fig. 3, from which $q=2.83$ and 2.6, for copper and aluminum, respectively. However the actual

[9] Read and Lauritsen, Phys. Rev. **45**, 433 (1934).
[10] Rutherford, Chadwick and Ellis, *Radioactive Radiations*, p. 473.

TABLE I. *Measured values of the mass absorption coefficient, μ/ρ, and the electronic absorption coefficient, μ_e, for carbon; and comparison with the Klein-Nishina values of the scattering per electron, σ_e.*

λ (X.U.)	μ/ρ (cm² g⁻¹)	Probable Error	Exp. Value[1] $\mu_e\times10^{25}$	Klein-Nishina Value[2] $\sigma_e\times10^{25}$	$\frac{\mu_e-\sigma_e}{\mu_e}\times100$
40	0.105	0.001	3.46	3.447	+0.5
50	0.114	0.001	3.76	3.734	0.7
60	0.120	0.001	3.96	3.969	−0.2
70	0.126	0.002	4.16	4.167	−0.2
80	0.132	0.002	4.36	4.336	+0.5
85	0.134	0.001	4.42	4.405	0.4
90	0.137	0.001	4.52	4.483	0.8
100	0.142	0.001	4.69	4.610	1.6
110	0.147	0.002	4.85	4.723	2.7
115	0.149	0.001	4.92	4.778	3.0
120	0.151	0.002	4.98	4.824	3.2
130	0.154	0.001	5.08	4.915	3.4
140	0.158	0.003	5.21	4.995	4.4
160	0.163	0.002	5.38	5.132	4.8
184	0.171	0.002	5.64	5.280	6.9
209	0.177	0.001	5.84	5.395	8.3

[1] $\mu_e=\mu_A/Z=\mu/\rho\cdot(A/ZN)$: A, atomic weight: Z, atomic number: N, Avogadro's number.
[2] In the calculation of the Klein-Nishina values of σ_e, given in the above table, the following values of the general physical constants were employed:
$e=4.767\times10^{-10}$ e.s.u. $\quad h=6.542\times10^{-27}$ erg·sec.
$m=0.9038\times10^{-27}$ g $\quad c=2.998\times10^{10}$ cm/sec.
Recently Bäcklin and Flemberg (Nature **137**, 655 (1936)) have reported a new value for e (4.800×10^{-10}) which is in good agreement with that utilized by Birge (Phys. Rev. **48**, 918 (1935)) (4.8036) in obtaining a new value of h (6.6286). Using $e=4.800\times10^{-10}$ and $h=6.6286\times10^{-27}$, an evaluation of the Klein-Nishina formula for σ_e gives 3.821 and $4.724(\times10^{-25})$ at 50 and 100 X.U., respectively. These are each some 2 percent greater than the values in Table I.

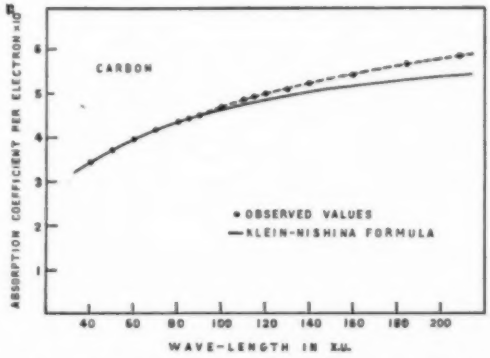

FIG. 1. The experimental values of μ_A/Z for carbon and the theoretical values of σ_e as calculated from the Klein-Nishina formula. The agreement in the region $40\leq\lambda\leq100$ X.U. is within experimental error, which confirms the Klein-Nishina formula for this wave-length region.

TABLE II. *The observed mass absorption coefficients; and the atomic and photoelectric coefficients* ($\times 10^{24}$).[1]

λ (X.U.)	Na(11)			Al(13)			K(19)			Ni(28)			Cu(29)		
	μ/ρ	μ_A	τ_A	μ/ρ	μ_A	τ_A	μ/ρ	μ_A	τ_A	μ/ρ	μ_A	τ_A	μ/ρ	μ_A	τ_A
50				0.113	5.02	0.17	0.115	7.41	0.32	0.126	12.2	1.7	0.129	13.5	2.7
55				0.117	5.20	0.17				0.148	14.3	3.5			
60	0.119	4.52	0.16	0.121	5.38	0.22	0.136	8.76	1.22	0.163	15.8	4.7	0.160	16.7	5.2
65										0.168	16.3	4.9			
70	0.126	4.78	0.20	0.131	5.79	0.37	0.144	9.27	1.35	0.187	18.1	6.4	0.182	19.1	7.0
75				0.135	6.00	0.48				0.195	18.9	7.0			
80	0.134	5.08	0.31	0.138	6.14	0.50	0.162	10.43	2.19	0.218	21.1	9.0	0.215	22.5	9.9
85				0.142	6.31	0.59									
90	0.140	5.30	0.37	0.144	6.40	0.57	0.180	11.59	3.07	0.250	24.2	11.7	0.259	27.2	14.2
95				0.147	6.54	0.64									
100	0.147	5.58	0.51	0.150	6.67	0.68	0.194	12.49	3.73	0.297	28.7	15.8	0.306	32.1	18.7
110	0.154	5.84	0.65	0.158	7.03	0.89	0.202	13.01	4.04	0.349	33.8	20.6	0.371	38.9	25.2
115				0.162	7.20	0.99									
120	0.161	6.11	0.80	0.168	7.47	1.20	0.228	14.68	5.51	0.420	40.6	27.1	0.434	45.5	31.5
125				0.175	7.78	1.46									
130	0.168	6.38	0.97	0.176	7.83	1.44	0.256	16.49	7.15	0.490	47.4	33.6	0.513	53.8	39.5
140	0.174	6.60	1.10	0.191	8.50	2.01	0.297	19.13	9.64	0.594	57.5	43.5	0.606	63.5	49.0
160	0.186	7.06	1.41	0.213	9.47	2.80	0.366	23.57	13.82	0.771	74.6	60.2	0.830	87.0	72.1
184[2]	0.208	7.89	2.09	0.240	10.67	3.81	0.459	29.56	19.53	1.10	106.5	91.7	1.17	122.6	107.3
209[3]	0.231	8.78	2.84	0.279	12.37	5.36	0.606	39.03	28.78	1.56	151.	136.	1.63	170.9	153.3

[1] $\tau_A = \mu_A - Z\sigma_e$. Values of σ_e are given in Table I. [2] W $K\beta$ radiation. [3] W $K\alpha_1$ radiation.

values of q are of little significance since the photoelectric absorption is, in the case of aluminum at 100 X.U., only 10 percent of the observed absorption, and consequently contains an unavoidably large experimental error.

The present experimental values of μ/ρ for carbon and aluminum are within one percent of those recently reported by Hahn[11] for $\lambda > 140$ X.U., but the present values differ from Allen's[5] in some cases by as much as 10 percent. It is to be noted, however, that Allen's value for carbon at 209 X.U. is but 2 percent greater than the scattering predicted by the Klein-Nishina formula, at 140 X.U. is about 1/2 percent greater, and at 81 to 90 X.U. is more than 8 percent greater than the predicted scattering. In view of the present measurements it is unlikely that the photoelectric absorption varies with wavelength in this manner.

In Fig. 4 the author's results for aluminum are plotted with the results of other investigators.[9, 11, 12] From the τ_A curve for aluminum, Fig. 3, it appears that at 50 X.U. the value of τ_A is greater than 0.12×10^{-24}. Assuming this minimum value, we have $\mu_A = 4.98\times10^{-24}$, which is approximately 2 percent greater than the

TABLE III. *The absorption coefficients determined for sulfur.*

λ (X.U.)	μ/ρ	$\mu_A\times10^{24}$	$\tau_A\times10^{24}$
75	0.142	7.51	0.72
100	0.172	9.09	1.71
120	0.200	10.57	2.85
130	0.219	11.58	3.72

[11] Hahn, Phys. Rev. **46**, 149 (1934).
[12] Chao, Phys. Rev. **36**, 1519 (1930).

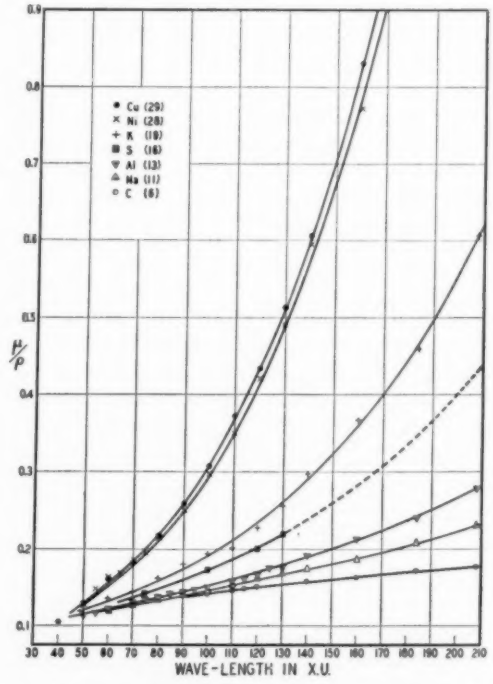

FIG. 2. Mass absorption curves for the elements studied.

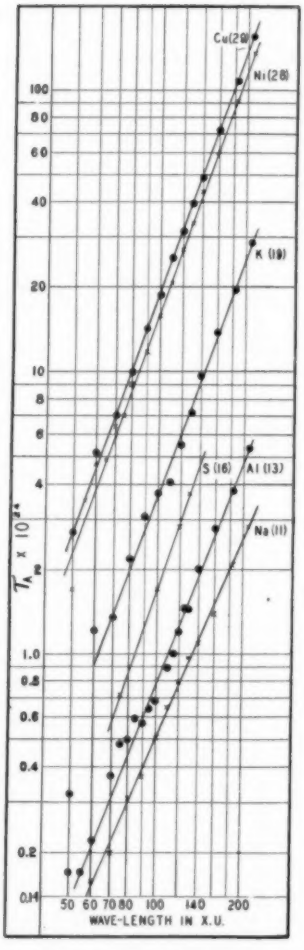

FIG. 3. The variation of the photoelectric absorption with wave-length.

value reported by Read and Lauritsen.[9] At the same wave-length their value for carbon is about 3 percent less than that predicted by the Klein-Nishina formula. These discrepancies may be due to the fact that Read and Lauritsen employed a much smaller resolving power than was used by the author.

Discrepancies exist between the previously reported results[3, 4, 5, 11] for nickel and copper and the present measurements in the region $140 < \lambda < 209$ X.U. Three independent determinations of μ/ρ for copper at 140 X.U. gave values within 2 percent of each other, but these values are 8 percent less than the value reported by Hahn.[11]

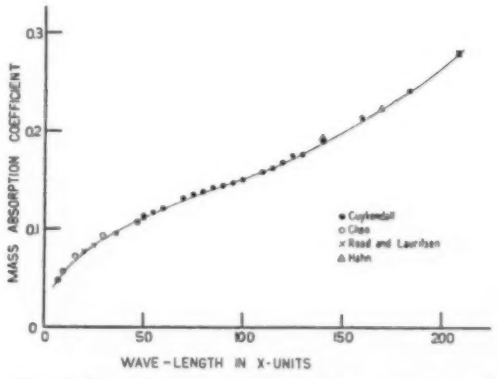

FIG. 4. The present results for aluminum plotted with those of Read and Lauritsen,[9] Hahn[11] and Chao[12] show the natural extension of the absorption measurements to the gamma-ray region. The form of the curve is explained as follows: At wave-lengths less than 75 X.U. the absorption is practically all scattering; at longer wave-lengths the photoelectric absorption becomes important, increasing to about 60 percent of the total absorption at 200 X.U.

Read[13] has measured the absorption in copper in the region 20 to 47 X.U.: a smooth curve through his results gives at 50 X.U. a value within 2 percent of the present result.

The probable errors given in Table I were calculated in the usual manner from the variations of the individual readings obtained during the determination of the mass absorption coefficient. After an interval of more than two months many of the values of μ/ρ were redetermined showing good agreement with the earlier results. Considering all the sources of error, the writer estimates that the values of μ/ρ given in Tables I, II, and III are in error by no more than 2 percent.

ACKNOWLEDGMENTS

The author is pleased to express his indebtedness to Professors F. K. Richtmyer and C. C. Murdock for their interest and advice during the course of this work, to Dr. L. G. Parratt for his criticism of the manuscript, to the Aluminum Company of America and the American Brass Company for their donation of the samples of aluminum and copper, respectively, to the I. E. duPont de Nemours & Company for the donation of, and to Drs. Jones and Gilbert of the R and H Chemicals Department for the preparation of the samples of sodium and potassium.

[13] Read, Proc. Roy. Soc. **A152**, 402 (1935).

The Absorption of Ultra-Short X-Rays by Elements of High Atomic Number

MATTHEW T. JONES, *Cornell University*

(Received May 11, 1936)

Employing a specially constructed two-crystal spectrometer and a 600-kilovolt x-ray machine, mass absorption coefficients have been measured, with an average probable error of 0.8 percent, for Pb(82), Ta(73), Sn(50), Ag(47), Mo(42), and Cb(41) in the wave-length range $30<\lambda<185$ X.U. Assuming the correctness of the Klein-Nishina formula for absorption due to scattering, the photoelectric absorption τ_a was calculated for the above elements. In the empirical equation $\tau_a=C_aZ^p\lambda^q$, p increases from 3.51 to 3.88 as λ decreases from 140 to 50 X.U., and q increases from 2.60 to 2.80 as Z decreases from 82 to 41. Agreements with data of other observers for Pb(82) are given. At 30 and 40 X.U., the present data for Pb(82) are about 10 percent higher than the theory developed by Hulme, McDougall, Buckingham and Fowler. New constants in Gray's empirical equation for τ_{Pb} are suggested of: $a=3.7321$, $b=1.03$ and $c=0.44$.

INTRODUCTION

WHEN a beam of monochromatic x-rays passes through an absorbing material, the law

$$I=I_0e^{-\mu_a(N/A)(\rho x)}, \tag{1}$$

is obeyed, where I_0 is the intensity of the incident beam, I the intensity after passing through a thickness x of absorber of density ρ, μ_a the total atomic absorption coefficient, N Avagadro's number, and A the atomic weight.

Theoretical and empirical laws have been developed expressing the variation of μ_a with Z, the atomic number, and λ the wave-length of the x-rays; the empirical laws take the form

$$\mu_a=\tau_a(Z,\lambda)+\sigma_a(Z,\lambda), \text{ with } \tau_a(Z,\lambda)=C_aZ^p\lambda^q, \tag{2}$$

where $\tau_a(Z,\lambda)$ is the true or photoelectric atomic absorption coefficient, $\sigma_a(Z,\lambda)$ is the atomic absorption coefficient due to scattering, C_a is a constant over a given wave-length range determined by the absorption limits.

In the wave-length range $0.1<\lambda<0.7$A, Richtmyer[1] determined $p=4$, $q=3$, $0.1<\sigma/\rho<1.0$, and $C_a=22.4\times10^{-27}$ for λ less than the K limit and $6<Z<82$; $\sigma/\rho=\sigma_a(N/A)$. Allen[2] made a large number of measurements in the range $0.081<\lambda<2.0$A and as a result advocates a value of $q=2.92$ although some of his values came out as low as 2.6. Jaeger[3] measured μ/ρ, the mass absorption coefficient, for Pb(82) in the region $30<\lambda<127$ X.U., employing the end-radiation method. Later Alichanjan and Kosman[4] made similar measurements in the range $25<\lambda<60$ X.U., introducing a correction for the effective wave-length when using the end-radiation method. Hahn[5] made very careful absorption measurements on Pb(82), Au(79), W(74), Ta(73), Ag(47), Cu(29), Al(13), C(6) and paraffin in the range $139<\lambda<208.6$ X.U. The data at 208.6 X.U. were taken with a two-crystal spectrometer; the rest of the data with the second crystal removed. Recently, Read[6] measured absorption coefficients for Pb(82) and Sn(50) in the range $20.2<\lambda<52.5$ X.U. using a single rocksalt crystal; the width of the band of rays used by him was about 5 X.U. Read estimates his experimental error on the lead data to be 2 percent.

In the region $4.7<\lambda<47$ X.U., Chao[7] measured absorption coefficients in Pb(82), Sn(50), and Al(13) employing gamma-rays. Gray[8] summarized gamma-ray data for Pb(82) and determined the constants in an empirical equation suggested by Ellis, to fit this summary, using Allen's data at 100 X.U.; this equation for τ, the linear photoelectric absorption coefficient, is

$$\log_{10}\tau=a+\log_{10}\lambda+c(\log_{10}\lambda)^2, \tag{3}$$

[1] F. K. Richtmyer, Phys. Rev. **17**, 264 (1921); **18**, 13 (1921); **27**, 1 (1926); **30**, 755 (1927).
[2] S. J. M. Allen, Phys. Rev. **24**, 1 (1924); **27**, 266 (1926); **28**, 907 (1927).
[3] R. Jaeger, Zeits. f. Physik **69**, 565 (1931).
[4] A. Alichanjan and M. Kosman, Zeits. f. Physik **90**, 779 (1934).
[5] T. M. Hahn, Phys. Rev. **46**, 149 (1934).
[6] J. Read, Proc. Roy. Soc. **A152**, 402 (1935).
[7] C. Y. Chao, Proc. Nat. Acad. Sci. **16**, 431 (1930); Phys. Rev. **36**, 1519 (1930).
[8] L. H. Gray, Proc. Camb. Phil. Soc. **27**, 103 (1931).

where $a=\bar{3}.6505$, $b=1.0$ and $c=0.480$. This law fits gamma-ray data within about 10 percent.

A large number of theoretical calculations have been made for $\tau(Z, \lambda)$; the best of them, calculated by wave mechanics, gives values for τ lower than experiment in the x-ray region. The most recent calculation by Hulme, McDougall, Buckingham and Fowler[9] gives values agreeing with Gray's Eq. (3) above. Their formula is valid for all wave-lengths and atomic numbers but is impractical for all but very short wave-lengths.

Of the theoretical calculations for $\sigma_a(Z, \lambda)$, the absorption due to scattering, the Klein-Nishina formula has been checked experimentally by Chao,[7] by Read and Lauritsen,[10] and by Cuykendall;[11] it represents the results within experimental error. These checks were carried out on the elements of low atomic number, C(6) and Al(13), and at short wave-lengths ($\lambda<100$ X.U.), because the photoelectric absorption may be considered negligible in this range.

Since for gamma-rays ($\lambda<50$ X.U.) the absorption due to scattering plays the major role and for x-rays ($\lambda>100$ X.U.), the photoelectric absorption is the larger part of the total, at least for the heavier elements, the intermediate region $30<\lambda<150$ X.U. for x-rays is an important one for the investigation of the variation of σ and τ with the wave-length and atomic number. In order to study the photoelectric absorption in this region, it is better to use the elements of high atomic number for which σ is small compared to τ. There are almost no reliable data in this region for monochromatic rays. End-radiation measurements are not very accurate and the radiation employed is not monochromatic. Any measurements in this region with single crystal spectrometers as monochromators were taken with very low resolving power of the spectrometers. Therefore a study was undertaken of the photoelectric absorption in the range $30<\lambda<200$ X.U. for elements of high atomic number.

[9] H. R. Hulme, J. McDougall, R. A. Buckingham, and R. H. Fowler, Proc. Roy. Soc. **A149**, 131 (1935).
[10] J. Read and C. Lauritsen, Phys. Rev. **45**, 433 (1934).
[11] T. R. Cuykendall, Phys. Rev. this issue.

Apparatus

The apparatus used consists of a 600-kilovolt x-ray machine and a two-crystal spectrometer described by Cuykendall and Jones.[12] The source of the x-rays is a cascade-type Coolidge tube, with a tungsten target, which is operated on two 300-kilovolt induction coils in series. The monochromator is a two-crystal spectrometer specially designed for use in the wave-length region $30<\lambda<215$ X.U. Transmission of the x-rays through the body of the crystals and reflection from internal planes instead of the usual reflection from the surface, is employed. An ionization chamber containing argon at 80 atmospheres pressure, and a FP-54 electrometer-tube system is used to measure the intensity of the reflected radiation. The width of the wave-length band separated from the continuous spectrum produced by the x-ray tube, is of the order of $1.8<\delta\lambda<1.0$ X.U., for $50<\lambda<215$ X.U.[12]

Results

The elements investigated were Cb(41), Mo(42), Ag(47), Sn(50), Ta(73) and Pb(82) in the range $30<\lambda<185$ X.U. All were of high purity and known to be free of any impurities which would affect the results beyond experimental error. The silver samples were 99.98 percent pure containing no lead; most of the impurity was oxygen. Table I gives a summary of the observed mass absorption coefficients μ/ρ, atomic absorption coefficients μ_a, and photoelectric atomic absorption coefficients τ_a. Each value is obtained from 9 to 12 pairs of observations with an average probable error of 0.8 percent.

The observed values of the atomic absorption coefficients for Pb(82) are plotted in Fig. 1 along with the data of other observers. Richtmyer's values at wave-lengths less than the K limit agree with the observations. Richtmyer's and Hahn's data at 208.6 X.U. agree with the observed value within experimental error; this was taken as a check. Allen's values, in the range $50<\lambda<110$ X.U., are from 40 to 60

[12] T. R. Cuykendall and M. T. Jones, Rev. Sci. Inst. **6**, 356 (1935).

TABLE I. *Observed absorption coefficients.*

λ (X.U.)	Pb(82) μ/ρ	Pb(82) $\mu_a\times10^{22}$	Pb(82) $\tau_a\times10^{22}$	Ta(73) μ/ρ	Ta(73) $\mu_a\times10^{22}$	Ta(73) $\tau_a\times10^{22}$	Sn(50) μ/ρ	Sn(50) $\mu_a\times10^{22}$	Sn(50) $\tau_a\times10^{22}$
30	0.22	0.752	0.499						
40	0.394	1.346	1.064						
50	0.600	2.052	1.745	0.458	1.372	1.100	0.246	0.482	0.295
60	0.900	3.077	2.751	0.689	2.064	1.774	0.314	0.615	0.416
70	1.455	4.975	4.634	1.018	3.049	2.745	0.430	0.842	0.634
80	1.829	6.254	5.896	1.357	4.065	3.747	0.607	1.189	0.972
90	2.490	8.513	8.145	1.819	5.448	5.120	0.800	1.567	1.343
100	3.248	11.11	10.73	2.435	7.293	6.956	1.020	1.998	1.767
110	4.079	13.94	13.56	3.014	9.027	8.681	1.222	2.394	2.158
120	5.150	17.61	17.21	3.770	11.29	10.94	1.587	3.108	2.867
130	6.412	21.93	21.52	4.553	13.64	13.28	1.912	3.745	3.499
140				5.476	16.40	16.03	2.310	4.524	4.274
160									
184.5									
208.6	5.108								

	Ag(47) μ/ρ	Ag(47) $\mu_a\times10^{22}$	Ag(47) $\tau_a\times10^{22}$	Mo(42) μ/ρ	Mo(42) $\mu_a\times10^{22}$	Mo(42) $\tau_a\times10^{22}$	Cb(41) μ/ρ	Cb(41) $\mu_a\times10^{22}$	Cb(41) $\tau_a\times10^{22}$
50	0.229	0.407	0.232	0.177	0.280	0.124	0.181	0.278	0.125
60	0.283	0.504	0.317	0.227	0.360	0.193	0.232	0.356	0.194
70	0.400	0.712	0.516	0.319	0.505	0.330	0.305	0.469	0.298
80	0.544	0.969	0.764	0.412	0.653	0.470	0.402	0.617	0.440
90	0.715	1.273	1.062	0.535	0.847	0.658	0.530	0.814	0.631
100	0.900	1.602	1.386	0.650	1.029	0.836	0.667	1.025	0.836
110	1.081	1.925	1.702	0.821	1.300	1.102	0.805	1.237	1.043
120	1.362	2.425	2.198	1.036	1.643	1.440	1.065	1.636	1.439
130	1.656	2.948	2.717	1.243	1.969	1.762	1.290	1.982	1.781
140	2.038	3.628	3.392	1.513	2.397	2.185	1.555	2.389	2.184
160				2.108	3.339	3.123	2.226	3.420	3.210
184.5				3.193	5.057	4.837	3.092	4.750	4.534

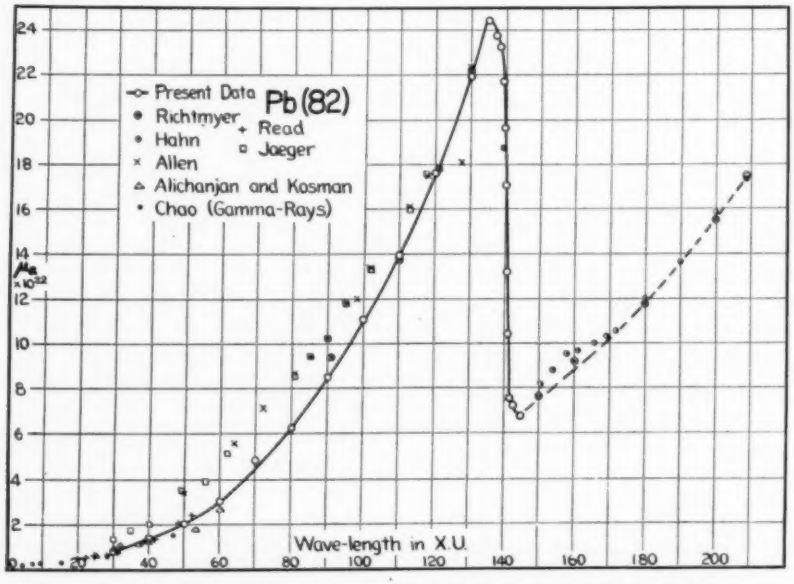

FIG. 1. Comparison of present values of μ_a for Pb(82) with those of other observers.

percent higher than the present data. This discrepancy could be accounted for by assuming that the radiation he employed was not monochromatic due to low resolving power of his apparatus in this region. Jaeger's data agree with Allen's but, as pointed out by Alichanjan and Kosman,[4] a correction should be made to the wave-length of the short-wave limit of their operating voltage, when employing the end-radiation method, to take into account the fact that a homogeneous beam of x-rays is never really reached by this method; the effective wave-length is longer than the short-wave limit. This would move Jaeger's data more in agreement with the present observations. Alichanjan and Kosman's data, for which this correction has been made, agree with the data herein reported. Read's data agree with the observed data within experimental error on the wave-length region covered by him. The gamma-ray measurements of Chao agree within 15 percent where they overlap with the present data.

Hahn's data for Ta(73) are lower than an extrapolation of the present data in the region $140<\lambda<160$ X.U. beyond the experimental error. His data for Ag(47) are higher in the same range. The data of Allen are consistently 10 to 50 percent higher than the present data. Read's data for Sn(50) fit on to an extrapolation of the observed data for $\lambda<50$ X.U.

The Klein-Nishina formula for the absorption due to scattering has been checked within experimental error;[7, 10, 11] therefore, if one assumes that the scattering per electron σ_e is independent of the atomic number, the photoelectric absorption τ_a per atom may be calculated from $\tau_a=\mu_a-Z\sigma_e$.* Plotting these values of τ_a against wave-length on a double logarithmic scale should give a straight line if q in Eq. (2) is constant; the slope of such a straight line gives the value of q. Fig. 2 is such a graph for the elements studied. The data for each element fall nearly on straight lines. Table II gives the values of q found from these curves.

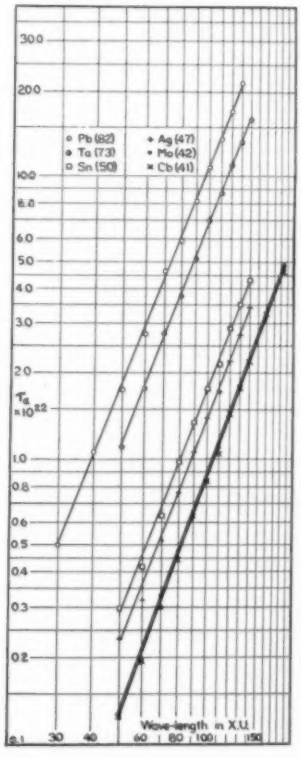

FIG. 2. τ_a plotted against wave-length for various elements.

In a similar manner, the exponent p, of Z in Eq. (2), may be determined from a double logarithmic plot of τ_a against Z. Fig. 3 is the graph obtained. Again the data fall nearly on straight lines. Table III gives the values of p. The variation of p agrees qualitatively with the theory[13] of photoelectric absorption which predict that $p\doteq 5$ as $\lambda\doteq 0$ and should decrease as the

TABLE II. *Experimental values of q in Eq. (2).*

Z	41	42	47	50	73	82
q	2.79	2.80	2.63	2.63	2.60	2.60

TABLE III. *Experimental values of p in Eq. (2).*

λ (X.U.)	p	λ (X.U.)	p
140	3.51	90	3.69
130	3.64	80	3.73
120	3.62	70	3.84
110	3.68	60	3.88
100	3.69	50	3.84

* As an extreme case, if, due to coherent scattering, σ_e were 5 percent greater for Pb(82) than calculated by the Klein-Nishina formula, at $\lambda=30$ X.U., τ_a would be less than 2 percent higher which is of the order of the experimental error and would not seriously affect the conclusions drawn herein.

[13] F. Sauter, Ann. d. Physik **9**, 217 (1931); **11**, 454 (1931).

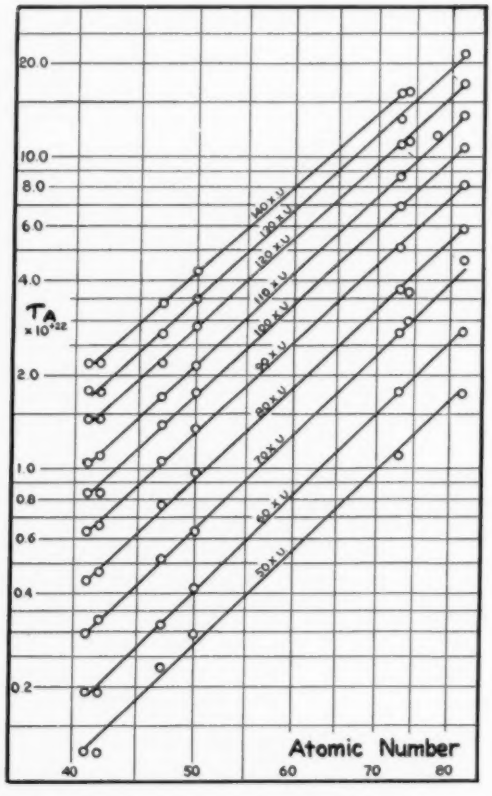

FIG. 3. τ_a plotted against atomic number for various wave-lengths.

wave-length increases. In the wave-length region here studied these data indicate that if there is a variation of q with λ, it is much less than that predicted by theory.

The agreement with Gray's empirical Eq. (3) is not good for the values of the constants given by him. Gray used Allen's data at 100 X.U. in the determination of his constants which partly explains the lack of agreement. Suggested values of the constants of Eq. (3) to fit the present data are: $a=\bar{3}.7321$, $b=1.03$ and $c=0.44$. Table IV gives the observed values, values calculated from Gray's equation, and values calculated using these new constants. Of course it is obvious that an equation in which q varies with wave-length can fit only approximately the present data for which q has been shown to be constant; therefore such an equation has no theoretical significance, but may be of practical use in irradiation work with hard x-rays.

TABLE IV. *Values of* $\tau_a \times 10^{22}$ *for Pb(82).*

λ (X.U.)	OBSERVED	CALCULATED FROM EQ. (3) using $a=\bar{3}.6505$, $b=1.0$, $c=0.48$	using $a=\bar{3}.7321$, $b=1.03$, $c=0.44$	CALC. FROM THEORY
30	0.50	0.45	0.49	0.47
40	1.06	0.92	0.98	0.91
50	1.74	1.64	1.70	
60	2.75	2.62	2.69	
70	4.63	4.06	4.07	
80	5.90	5.90	5.82	
90	8.14	8.26	8.02	
100	10.73	11.20	10.74	
110	13.56	15.51	14.63	
120	17.21	19.26	17.98	
130	21.52	24.45	22.63	

Calculations taken from the theoretical photo-electric absorption curve given by Hulme, McDougall, Buckingham and Fowler[9] for Pb(82) are given in the last column of Table IV. The calculated values are about 10 percent lower than the observations.

The author wishes to express his appreciation to Professor F. K. Richtmyer for his assistance and encouragement throughout the work and to the Raritan Copper Works, Perth Amboy, N. J., for donating the silver samples.

Mechanical Detection and Measurement of the Angular Momentum of Light

RICHARD A. BETH,* *Worcester Polytechnic Institute, Worcester, Mass. and Palmer Physical Laboratory, Princeton University*

(Received May 8, 1936)

The electromagnetic theory of the torque exerted by a beam of polarized light on a doubly refracting plate which alters its state of polarization is summarized. The same quantitative result is obtained by assigning an angular momentum of $\hbar$ ($-\hbar$) to each quantum of left (right) circularly polarized light in a vacuum, and assuming the conservation of angular momentum holds at the face of the plate. The apparatus used to detect and measure this effect was designed to enhance the moment of force to be measured by an appropriate arrangement of quartz wave plates, and to reduce interferences. The results of about 120 determinations by two observers working independently show the magnitude and sign of the effect to be correct, and show that it varies as predicted by the theory with each of three experimental variables which could be independently adjusted.

ELECTROMAGNETIC FIELD THEORY

THE moment of force or torque exerted on a doubly refracting medium by a light wave passing through it arises from the fact that the dielectric constant $\mathbf{K}$ is a tensor. Consequently the electric intensity $\mathbf{E}$ is, in general, not parallel to the electric polarization $\mathbf{P}$ or to the electric displacement

$$\mathbf{D}=\mathbf{K}\mathbf{E}=\mathbf{E}+4\pi\mathbf{P}$$

in the medium. The torque per unit volume produced by the action of the electric field on the polarization of the medium is

$$\mathbf{l}=\mathbf{P}\times\mathbf{E}=(\mathbf{D}\times\mathbf{E})/4\pi. \qquad (1)$$

Following Sadowsky and Epstein[1] we may calculate this torque for a simple case as follows: Assume a doubly refracting medium of permeability unity and take as x, y, and z axes the principal axes of the tensor $\mathbf{K}$ for the light frequency in question. Denote the principal values of $\mathbf{K}$ by n_x^2, n_y^2 and n_z^2 so that n_x, n_y and n_z will be the principal indices of refraction. Let the electric components of a plane light wave propagated in the $+z$ direction be given by

$$\mathbf{E}=A\cos\theta\cos(Z_1+\Delta),\quad A\sin\theta\cos(Z_1-\Delta),\quad 0,$$

$$\mathbf{D}=\mathbf{K}\mathbf{E}=n_x^2A\cos\theta\cos(Z_1+\Delta),\quad n_y^2A\sin\theta\cos(Z_1-\Delta),\quad 0, \qquad (2)$$

where $Z_1=\omega(t-nz/c)$; $n=(n_y+n_x)/2$,

$$\Delta=\pi z(n_y-n_x)/\lambda;\quad \omega=2\pi c/\lambda.$$

For any value of z (in particular $z=0$) for which the wave plate thickness Δ/π is a whole number the light is plane polarized and E makes an angle $+\theta$ with the x axis.

The torque per unit volume at any point in the crystal is calculated from (2) according to (1)

$$\mathbf{l}=0,\quad 0,$$

$$(A^2/8\pi)(n_x^2-n_y^2)\sin 2\theta\cos(Z_1+\Delta)\cos(Z_1-\Delta)$$

and the time average value of the z component is

$$(A/4\pi)^2(n_x^2-n_y^2)\sin 2\theta\cos 2\Delta.$$

Integrating from z_1 to z_2 we get the torque per unit area on the crystal between these values:

$$L=-(A/4\pi)^2n\lambda\sin 2\theta(\sin 2\Delta_2-\sin 2\Delta_1). \qquad (3)^2$$

This torque, which has hitherto been generally considered too small for experimental detection, was detected and measured in the present experiment.[3]

---

* Member of the Physics Department, Worcester Polytechnic Institute. Preliminary work and final calculations were carried on at Worcester. Experimental work was done on leave-of-absence from Worcester as Research Associate at Palmer Physical Laboratory, Princeton University. Additional measurements were made by Mr. W. Harris at Princeton, as will be explained later.

[1] A. Sadowsky, Acta et Commentationes Imp. Universitatis Jurievensis **7**, No. 1–3 (1899); **8**, No. 1–2 (1900). P. S. Epstein, Ann. d. Physik **44**, 593 (1914). The derivation is repeated here because the first articles are in Russian and relatively inaccessible, while in the last there seems to be a misprint in the result. I wish to thank Dr. Boris Podolsky for translating parts of Sadowsky's articles for me from the Russian. I am also deeply indebted to Professor A. Einstein not only for his advice in checking Professor Epstein's calculation but also for several interesting discussions about the experimental part of the work here reported.

[2] J. H. Poynting, Proc. Roy. Soc. **A82**, 560 (1909), infers from an ingenious mechanical analogy that circularly polarized light should exert a torque equal to the light energy per unit volume times $\lambda/2\pi$ on unit area of a quarter-wave plate which makes the light plane polarized. This result, which neglects surface reflections, is contained in (3).

[3] R. A. Beth, Phys. Rev. **48**, 471 (1935); also Annual Meeting of the Am. Phys. Soc., St. Louis, Missouri, January 1, 1936. A. H. S. Holbourn, Nature **137**, 31 (1936), also reports successful measurement of the effect.

Quantum Theory

It is worth observing that (3) may be derived from the quantum theory by assigning an angular momentum or spin of $\hbar(-\hbar)$[4] to each photon of left (right) circularly polarized light, the spin axis being in the direction of propagation of the light.[5]

Consider an elliptically polarized light wave, propagated in the $+z$ direction in a vacuum, whose components in the directions of the principal axes of the ellipse (phase difference $=\pi/2$) have amplitudes X_0 and Y_0. Let the components of the same wave, when resolved along an arbitrary pair of perpendicular x and y axes in the plane of the ellipse, be given by

$$\mathbf{E}=X\cos(Z+\Delta),\quad Y\cos(Z-\Delta),\quad 0, \tag{4}$$

where $Z=\omega(t-z/c)$ and 2Δ is the phase angle by which the y component lags behind the x component of the wave. It may be shown that[6]

$$XY\sin 2\Delta=X_0Y_0,\quad X^2+Y^2=X_0^2+Y_0^2. \tag{5}$$

If we now regard the wave (4) as the superposition of left and right circularly polarized components of amplitudes L and R, respectively, calculation shows that

$$L^2-R^2=XY\sin 2\Delta,\quad L^2+R^2=(X^2+Y^2)/2.$$

The number of left circularly polarized photons transmitted per unit area per second is the Poynting energy flow $cL^2/4\pi$ divided by the energy per photon $2\pi\hbar\nu=2\pi\hbar c/\lambda$, or $\lambda L^2/8\pi^2\hbar$. Multiplying by $\hbar$ gives $\lambda L^2/8\pi^2$, the angular momentum transmitted per unit area per second by the left circularly polarized component. Taking account of the similar expression for the right circularly polarized component, the angular momentum transmitted per unit area per second by the wave (4) is

$$M=\lambda(L^2-R^2)/8\pi^2=\lambda XY\sin 2\Delta/8\pi^2 =\lambda X_0Y_0/8\pi^2. \tag{6}$$

It is well known that the linear momentum transmitted per unit area per second is the energy flow divided by c, in this case:

$$(L^2+R^2)/4\pi=(X^2+Y^2)/8\pi=(X_0^2+Y_0^2)/8\pi.$$

Thus the angular and linear momenta are proportional to the natural invariants (5) of the wave (4). For $X_0=Y_0$ their ratio is $\lambda=\lambda/2\pi$, which is another form of Poynting's result.[2]

The value (6) of the angular momentum, which is independent of the quantum constant $\hbar$, can be derived from the linear momentum (Poynting vector divided by c) in a finite beam, but the elementary method given is more descriptive in bringing out the fact that the quantum theory leads to the same value (3) as the wave theory for the torque on a section of a crystal.

To show this equivalence we have now to obtain the angular momentum for a wave (2) *in the crystal* from the expression (6) for a wave *in a vacuum*, by placing the face of the crystal at $z=z_1$ (vacuum for $z<z_1$) and using the conservation of angular momentum and Fresnel's expressions for the amplitudes of the reflected and transmitted waves. In the reflected wave the y component of amplitude $Y(n_y-1)/(n_y+1)$ lags behind the x component of amplitude $X(n_x-1)/(n_x+1)$ by the phase angle 2Δ. We get the angular momentum transmitted through the face $z=z_1$ by calculating (6) for the direct and reflected waves in the vacuum (taking account of direction of transmission of each) and assuming the conservation of angular momentum at the face

$$M_1=XY(n_x+n_y)\lambda\sin 2\Delta/4\pi^2(n_x+1)(n_y+1).$$

Using Fresnel's expressions for the amplitudes, we identify the transmitted wave *in the crystal* with (2) at $z=z_1$ by choosing

$$A\cos\theta=2X/(n_x+1);\quad A\sin\theta=2Y/(n_y+1);$$
$$\Delta=\Delta_1=\pi z_1(n_y-n_x)/\lambda.$$

Hence the angular momentum transmitted by (2) at $z=z_1$ is

$$M_1=(A/4\pi)^2n\lambda\sin 2\theta\sin 2\Delta_1. \tag{7}$$

It can now be seen directly that the torque (3) is equal to the excess of the angular momentum (7) per unit area per second flowing into a section of the crystal at $z=z_1$ over that flowing out at $z=z_2$. Hence both the field and the

---

[4] $\hbar=h/2\pi$.

[5] A. E. Ruark and H. C. Urey, Proc. Nat. Acad. Sci. **13**, 763 (1927); Harnwell and Livingood, *Experimental Atomic Physics* (1933), p. 81; Brillouin, *Les Statistiques Quantiques*, Chap. III (1930).

[6] See, e.g., Schuster and Nicholson, *Theory of Optics*, third edition, pp. 14, 15 (1924), especially Eqs. (15) and (17).

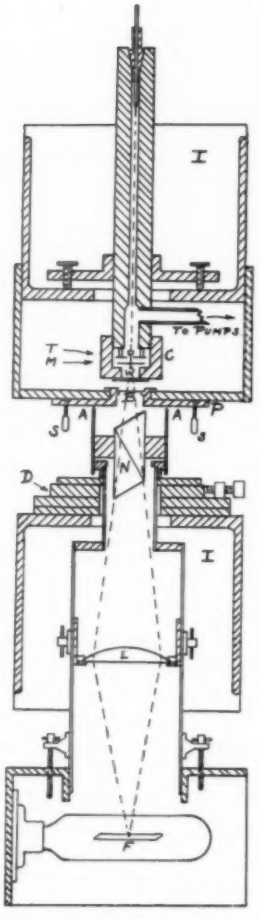

FIG. 1. Diagram of apparatus.

quantum theories predict the same value for the effect which has been measured in the present experiment.

APPARATUS

The basic idea used in detecting and measuring the effect[7] is to observe the deflection of a quartz wave plate hung from a fine quartz fiber when suitably polarized light is sent through the plate. In order to increase the effect to be measured and to avoid as far as possible interfering effects due to mechanical and electrostatic disturbances,

[7] See Poynting, reference 2, A. Kastler, Société des Sciences physiques et naturelles de Bordeaux, Jan. 28, 1932. R. A. Beth, abstract, Boston Meeting, American Physical Society, Phys. Rev. **45**, 296 (1934).

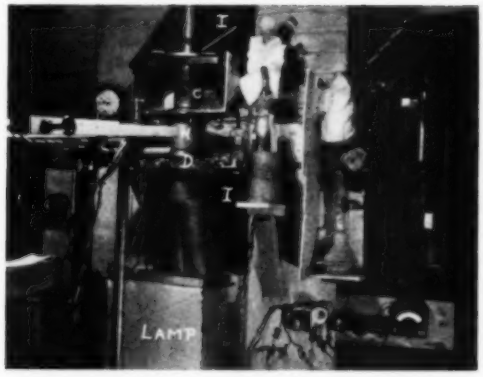

FIG. 2. Photograph of apparatus.

stray heating effects, radiometer and gas effects, and variations in light pressure, the apparatus was constructed as shown in Figs. 1, 2, 3, and 4. Some of the precautions taken to avoid these interferences may have been unnecessary, but they were sufficient.

The whole apparatus is supported on the heavy cast iron brackets I in Fig. 1, each $12'' \times 12''$, which are bolted to a brick pier to avoid mechanical disturbances, especially torsional vibrations of a period comparable to that

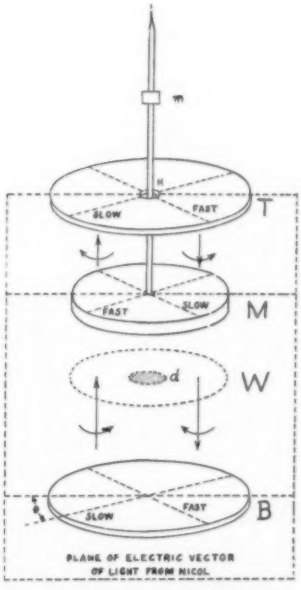

FIG. 3. Wave plate arrangement.

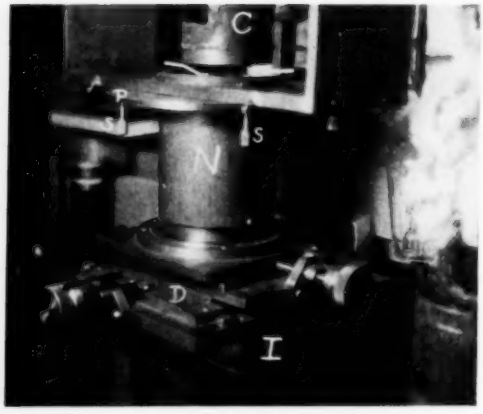

FIG. 4. Detail showing method by which light beam could be given lateral adjustment.

of the torsional pendulum formed by the one-inch circular wave plate M hanging at the bottom of the quartz fiber (about ten minutes). The fiber is about 25 centimeters long and hangs in a quarter inch hole bored lengthwise through a copper cylinder two inches in diameter. The upper end of the fiber is attached with a bit of flake shellac to a conical copper plug which was carefully ground in place and sealed with Apiezon grease. Thus the zero position as well as the amplitude of the torsional pendulum can be changed while the chamber is evacuated.

The hanging plate and the fixed plate above it, Fig. 3, are located in the cylindrical vacuum chamber C which is of copper, three inches in diameter with walls one-half inch thick. The heavy copper chamber is intended to eliminate unequal heating effects from the room as well as to shield off stray light and electrostatic disturbances.[8]

The chamber was evacuated through wide tubing by a high speed diffusion pump and three liquid-air traps. A two-stage diffusion pump and forepump provided the forevacuum for the high speed pump. According to the rated air calibration of the Western Electric ionization gauge, pressures below 10^{-6} mm of mercury existed in the chamber while the effect was being measured; no noticeable fluctuations appeared in the actual measurements which might be ascribed to radiometer or gas effects.

Light from a three-millimeter tungsten ribbon filament F is focused by the fused quartz lens L, 10.7 centimeters in diameter, through a large Nicol prism N, the lower plate B (Fig. 3), the fused quartz window W, and the hanging plate M, on the reflecting layer of aluminum on the top of the upper plate T in the chamber. The maximum deviation of the light from the vertical was about 10°. W has a circular aperture one inch in diameter. A round one-quarter inch copper disk d fastened in the middle of W prevents light from passing through the hole H in the top plate T. With this arrangement no light energy reaches the fiber and most of the energy is reflected out of the vacuum chamber altogether, thus minimizing fluctuations in the position of the pendulum due to unequal heating of the fiber and light pressure on the small mirror m. These undesirable effects are found to be present if the shield d is removed.

The lower plate B is placed outside the vacuum chamber in a brass ring bushing held so it is free to turn in a brass frame attached to the upper cast iron bracket. The position of the lower wave plate may be read on a circular scale by means of a pointer attached to the bushing. A circular brass plate P attached to the under side of the bushing carries adjustable stops S, and the plate may be rotated from one stop to the other while observing the swing of the pendulum (with a telescope placed in front of the apparatus) by means of cords running in grooves on the edge of the plate P. Frame, plate P, cords, stops, pointer and circular scale are visible at the top of Fig. 4.

The ideas underlying the wave plate arrangement, Fig. 3, may be qualitatively understood as follows. The light coming upward through the plates is reflected by the aluminum player on the top side of T, passing downward again through the plates. For a certain wave-length λ_0, B and T are quarter wave plates with their axes as shown at 90° to those of the hanging half-wave plate M. If light of wave-length λ_0 from the Nicol, plane polarized at $\theta=45°$, enters the bottom plate B, both direct and reflected beams will be circularly polarized in each space between the plates in the directions indicated by the

[8] I wish to thank Professor G. P. Harnwell for this and many other helpful suggestions concerning the mechanical and optical design of the apparatus.

curved arrows. Thus the angular momentum delivered per second to the half-wave plate M is almost four times what could be obtained by simply absorbing the same amount of circularly polarized light.

For wave-lengths λ different from λ_0 it will be seen that, because of the alternate advancing and retarding of each component with respect to the other, light in both direct and reflected beams is plane polarized at the initial angle θ at the bottom of B, the middle of M, and the top of T. If the plates vary somewhat from the exact specifications these levels of plane polarization will be correspondingly shifted. In general the light will be elliptically polarized in each space between the plates. Careful consideration shows that the angular momentum delivered to M is in the same sense as that for λ_0 for all wave-lengths λ for which

$$(n_y - n_x)_\lambda/\lambda < 2(n_y - n_x)_{\lambda_0}/\lambda_0$$

or, approximately, $\lambda > \lambda_0/2$.

If the lower plate B is rotated 90° from the position shown, the torque due to light of wave-length λ_0 will be just reversed. For this position the contributions to the torque of other wave-lengths is not easily considered qualitatively, but detailed calculation shows, as might be expected, that the integrated torque for all values of λ used is smaller in magnitude and opposite in direction compared to the torque similarly calculated for the position shown in Fig. 3. The torque is a continuous function of the position angle of the bottom plate, and its value can, with some labor, be calculated for each position.

The design wave-length λ_0 is determined on the basis of (3) by noting that A^2 is practically proportional to the energy in the light at each wave-length, and that λ enters as a factor. The energy distribution has a rather sharp peak in the region just above 1.0 μ for the tungsten filament temperatures to be considered. By a series of trial calculations $\lambda_0 = 1.2\ \mu$ was chosen to make the light torque a maximum.

The actual plates used, of course, vary somewhat from the ideal specifications. The most accurate plates obtained were made to within a few percent of the specified thickness by the Bryden Company of Waltham, Massachusetts, whom I wish to thank for this excellent cooperation. For the purposes of the exact calculations the plates were measured by means of a Babinet type compensator with sodium light. From the known values of the refractive indices of quartz[9] the retardation was then calculated for each plate for all wave-lengths contributing to the effect.

Besides almost quadrupling the torque compared to what would be obtained if the light were simply absorbed, and furthermore reducing heating, radiometer, and gas effects in the vacuum chamber, this plate arrangement greatly reduced difficulties due to radiation pressure. The disk M cannot be mounted exactly at right angles to the fiber axis, nor can the light be projected exactly in a vertical direction. Thus the resultant light pressure integrated over the disk will not be quite vertical and will produce a "light pressure torque" unless its line of action lies in a vertical plane containing the fiber axis. Without special precautions this torque might very easily mask the effect to be detected and measured.[10]

A tungsten filament light source was chosen, at a sacrifice of light intensity compared to an arc, in order to keep the resultant light pressure on the disk M as steady as possible, both in position and magnitude, and to give a steady and reproducible spectral energy distribution for purposes of calculation. The undesirable resultant light pressure on the disk M is decreased in the plate arrangement described, first, because most of the energy is allowed to pass through the disk and, secondly, because the pressure due to surface reflections and absorption for the upward beam is largely cancelled by the similar pressure for the beam reflected downward.

Finally, the moment arm for the residual light pressure can be varied by shifting the entire light beam parallel to itself. This is done by mounting the entire optical system up to $A-A$ in Fig. 1 on the double slide D, which in turn is supported in the lower of the two cast iron brackets I. The detail view, Fig. 4, shows the two micrometer screws by which the lateral

[9] *International Critical Tables*, VI, 341–342.

[10] Besides the smallness of the effect itself, the light pressure torque is perhaps the greatest difficulty in this experiment. I wish to thank Professor A. Kastler of the University of Bordeaux for a personal communication emphasizing this fact.

motion in two coordinates is produced. These are calibrated in thousandths of an inch so that any particular setting is easily repeated at a later time. By using this arrangement and leaving the lower wave plate B in a fixed position, the change in the sum of light torque, and light pressure, radiometer, and gas effect torque produced by a ten-percent change in filament current was measured for various settings of one of the double slide screws, the other being kept fixed. The results when plotted give a smooth curve crossing the zero torque line when the filament image lies across the middle of the window W as nearly as the eye can judge. This indicates that the spurious torques are probably of the nature anticipated and, in any event, can be held steady and made very small by appropriate setting of the double slide. In making the measurements of the light torque effect itself, the filament current was held constant to better than one percent, and the filament image was placed across the middle of the window. Care was also taken to use the same lengthwise portion of the filament in all cases.

The entire optical system can be rotated in its support on the double slide. Changes in the angle θ so produced are read on the circular scale visible in Fig. 4 on top of the double slide and below the Nicol housing N.

As described below, changes in the light torque effect corresponding to definite rotations of the bottom plate were measured and found to be reproducible for the same settings to within a few percent. When the bottom plate was removed, or when it was replaced by a fused quartz plate, rotation in the same manner produced no measurable effect. Hence it may be assumed that rotating the lower plate leaves the light energy, light pressure, heating, radiometer and gas effects sensibly unchanged. In other words, the apparatus used successfully eliminates the interfering effects, and enhances the light torque effect to be measured.

Measurements

The apparatus constructed according to the plan described showed the effect in the predicted direction and of about the predicted magnitude at the first trial on July 10, 1935. With this, the first aim, that of *detecting* the effect, was accomplished. The second aim, that of *measuring* the effect, was carried out by a resonance method (see reference 7). One of the first series of measurements taken is shown in Fig. 5, which illustrates both the definiteness of the effect observed and the kind of minor fluctuations encountered.

At the top of Fig. 5 are given the readings $a_\nu(\nu=0, 1, 2, \cdots)$ in centimeters on the scale (338 centimeters from the fiber axis) corresponding to the end points of the swing of the torsional pendulum. Tenths of millimeters on the scale could be estimated by means of the cross hairs in the telescope. The bottom plate B was in the position shown in Fig. 3 ($\theta=45°$, right stop R) while the readings a_0 to a_4 were being taken, but was turned 90° to the left (to $\theta=-45°$, to left stop L) at the instant at which the end point a_5 was read. The change in light torque produced by this rotation of B was such as to *oppose* the swing of the pendulum from a_5 to a_6. At a_6 the plate B was turned back to R, the torque change again opposing the ensuing swing from a_6 to a_7. The plate was turned similarly in "antiresonance" at a_7 and a_8 as indicated, but was then left in the position R when a_9, a_{10} and a_{11} were

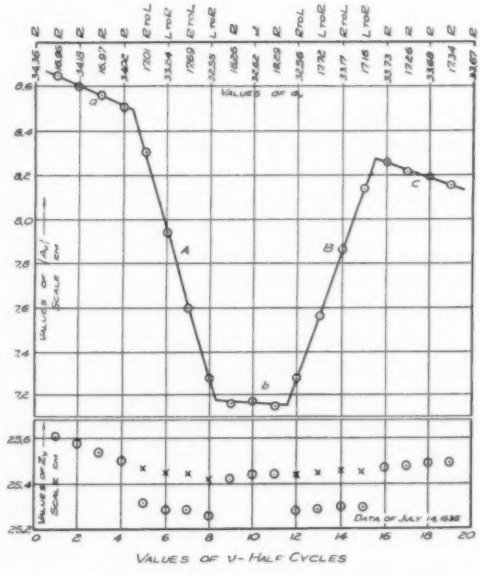

Fig. 5. Effect of light torque in resonance and out of resonance on the vibration amplitude of the torsion pendulum.

read. At a_{12} the plate was turned R to L, the change in torque now *aiding* the swing of the pendulum between a_{12} and a_{13}. At a_{13} the plate was turned L to R. This "resonance" turning was continued at a_{14} and a_{15}, and then the plate was again left in the position R for the drift readings a_{16} to a_{20}. For most of the readings taken another "antiresonance" series was added to the schedule described, and, for the readings taken by Mr. Harris, the "drift" periods were shortened while the "resonance" series in the middle of the schedule was lengthened to six half-cycles.

From the end-point readings taken according to such a schedule $4A_r = -a_{r-1} + 2a_r - a_{r+1}$ and $4Z_r = a_{r-1} + 2a_r + a_{r+1}$ were calculated. The absolute values of the "amplitudes" A_r are plotted in the upper part of Fig. 5 and the "zeros" Z_r (circles) in the lower part. For small values of damping (see "drift" slopes) the arithmetic means used differ by much less than the experimental error from the ideally correct geometric means for the quantities calculated.

From each such set of readings we wish to determine the value of the change in light torque on the hanging plate M when the bottom plate B is turned R to L or L to R. Since the torsional amplitude of the pendulum was at most a few degrees, we may assume that the light torque on M was a constant for a given position of the bottom plate B. We may consider a change in the position of the bottom plate to be equivalent to a change in the equilibrium position about which the torsional pendulum executes its oscillations. Let x be the corresponding change in scale reading. Careful consideration shows that, leaving damping out of account, the change in A_r per *cycle* must then be $2x$ during "resonance" or "antiresonance" sequences. With a small amount of damping, x is therefore very nearly equal to the average of the rates of change of A_r per *half-cycle* during "resonance" and "antiresonance." For example, in Fig. 5, the magnitudes of the slopes A and B, by least squares, are 0.341 and 0.289 centimeter per half-cycle, respectively. Hence $x = 0.315$ centimeter.

This method of taking readings and calculating affords several checks on the self-consistency of the sequence of readings a_r used to determine one value of x. For example, the damping slopes a, b, and c should be approximately equal to $(A-B)/2$ in magnitude. Furthermore $Z_r + x/2$ during the "resonance" and "antiresonance" intervals (plotted as crosses) should form a smooth sequence with the values of Z_r during the drift intervals. Slight disturbances, such as between a_9 and a_{10}, may be taken into account in evaluating these diagrams.

The quartz fibers were made in a gas-oxygen blast flame. Of those which seemed straight and uniform over a length of a foot or so, the *finest* (*small* K)[11] was taken. K for the first pendulum, with which the measurements of Fig. 5 were taken, was 8.52×10^{-6} dyne-cm/radian, or 1.26×10^{-8} dyne-cm/scale centimeter. Hence the change in light torque in Fig. 5 was 3.97×10^{-9} dyne-cm. This first fiber was accidentally broken and most of the measurements were taken with the second fiber for which K was 10.1×10^{-6} dyne-cm/radian or 1.50×10^{-8} dyne-cm/scale centimeter. The period in the latter case was about nine minutes, so that most of the determinations of x required consecutive observation of end-points for practically two hours. I made about 80 determinations during July, August and September, 1935, and Mr. Wilbur Harris made about 40 determinations during October, November and December, 1935, after I had left Princeton. Each of us worked in the absence of the other, and each made determinations of the three types to be described. Mr. Harris used a different bottom plate from the one

[11] With regard to the choice of the torsion constant K (in dyne-cemtimeters per radian) for the fiber, the following is of interest. During a "resonance" interval the amplitude (neglecting damping) increases by an amount $2Nx$ in N cycles. For a given torque change, x is inversely proportional to K. The number of cycles in a given time is directly proportional to $\sqrt{K}$, assuming the moment of inertia of the pendulum is a constant. Hence the change in amplitude $2Nx$ in *a given time* is inversely proportional to $\sqrt{K}$. In other words, the time required to achieve a given increase in amplitude by the resonance method varies directly as $\sqrt{K}$, other factors being constant. *Increasing* K in this experiment would therefore involve an increase in the time required for each measurement, a disadvantage which was not present in the corresponding case of the Einstein-de Haas experiment, in which the *impulse* per half cycle was independent of the length of the cycle. Nevertheless, Professor Einstein has pointed out that it would also be worth while in this experiment to *increase* K considerably, in spite of the increase in time required to achieve a given change in amplitude, because then the ratio of the energy in the effect desired to the energy of random disturbances would become much more favorable. Furthermore, it is an advantage to have the end-point readings a_r come at shorter intervals insofar as the possible segregation of the larger random disturbances is concerned.

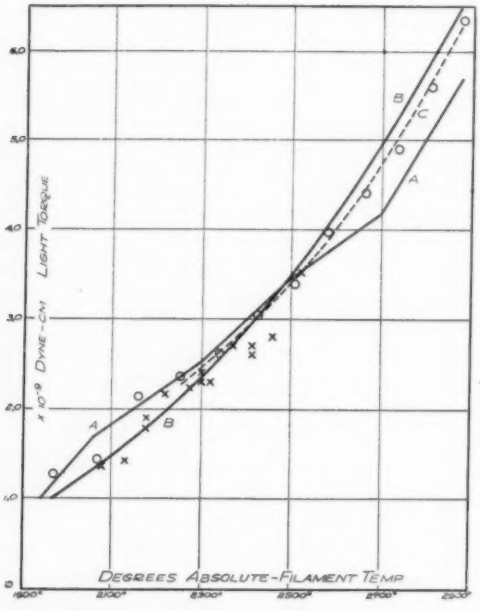

FIG. 6. Comparison of theory and experiment. Type I measurements: light torque as a function of filament temperature.

which I used, which seems to eliminate the possibility that the results, which were throughout consistent, could have been influenced by irregular patches of "infrared dirt" on the clear crystal quartz plates. Mr. Harris also investigated very thoroughly whether any effects were obtainable in the absence of the bottom plate, and found absolutely nothing. These checks were invaluable in substantiating the results of the present experiment, and Mr. Harris deserves much credit for the thoroughness and enthusiasm with which he carried out the tedious observations.

Three types of measurements, presented in Figs. 6, 8 and 9, were taken to show that the effect varies as required by the theory. The crosses represent my determinations and the circles those of Mr. Harris. Each point is derived from observations over a period of one and one-half to two hours as described in connection with Fig. 5. The smooth curves give the corresponding theoretical variation in each case.

For type I (Fig. 6) the torque change was measured for various filament temperatures as determined by the current through the lamp. The bottom plate was turned between stops at $\theta=45°$ and $\theta=-45°$, and the plane of polarization of the Nicol was at 45° to the axes of the plates as in Fig. 3. Mr. Harris' values (circles), taken consecutively, without shifting the position of the lamp, form the smoothest sequence obtained. The scattering of my values (crosses) taken with a different bottom plate is partly explained by the fact that I did not make these determinations consecutively, but shifted the lamp position a number of times for other readings. The total amount of light entering the plate system changes rather sharply with the position of the lamp in its socket and the setting of the double slide because of the presence of the small light shield d in the middle of the window W. The measurements previously reported[12] of this type, were made with a different lamp and fiber, and were made with a somewhat larger light shield on the window W. The values were therefore somewhat smaller than those shown in Fig. 6, but the magnitudes increased in a similar way with temperature.

The torque to be expected at various filament temperatures was calculated from (3) and the spectral energy distributions as follows. From the Poynting vector, the energy flow in the plate M is $A^2(n_x\cos^2\theta+n_y\sin^2\theta)c/8\pi$ or, practically, $A^2nc/8\pi=2\pi c(A/4\pi)^2n$ ergs/cm²-sec. Hence, if $J_\lambda' d\lambda$ is the total energy flow (integrated over the area of the plate) in M in the wave-length range λ to $\lambda+d\lambda$, the net torque on the plate from the energy flow in this wave-length range will be $L_\lambda' d\lambda$ dyne-centimeters, where

$$L_\lambda'=\sin 2\theta_\lambda'(\sin 2\Delta_1-\sin 2\Delta_2)\lambda J_\lambda'/2\pi c.$$

Here $\tan\theta_\lambda'$ is, in general, the ratio of the amplitudes of the components of the light in the directions of the axes of the plates T and M. $\theta_\lambda'=\theta$ only when the position of the bottom plate B is such that the directions of its axes coincide with those for M and T. If the total energy flow entering the plate system in this wave-length range is $J_\lambda d\lambda$ ergs/sec., we set $J_\lambda'=J_\lambda F_{\lambda\eta}$ for each of the light beams contributing to the effect (enumerated by the index η), and compute $F_{\lambda\eta}$ using Edison Pettit's values for the reflectivity of aluminum (top surface of T)[13] and the re-

[12] R. A. Beth, Phys. Rev. **48**, 471 (1935).
[13] Edison Pettit, Pub. Astronom. Soc. Pacific **46**, 27 (1934).

fractive indices of quartz, which enter into Fresnel's expressions for the transmitted and reflected intensities at the plate surfaces. The absorption in the quartz plates may be neglected because the light has been filtered through the fused quartz lens L and the calcite and Canada balsam of the Nicol prism. From the theory for elliptically polarized light, the angles θ_λ' and the phases 2Δ may be calculated for each beam and each wave-length and for any position of the bottom plate, because the incoming light from the Nicol is plane-polarized, and the plate thicknesses, as measured by the compensator in wave plates for sodium light, were: $T=0.649$, $M=1.051$, $B_1=0.535$ (my torque measurements), $B_2=0.454$ (Harris' torque measurements). The whole torque on M is then

$$L=\int L_\lambda J_\lambda d\lambda \text{ dyne-centimeters,} \qquad (8)$$

where the torque factors L_λ are given by

$$L_\lambda=\sum_\eta \lambda F_{\lambda\eta}\{\sin 2\theta_\lambda'(\sin 2\Delta_1-\sin 2\Delta_2)\}_{\lambda\eta}/2\pi c \text{ seconds.} \qquad (9)$$

The torque factors L_λ were calculated for the sum η of the effects of the main beam going upward through M, the main beam reflected downward from the aluminized top surface of T, and for the reflections of these beams at the surfaces of B, W, M, and T, repeated surface reflections being neglected. These values of (9) are shown in Fig. 7, the angles denoting the azimuthal position of the bottom plate; at 45° the direction of the "fast" axis of B coincides with the direction of the "slow" axis of M and the "fast" axis of T (see Fig. 3). The full curve refers to the calculations for B_2, the dotted curve to those for B_1.

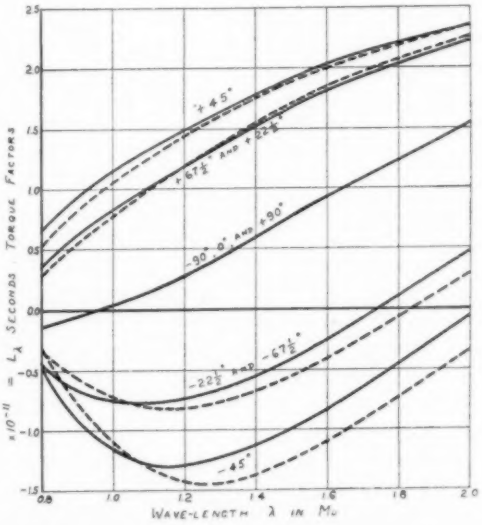

FIG. 7. Torque factor as a function of wave-length.

Using a rocksalt spectrometer and thermocouple arrangement Mr. Harris compared the amount of radiation from a black body at a known temperature (radiation from the interior of a furnace made out of an alundum cylinder $2\frac{1}{2}$ inches in diameter and a foot long at 766°C and 784°C was used) with the amount of radiation coming through the Nicol in the same solid angle at intervals of 0.1 μ for each of six different lamp currents. The energy factors J_λ were computed in absolute terms from these measurements using calculated values of black body radiation, Lambert's law, and constants of the optical system to determine the solid angle of the cone of light entering the plate system from the Nicol.

Replacing the integral in (8) by the corresponding sum for 0.1 μ intervals from 1.0 μ to 2.0 μ inclusive, the change in total torque from $\theta=45°$ to $\theta=-45°$ for each of the six filament currents and for the bottom plate B_2 was obtained. These theoretical torque values are plotted against the temperatures, 1948°, 2069°, 2297°, 2506°, 2701° and 2879° absolute, corresponding to the filament currents used, in Fig. 6 and connected by straight lines A. The irregularity of this broken line A indicates the difficulties encountered in making the energy determinations. The principal sources of error are: The spectrometer was not set up especially for this purpose, but was originally designed for somewhat longer wave-lengths; the solid angle of the light cone is difficult to determine with accuracy; the neglected effect below 1.0 μ is probably not exactly compensated by assuming that the Nicol actually polarizes all the light out to 2.0 μ. There is reason to believe, from the energy measurements themselves, that the energies computed for the upper two temperatures are somewhat too low. The root-mean-square deviation of the measured torques (circles) from

the computed values A is 0.29×10^{-9} dyne-centimeter.

A second attempt was made to get the values of the energy factors J_λ in absolute terms by extrapolating the tungsten emissivities given by Forsythe and Worthing[14] (assuming the emissivity to be a linear function of temperature at each wave-length), multiplying by the black body radiation at the temperature of the filament, taking account of the solid angle of radiation collected from each point on the filament by the lens L, and making an allowance for the reflections from the surfaces of the bulb of the lamp, the lens, and the Nicol prism. The change in torque at each temperature was calculated from (8) as before, the integral in this case being replaced by the corresponding sum for $0.2\ \mu$ intervals from $0.8\ \mu$ to $2.0\ \mu$ inclusive. The results must be reduced by about 15 percent to give the curve B in Fig. 6. This 15 percent may be caused by the absorption of the Canada balsam in the Nicol, by nonpolarization of the light near $2.0\ \mu$, and by inaccuracies in the emissivities used. The root-mean-square deviation of the circles from the curve B *as drawn* is 0.24×10^{-9} dyne-centimeter. It should be emphasized that the uncertainties in B leave the *absolute value* in considerably greater doubt than in the case of A.

An important conclusion from Fig. 6 is, however, that the *slope* and *shape* of the theoretically determined curves A and B agrees within the limits of error with the trend of the measured torque values. The trend of B relative to the torque values (measured for certain lamp *currents*) depends on the current-temperature calibration of the lamp which was extrapolated from one value at 2941° absolute by comparison with the calibration for a similar lamp, while the trend of A relative to the torque values measured does not depend on this calibration, the energy distributions having been measured for given lamp *currents* also. The dotted smooth curve C, empirically fitted to the upper nine of Harris' torque measurements, appears as a natural compromise between the trends of A and B. Half of the circles lie within one percent of this curve. Their root-mean-square deviation from the curve is 0.054×10^{-9} dyne-centimeter.

[14] Forsythe and Worthing, Astrophys. J. **61**, 151 (1925).

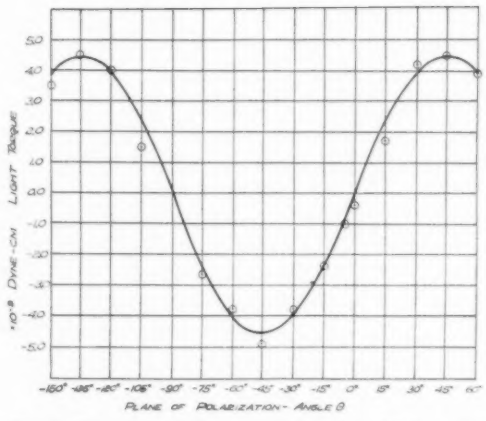

FIG. 8. Type II measurements: variation of light torque with angle between plane of polarization of light and the axes of the plates.

If we choose to think of C as an empirical calibration curve, this indicates that we may determine the temperature of the lamp in this range with a probable error of about 7° by measuring the torque with the accuracy attained by Mr. Harris, the lamp position being left unchanged.

The type I measurements may be regarded as a test of the factors $\lambda J_\lambda/2\pi c$ in the calculation of the torque from (8) and (9).

For the type II measurements (Fig. 8) the lamp current, and therefore the light intensity, was maintained constant and the plate B_2 was rotated between the same stops as in type I, but the plane of polarization of the light was rotated to various angles θ with the axes of the plates. These measurements are intended to test the factor $\sin 2\theta$ in the formula for the torque. The root-mean-square deviation of the measured values from the computed sine curve shown is 0.34×10^{-9} dyne-centimeter. A small systematic deviation from the sine curve may be due to the difficulty encountered in lining up the plate axes accurately in setting up the apparatus. In setting the angle θ the whole lamp housing and optical system, including the Nicol, was rotated and the double slide reset as described. Because of the presence of the light shield d this causes a greater scattering of the measurements than would be obtained if the lamp could be left fixed in position.

The measurements shown were made by Mr. Harris. In my measurements of this type only a

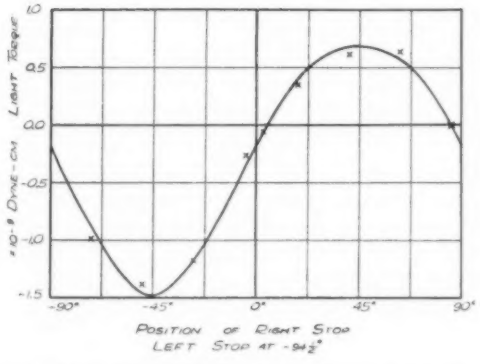

FIG. 9. Type III measurements: light torque as a function of position of the right stop.

quarter cycle of a sine curve was covered, but at 15° intervals. These points also form a smooth segment of a sine curve; though the root-mean-square deviation is considerably less, the test is not as critical and the result not as interesting as the full cycle curve shown.

For the type III measurements (Fig. 9) the light intensity was again maintained constant and the plane of polarization of the optical system was again put at 45° to the directions of the axes of plates M and T as in type I. The left stop was fixed at $-94\frac{1}{2}°$ and measurements made for different positions of the right stop. Since the torque for B_1 at the left stop was constant, the curve shows how the light torque in this plate system varies with the position of the bottom plate. The elliptical polarization produced by the bottom plate depends on its position, and these measurements are, therefore, in the main a test of the phase factors $(\sin 2\Delta_1 - \sin 2\Delta_2)$ in the formula. From the torque factors of Fig. 7 the smooth curve shown in Fig. 9 was calculated from the energy distribution. The root-mean-square deviation of the measured values of the torque from this curve is 0.073×10^{-9} dyne-centimeter. This very good agreement is again to be expected because the lamp position was left fixed. Mr. Harris also made measurements of this type, but did not cover a whole cycle. They are in similar agreement with the predicted values.

CONCLUSION

The change in the angular momentum of polarized light in passing through a crystal plate has been detected and measured with the apparatus described. This conclusion rests on the fact that the measured effect agrees in sign and, within the limits of error, in magnitude with the effect as predicted both by the wave and by the quantum theories of light. In particular it has been shown that the effect varies as required by the theory with each of three experimental variables studied: filament temperature (light intensity), azimuth of the plane of polarization, and position of the bottom plate.

I am deeply indebted to Professor A. W. Duff of the Worcester Polytechnic Institute who first suggested this problem to me and who personally helped me with the purchase of apparatus in the preliminary stages of the investigation. I wish to thank the National Research Council for a Grant-in-Aid for the purchase of apparatus and the Palmer Physical Laboratory of Princeton for providing all the specially made apparatus and technical assistance as well as for the hospitality of the Laboratory. In particular I wish also to thank Professors Harnwell, Einstein, Condon, Robertson, Shenstone, Bleakney, and Dr. Barnes of Princeton for their willing helpfulness in discussing the work with me on numerous occasions. Dr. S. N. Van Voorhis and Messrs. C. W. Curtis and C. W. Lampson of Princeton helped me both with suggestions about experimental details and in actually taking readings. Mr. Curtis shared the work of taking readings with me for many weeks. The very valuable part of the work done by Mr. W. Harris has been noted in detail above. Finally, I want to thank Mr. A. H. S. Holbourn of the Clarendon Laboratory, Oxford, for his interesting correspondence with me about the problem.

The Paschen-Back Effect of Hyperfine Structure

III. Separation of Hg_{199}

J. B. GREEN, *Mendenhall Laboratory of Physics*

(Received May 15, 1936)

It has been possible, by a judicious choice of field strength to separate the magnetic components due to the 199 isotope of mercury. Five lines have been studied, $\lambda\lambda 3125(^3P_1\,^3D_2)$, 5461, 4358, $4047(^3P\,^3S)$. A practically complete Paschen-Back effect is observed, each ordinary Zeeman component being accompanied by two satellites due to the nuclear spin $i=\frac{1}{2}$ of Hg_{199}. There is excellent agreement between the theory and experiment even to the slight asymmetries observed. Some comments on the recent work at the French Academy express doubt of the reality of their findings.

THE hyperfine structure of the mercury lines has been studied by numerous investigators, particularly Schüler and his collaborators.[1] They have been able to show that the very strong principal component (which is complex under very high resolution) can be attributed to the even isotopes of mercury, while the weaker satellites are due to the two odd isotopes, 199 and 201. A careful analysis seems to prove that the complexity of satellites can be correctly accounted for if we assign a nuclear spin of $\frac{1}{2}$ to the 199 isotope and a nuclear spin of $3/2$ to the 201 isotope.

The effect of the application of an external magnetic field to a line showing hyperfine structure is to increase greatly the complexity of the pattern, each line giving its Zeeman pattern to the total; but as the field increases, and finally becomes very strong, certain simplifications occur which may be described briefly as follows.[2]

For very strong magnetic fields the energies of the various levels may be represented by $(A \ll \omega)$

$$W = m_j g\omega + A m_i m_j, \tag{1}$$

the first term on the right side of the equation being the ordinary Zeeman level without hyperfine structure and the second term due to the hyperfine structure. This means that instead of each single Zeeman level there will be $2i+1$ levels (corresponding to the $2i+1$ values of m_i) separated by amounts proportional to Am_j, and the lines due to transitions between these levels will be given by

$$W_1 - W_2 = \omega(m_{j_1} g_1 - m_{j_2} g_2) + (A_1 m_{j_1} - A_2 m_{j_2}) m_i \tag{2}$$

with selection rules $m_{j_1} = m_{j_2} \pm 1$ or $m_{j_1} = m_{j_2}$ and $\Delta m_i = 0$. The first term gives the position of the ordinary Zeeman component, and the second term shows that instead of this one component, there will be $2i+1$ components separated by amounts

$$A_1 m_{j_1} - A_2 m_{j_2}.$$

Thus, in the case of an element containing only one isotope, the Paschen-Back effect of hyperfine structure gives an immediate means of determining i, the nuclear spin, provided A is large enough to allow the resolution of the separate components. This was the case for Tl and Bi where one isotope predominates. But in the case of Hg, where we have a large number of isotopes each with its own nuclear spin, it is not so easy to separate the components belonging to each of them. Whereas in Tl, where $i=\frac{1}{2}$, each of the ordinary Zeeman components yielded $2i+1$ or 2 components; in Hg, we should find the ordinary Zeeman components due to the even isotopes, 2 components due to isotope 199, and 4 components due to isotope 201.

But the hyperfine structure constants A of Hg_{201} are much smaller than those of Hg_{199} and the four components of each line of Hg_{201} are therefore crowded together and practically unresolvable by the grating, and should merge with the lines due to the even isotopes, whose isotopic

[1] See Schüler and Jones, Zeits. f. Physik **77**, 801 (1932) for a complete list of references.

[2] For a complete account, see Green and Wulff, Zeits. f. Physik **71**, 593 (1931).

Fig. 1. HgI $^3S_1$ $^3P_2$ II order.

Fig. 2. HgI $^3S_1$ $^3P_1$ II order.

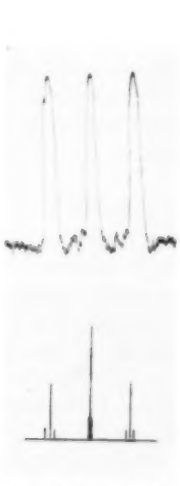

Fig. 3. HgI $^3S_1$ $^3P_0$ II order.

FIG. 4. HgI $^3P_1$ $^3D_2$ III order.

displacements are also extremely small, and should appear as one line. The pattern to be expected is therefore the ordinary Zeeman pattern, but each line accompanied by a satellite on each side, due to isotope 199.

An examination of Eqs. (1) and (2) shows that while the first term is proportional to the field strength, the second term depends only on the hyperfine structure constant. To be sure, this is true only when $A \ll \omega$, but experimentally, the condition is reached for comparatively low field strengths. The picture will then appear, as we increase the field strength, of a group of lines whose separations increase proportionally with the field strength (the ordinary Zeeman components) each accompanied by two satellites whose separation remains almost constant. Thus, unless the field strength is properly chosen, the satellites of one particular line may actually be beyond one of the other lines of the pattern. Furthermore, the satellites are quite faint in comparison with the principal lines, so that the latter must be very strongly overexposed in order to bring out the weaker satellites. This always involves the difficulty that in developing, the overexposed images tend to spread and unless the faint satellites are well-separated from the principal lines, they will be lost in the background. It is therefore necessary to choose a field-strength and lines with such values of the hyperfine structure constant A, that the satellites fall about midway between the main Zeeman components. This is not possible, of course, for all of the components and all of the satellites simultaneously, but the conditions have been fulfilled in a sufficiently large number of cases to make the results worth reporting.

A field strength of about 36,000 gauss was used, ($\omega = 1.70$ cm^{-1}) and the ^3S ^3P triplet ($\lambda\lambda$5461, 4358, 4047) was studied, as well as $^3P_1$ $^3D_2$ (λ3125) which is particularly interesting because of the fact that the $^3D_2$ has a negative hyperfine structure constant.[3]

The results are shown pictorially in Figs. 1 to 4. The upper half of each figure is a microphotogram of the line, and below is the pattern as calculated from the exact formulas of Goudsmit and Bacher.[4] The exact calculations show asymmetries not mentioned in the discussion above, and these asymmetries are apparent on both the observed and calculated pictures shown in the figures. That the principal lines are all overexposed is shown by the fact that all the principal

[3] The apparatus and method used have been described by Green and Loring, Phys. Rev. **46**, 888 (1934).

[4] Goudsmit and Bacher, Zeits. f. Physik **66**, 13 (1930).

peaks are of the same height except for the weakest lines of the patterns. The satellites appear on the microphotograms as subsidiary peaks where they are well-resolved and as points of inflection where the resolution is not very good. Of course, all the satellites do not appear. Some of them are too close for the resolving power available.

The Zeeman effect of the Hg lines is being studied in detail at the French Academy of Sciences[5] using their large magnet which provides fields up to about 60,000 gauss. Certain irregularities seem to show up, but there is a doubt in the author's mind of the reality of these, principally because of the effect of the unresolved h.f.s. components. If, for example, we label the principal components of λ4358 with the numbers 1 to 6, the components 2 and 5 separate proportionally with the field strength, while 1 and 6 seem to separate more rapidly. This would seem to indicate that something was affecting $^3S_1$ but not $^3P_1$. The same sort of thing happens with λ5461, indicating perhaps a similar cause for the behavior of $^3P_2$. The meagerness of the report makes it very difficult to comment upon, but in view of all of the work done on h.f.s., it would seem that any discussion of the peculiar behavior of the Zeeman components of a line cannot entirely neglect the effects of the Paschen-Back effect of the h.f.s. components, which tend to spoil any effect that concerns itself only with the linearity of position and field-strength.

In conclusion, the author wishes to express his thanks to Professor R. A. Loring, of the University of Louisville, for his assistance in part of the experimental work connected with this paper.

[5] Dupouy and Jacquinot, Comptes rendus **201**, 543 (1935). Jacquinot and Belling, ibid. **201**, 778 (1935).

JULY 15, 1936 PHYSICAL REVIEW VOLUME 50

The Diffusion and Absorption of Neutrons in Paraffin Spheres*

DON M. YOST AND ROSCOE G. DICKINSON, *Gates Chemical Laboratory and Kellogg Radiation Laboratory, California Institute of Technology*

(Received May 11, 1936)

Measurements are described of the activities imparted to silver and to indium detectors placed in paraffin spheres of various sizes with a radon-beryllium source of neutrons located at the center. The results are discussed with the aid of diffusion theory. Reasonably good quantitative agreement is obtained at distances from the source greater than about 8 cm. Various independent estimates are made of the mean free path of the neutrons in paraffin, their specific absorption rate constant, and the ratio of the latter to the diffusion constant. The mean free path is found as 0.53 cm; the ratio of the specific absorption rate constant to the diffusion constant as 0.026 cm^{-2}.

FOLLOWING the discovery of Fermi[1] and his co-workers that hydrogen containing substances are effective in slowing down the neutrons from a radon-beryllium source, several investigators have made experiments to determine the velocities of the slow neutrons produced. The results of various experimenters[1, 2, 3] have shown that the velocities are comparable with thermal velocities. Dunning[4] and others, by means of a velocity filter, found that the neutrons slowed down by paraffin had a velocity distribution at room temperature substantially that predicted by Maxwell's law. These results suggested that, under definite and simple geometrical conditions, the behavior of slow neutrons in paraffin might be more closely studied from the point of view of diffusion. The method of experimentation adopted consisted in deter-

* Contribution No. 545.

[1] Fermi, d'Agostino, Rasetti and Segrè, Proc. Roy. Soc. **A146**, 483 (1934); Amaldi, d'Agostino, Fermi, Pontecorvo, Rasetti and Segrè, Proc. Roy. Soc. **A149**, 522 (1935).

[2] Westcott and Bjerge, Proc. Camb. Phil. Soc. **31**, 145 (1935); Westcott and Niewodniczański, Proc. Camb. Phil. Soc. **31**, 617 (1935); Bjerge and Westcott, Proc. Roy. Soc. **A150**, 709 (1935).

[3] Moon and Tillman, Nature **135**, 904 (1935).

[4] Dunning, Pegram, Fink, D. P. Mitchell and Segrè, Phys. Rev. **48**, 704 (1935); Fink, Dunning, Pegram, and Mitchell, Phys. Rev. **49**, 103 (1936).

mining the activity produced in indium and silver detectors placed inside paraffin spheres of different diameters at measured distances from a source located at the center.

Experimental Procedure

Four paraffin spheres were used; their diameters were 20, 25, 35, and 51 cm, respectively. The smaller ones were spherical to within two or three millimeters and the largest to within five millimeters. A cylindrical hole, 7 cm in diameter, was bored radially to the center of each sphere, and fitting easily into this hole was a stack of paraffin cakes. The two larger surfaces of each cake was so curved that a thin flexible detector placed between any two cakes would have all points on its surface equidistant from the source located at center of the sphere.

The detectors were thin, circular disks of silver and indium with several small sectors cut out in order to make them conformable to the curved surfaces of the paraffin cakes. The thickness of the indium detector was 0.005 cm and that of the silver 0.02 cm. The spheres and detectors are shown in Fig. 1.

A 3-mm×5-mm cylindrical brass capsule containing powdered beryllium and radon (300 millicuries or less) served as the source of neutrons.

In an experiment the detector used was left in some one position for a time sufficient for the activity to become practically saturated (7 to 12 half-lives). The activity was measured with a quartz fiber electroscope. Readings were begun at a fixed time (Ag, 30 sec.; In, 60 sec.) after removal of the detector from the sphere and were continued at suitable intervals for a definite period of time (Ag, 6 min.; In, 15 min). The total reading for the period, after correcting for nonlinearity of scale, for background, and for radon decay, was taken as the activity, β, for that experiment.

The half-lives of the two activities of silver were determined with the electroscope used and were found to be 23.5 sec. and 2.15 min., respectively.

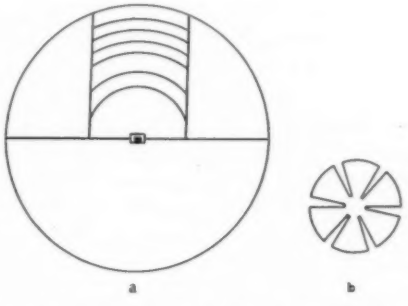

Fig. 1. (a) Cross section of the 10-cm paraffin sphere showing arrangement of the cakes between which the detector was placed. (b) The detector drawn to the same scale.

Results of the Experiments

The results of the experiments are shown graphically in Figs. 2 and 3 where βr is plotted against r the distance of the detector from the center of the sphere in cm. Because of the strong activity and relatively long half-life of indium the best accuracy was obtained with it as the detector.

Discussion of the Results

If it is assumed that the neutrons diffuse through the paraffin according to the ordinary diffusion laws, and that the absorption by the thin detector does not cause appreciable disturbances, and further that the neutrons are absorbed in the paraffin at a rate, ac, proportional to the concentration, then

$$D\nabla^2 c - ac = \partial c/\partial t$$

where D is the constant diffusion coefficient and a is the specific absorption rate constant. Under the steady state conditions of the experiments $\partial c/\partial t = 0$. The equation becomes then

$$D\nabla^2 c - ac = 0. \qquad (1)$$

The general solution, for the present case of spherical symmetry, may be written in either of the forms

$$cr = (A/\alpha)\sinh \alpha r + Be^{-\alpha r}$$

$$= B \sinh \alpha(r+k_1)/\sinh \alpha k_1; \quad \alpha^2 = a/D. \qquad (2)$$

A, B and k_1, are constants of integration and are related to each other by the equation

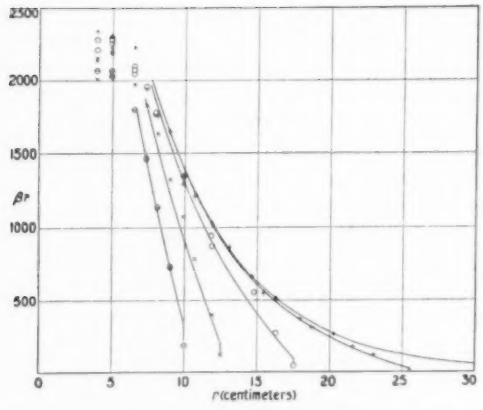

FIG. 2. Plots of βr *vs.* r for the indium detector in spheres of radii 10, 12.5, 17.55, and 25.55 cm, respectively, from left to right. The curves for the spheres of various radii were drawn using Eq. (5). The top curve is for a sphere of infinite radius.

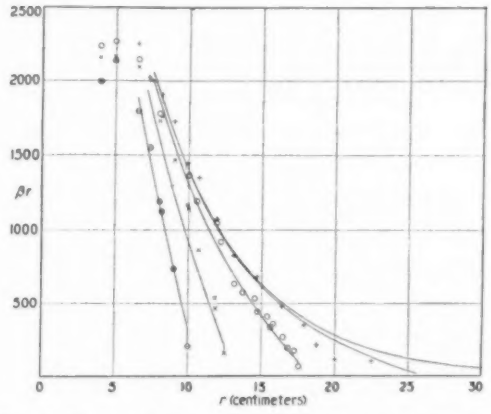

FIG. 3. Plots of βr *vs.* r for the silver detector. The solid curves are identical with those of Fig. 2.

$A=\alpha B/\sinh \alpha k_1$. B is directly proportional to the strength of the source when the source is placed at the center of the sphere. In case $a=0$, $cr=Ar+B$.

There are two particular solutions contained in (2) which will be required later, namely,

$$cr=Be^{-ar} \tag{3}$$

when the source is central and the sphere is of infinite radius, and

$$cr=(A'/\alpha)\sinh \alpha r \tag{4}$$

when the source is uniformly distributed over the surface of a finite sphere.

In order to relate the concentrations in one sphere with a central source to those in a sphere of different radius a boundary condition may be introduced as follows. The net outward flux of neutrons across a spherical surface just inside the paraffin is equal to the rate of escape of neutrons from the surface. The first quantity is equal to $-4\pi r^2 D\partial c/\partial r$; if the rate of "evaporation" of the neutrons per unit area be assumed proportional to the concentration prevailing a short distance under the surface, then

$$-D(\partial c/\partial r)_{r=r_0}=k_2 c_{r=r_0},$$

where r_0 is the radius of the sphere. The use of this boundary condition leads to the particular solution

$$cr=B\sinh \alpha(r+l-r_0)/\sinh \alpha(l-r_0), \tag{5}$$

where $l=(1/\alpha)\sinh^{-1}[\alpha/\{(1/r_0-k_2/D)^2-\alpha^2\}^{\frac{1}{2}}]$.

The equations derived involve the concentration of neutrons, while the measured quantity is β, the activity of a detector. The number of neutrons per unit time entering the detector will depend on both the concentration in its neighborhood and the velocity distribution; of the neutrons entering, the fraction captured by the detector may again depend on the velocity distribution.[5] Proportionality between β and c may safely be expected, then, only in regions of constant velocity distribution; this doubtless excludes regions close to the central source. Moreover, in regions where the velocity distribution is not constant it is not likely that D, a, and k_2 remain constant as assumed in Eqs. (1) to (5). However, in order to see to what extent the observations are in harmony with the hypothesis, we have assumed Eqs. (1) to (5) and have placed $\beta=k'c$, with k' constant for a given detector. Similarly, with the detector placed on the surface of a sphere the activity β_0 is assumed proportional to f_0, the flux of neutrons from the surface: $\beta_0=k_0' f_0$. If one assumes that the capture cross section of indium or silver is a constant, and further that the velocity distribution of the neutrons is Maxwellian, then it may easily be

[5] For recent experiments and theory on absorption see Rasetti, Segrè, Fink, Dunning and Pegram, Phys. Rev. **49**, 104 (1936). Breit and Wigner, Phys. Rev. **49**, 519 (1936).

TABLE I. *Total fluxes measured by indium.*

SPHERE RADIUS, r_0	ACTIVITY, β_0 (Mean)	FLUX, $r_0^2\beta_0$
10.0	18.7	1870
12.5	9.83	1540
17.55	2.61	800
25.55	0.53	340

shown that $k'=bn\sigma(2kT/\pi m)^{\frac{1}{2}}$ and $k_0'=bn\sigma$ where n is the number of nuclei per cm² in the detector and b is an instrument constant. If, on the other hand, the capture cross section $\sigma=\sigma_0/v$, then $k'=bn\sigma_0/2$ and $k_0'=(bn/2)(\pi m/2kT)^{\frac{1}{2}}$. In either case $k'/k_0'=(2kT/\pi m)^{\frac{1}{2}}$.

There appears to be some justification for the assumption of constancy of k' in the fact that the curves for silver and indium are superposable throughout. Silver and indium are known to be activated by neutrons of different qualities.[6] Also the ratio of the 23.5-sec. activity of silver to the 2.15-min. activity remains substantially constant. It does not follow, but it does appear possible that the neutrons which cause activation are all at the same "temperature," and, from Dunning's velocity filter experiments, the temperature corresponds to that of the paraffin. It is recognized, of course, that in the region near the source the velocity distribution is presumably not Maxwellian.

On the assumption that k', D and a are constants, independent of r, it may be immediately concluded that, since the values for βr do not fall on a straight line, some absorption of the neutrons in the paraffin occurs. Moreover, since the total outward flux, $r_0^2\beta_0$, as measured by detectors placed on the surfaces of the spheres, decreases with increasing radius of the spheres it follows that absorption takes place in the paraffin if k_0' remains constant after the neutrons have traversed 10 cm or more of paraffin. The total fluxes are presented in Table I.

In order to compare the predictions of the theory with the observations in the region $r \gtrless 8$ cm, the following procedure was used. Eq. (2) was fitted to a smoothed curve drawn through the points for the 51-cm sphere. A satisfactory fit was obtained with 0.16 cm^{-1} as the value for α. Eq. (5) was then used to construct the predicted curves for the other spheres. The agreement with the observations may be seen in Figs. 2 and 3. It is satisfactory for all but the 25-cm sphere where the deviations are somewhat greater than the experimental error. Evidently then, had independent values of α been conversely calculated from the relative activities near the surfaces of the various spheres, substantially the same value of α as before would have been obtained.

A value for α may be obtained in still another manner as follows. At a given distance r from the center, the activity produced in a detector increases with the radius r_0 of the sphere. The increase must be due to neutrons which have been at larger distances and then diffused back to r. The difference in the activity (times r) at r for two different spheres of radii r_0 and r_0' will evidently be

$$\Delta=\beta' r-\beta r=\frac{A''(r_0')-A''(r_0)}{\alpha}\sinh \alpha r$$

and
$$(1/\Delta)(d\Delta/dr)=\alpha \coth \alpha r. \qquad (6)$$

Application of relation (6) to the observations yielded an average value of 0.23 for α. This is appreciably higher than the value given above, but the errors involved are also considerably greater. For the present it can only be said that the two results are quite closely of the same order of magnitude.

An estimate of the value of a was made in the following manner. The total rate of absorption of neutrons in a sphere is equal to $\int_0^{r_0}4\pi r^2 a c dr$; and the total flux of neutrons from the sphere equal to $4\pi r_0^2 f_0$. The sum of these is equal to the rate of issue of neutrons from the source, so that for two experiments with equal sources but different spheres of radii r_0 and r_0' the sums are equal. Assuming a constant

$$a=\frac{r_0'^2 f_0'-r_0^2 f_0}{\int_0^{r_0} r^2 c dr-\int_0^{r_0'} r^2 c' dr}$$

$$=\frac{r_0'^2\beta_0'-r_0^2\beta_0}{\int_0^{r_0} r^2\beta dr-\int_0^{r_0'} r^2\beta' dr}\,\frac{k'}{k_0'}.$$

The last member also assumes constancy of k_0' and k'. At first sight these assumptions seem especially objectionable since the integrations extend from the origin; however, at the smaller

[6] C. H. Collie, Nature **137**, 614 (1936).

TABLE II. *Mean free path of neutrons in paraffin from indium measurements.*

r_0(cm)	β_0	$-(\partial\beta/\partial r)$	λ(cm)
10.0	18.7	48.9	0.58
12.5	9.83	26.9	0.55
17.55	2.61	8.3	0.47
25.55	0.53	1.5	0.53
		Mean	0.53 cm

r's, β and β' do not greatly differ, and the contribution to the denominator of distances under 6 or 7 cm is at most only a few percent. From graphical evaluation of the integrals, values of a of from 0.99 to $1.22\times10^{-2}k'/k_0'$ with a mean of $1.13\times10^{-2}k'/k_0'$ were obtained. With k'/k_0' equal to that for a Maxwellian distribution of 295°K, a becomes $1.41\times10^3\pm0.08$ sec.$^{-1}$.

Finally, from a consideration of the behavior of the neutrons at and near the surface of a sphere, a value of their mean free path λ and the diffusion coefficient, $D=\frac{1}{3}(8kT/\pi m_n)^{\frac{1}{2}}$, may be calculated. By kinetic theory considerations it may be shown that the net flux, in the direction of increasing r, of neutrons through unit area of a detector placed normal to the concentration gradient $\partial c/\partial r$ is $-\frac{1}{3}\lambda v\partial c/\partial r$, where v is the mean velocity; similarly the gross flux is $\frac{1}{2}cv$. The net flux is measured by a detector placed on the surface of the sphere and the gross flux by a detector just inside the surface. From this it can readily be shown that

$$\lambda=-(3/2)\beta_0/(\partial\beta/\partial r),$$

where the derivative is taken a short distance inside the surface. The values of λ obtained for the several spheres are given in Table II. The fact that λ is about the same for all spheres does not necessarily imply a constancy of the temperature of the slow neutrons. On the assumption that $T=295°$, $D=4.4\times10^4$.

From the independently determined values of a and D, a value of $\alpha=(a/D)^{\frac{1}{2}}=0.18$ cm^{-1} was calculated which is in very good agreement with the value 0.16 cm^{-1} found above.

The measurements also permit calculations of cross sections for scattering, and cross sections for capture.[7] That for scattering, σ_s, may be obtained from the mean free path through the relation $\sigma_s=\frac{3}{4}N\lambda$ where N is the number of scattering nuclei per unit volume. If hydrogen alone be assumed to scatter, then $\sigma_s=18\times10^{-24}$ cm^2. If, however, a scattering cross section of 4×10^{-24} be allowed for carbon,[8] that for hydrogen becomes 16×10^{-24}. The cross section for absorption may be obtained from the specific absorption rate constant through the relation $\sigma_c=(a/N)(\pi m_n/8kT)^{\frac{1}{2}}$ where m_n is the mass of the neutron. The results of Fleischmann[9] and of Kikuchi, Husimi and Aoki[10] indicate that protons are mainly responsible for capture in paraffin. On the assumption of capture by hydrogen alone, our value of a leads to $\sigma_c=7.3\times10^{-26}$ cm^2; Kikuchi obtained 3.0 to 8.3×10^{-26} cm^2. If we take $\sigma_c=\sigma_0/v$ then $\sigma_0=a/N$, independently of any assumed temperature. The value calculated becomes $\sigma_0=1.8\times10^{-20}$ cm^2 sec.$^{-1}$, and this would be the cross section for neutrons of unit velocity. These values for σ_c and σ_0 are presumably lower limits.

The writers are indebted to Professor C. C. Lauritsen for helpful suggestions and the use of an electroscope, and to Mr. J. E. Walstrom for assistance in the preparation of the neutron sources.

[7] It has been emphasized by A. C. G. Mitchell that, in most cases, absorption and scattering cross sections have not been separated. Mitchell, Murphy and Langer, Phys. Rev. **49**, 400 (1936).

[8] Dunning, Pegram, Fink and D. P. Mitchell, Phys. Rev. **48**, 265 (1935). Dana P. Mitchell, Phys. Rev. **49**, 453 (1936). A. C. G. Mitchell, Murphy and Langer, Phys. Rev. **49**, 400 (1936).

[9] Fleischmann, Zeits. f. Physik **97**, 242 (1935).

[10] Kikuchi, Husimi and Aoki, Proc. Phys. Math. Soc. Japan **18**, 35 (1936); Nature **137**, 30 (1936).

Scattering of Slow Neutrons. II

ALLAN C. G. MITCHELL, EDGAR J. MURPHY AND MARTIN D. WHITAKER, *Department of Physics, New York University, University Heights*

(Received May 25, 1936)

The scattering of slow neutrons from various materials has been measured with several different detectors. The scattering cross section for a number of elements has been determined and the results given in a table. With suitable filters, the scattering curves for several of the Fermi groups have been investigated. The differences between the groups show up most markedly when the scatterer is itself a good absorber of one of the groups. The effect of temperature on the activation of In has been investigated, and the temperature ratio $J_{90}=\frac{\text{activity at liquid air temperature}}{\text{activity at room temperature}}$ found to be 1.08 for the *D* neutrons and 1.21 for the *C* neutrons.

1. INTRODUCTION

IN several recent papers[1, 2, 3] we have reported on some investigations of the scattering of slow neutrons by various metals. The experiments were originally designed to see whether the elements showing large "absorption cross sections" also showed large scattering cross sections, since the original theories of interaction[4] predicted such an effect. Experiments on the metals Ag, Cd and Hg as scatterers failed to show any large scattering and indeed the shape of the scattering curves indicated that the large absorption cross section was due to capture, the scattering cross section being normal. These facts are in agreement with the theory of Breit and Wigner[5] who show that scattering and capture are complementary.

Further experiments[3] with Rh and In detectors showed marked differences in the scattering curves for the same metal with various detectors. A large part of these differences can be accounted for by absorption in the detector, since many substances have been shown to exhibit marked absorption bands by Fermi and his collaborators.[6] In other cases, discussed below, we have been able to show marked differences in the form of the scattering curves due to the various groups discussed by Fermi.

Finally, using the method of Moon and Tillman[7] and Rasetti and Fink,[8] we have investigated with an indium detector the temperature coefficient of the C and D neutrons.

2. APPARATUS AND METHOD

The apparatus used was the same as that previously employed.[1] A cylindrical block of paraffin, 15 cm in diameter and 17 cm high, contained a Ra-Be bulb located on the axis 6 cm from the top surface. The detectors were thin sheets of the metals Ag, Rh and In of dimensions 6 by 10 cm. These were placed on top of the paraffin cylinder and the scatterer, usually blocks of metal the same size as the detector, were placed on top of the detector. In some cases a sheet of Cd metal, containing 0.218 g/cm^{-2}, was interposed between the paraffin and the detector. This served as a filter to cut out neutrons of the *C* group. After irradiation for a given length of time the detectors were placed around a Geiger-Müller tube counter and the activity obtained with the help of a thyratron "scale of two" recording system. In some experiments a "scale of four" counter was also used and gave results in substantial agreement with those obtained with the "scale of two" counter. In the previous communications the percent scattering, defined as the percentage ratio of the activity of the detector with a thickness x of scatterer minus the activity without scatterer divided by the activity without scatterer, was plotted as a function of the thickness of the scatterer.

In view of the rather large variations in

[1] A. C. G. Mitchell and E. J. Murphy, Phys. Rev. **48**, 653 (1935).
[2] A. C. G. Mitchell, E. J. Murphy and L. M. Langer, Phys. Rev. **49**, 400 (1936).
[3] A. C. G. Mitchell, E. J. Murphy and M. D. Whitaker, Phys. Rev. **49**, 401 (1936).
[4] H. A. Bethe, Phys. Rev. **47**, 747 (1935); E. Amaldi, O. d'Agostino, B. Pontecorvo, F. Rasetti and E. Segrè, Proc. Roy. Soc. **A149**, 522 (1935); Perrin and Elsasser, Comptes rendus **200**, 450 (1935).
[5] G. Breit and E. Wigner, Phys. Rev. **49**, 519 (1936).
[6] E. Amaldi and E. Fermi, Ricerca Scientifica; (VI) **2** (1935).
[7] P. B. Moon and J. R. Tillman, Proc. Roc. Soc. **A153**, 476 (1936).
[8] F. Rasetti and G. A. Fink, New York meeting, Phys. Rev. **49**, 642A (1936).

absorption coefficient for the various groups of slow neutrons exhibited by the several detectors which we used, we measured their absorption. This was accomplished by using the actual detectors as absorbing sheets and measuring the fraction transmitted with the help of a detector of the same material. In certain cases a Cd filter ($0.218\,g/cm^{-2}$) was used to absorb the C neutrons. The time of irradiation of the materials was the same as that used in the scattering experiments (see below). The results of the absorption experiments are given in Table I.

To get the true scattering fraction from the curve of percentage scattering, as defined above, it is necessary to correct the results for absorption in the detector. If y is the fraction of neutrons absorbed, then $1-y$ is the fraction getting through to the scatterer. If $a(x)$ is the fraction of these scattered from a thickness x of scatterer, then the number of these recorded by the detector is $a(x)y(1-y)$. The percentage scattering as it is defined above, and has been used in our previous papers is $a(x)(1-y)\cdot 100$. Hence to get the true fraction of neutrons scattered the results must be divided by $(1-y)$, the fraction transmitted by the detector. All curves published in this paper have been corrected and a corrected table of relative cross section is also given.

The time of irradiation depended on the period of the detector used and was also governed to some extent by practical considerations. The In (54-minute period) detectors were irradiated for 15 minutes and readings were taken at 1, 5 and 9 minutes after the end of irradiation. The Ag (22 sec., 2.2 min.) was irradiated 6 minutes and readings were taken at 1 and 5 minutes after irradiation; while the Rh (44 sec., 3.9 min.) was irradiated 5 minutes and readings taken at 1 and 5 minutes also at 2 and 6 minutes after irradiation.

In order to test whether there was a difference in the scattering as detected by the different periods of Ag, the following experiments were performed. The detector was irradiated for 10 seconds and counting began 30 seconds after removal of the foil. In this manner scattering curves were run for Ni and C and gave substantially the same results as were obtained for the combined periods. Furthermore, one run was made to measure the scattering of a certain thickness of Ni, in which the Ag detector was irradiated 6 minutes and the counting was not started until 6 minutes after irradiation, so that the activity of the thirty second period had practically disappeared. This point lay on the curve determined by the other groups of measurements. The scattering from the metals Ni and C, with an Ag detector, is, therefore, independent of the period used in the detection. This is probably also true for the other scatterers with the possible exception of Ag.

TABLE I. *Absorption measurements.*

DETECTOR	THICKNESS (g/cm^{-2})	FRACTION TRANSMITTED
Ag	0.105	0.93
Ag (filtered)	0.105	0.73
Rh	0.124	0.80
Rh (filtered)	0.124	0.55
In	0.109	0.82

3. RESULTS

Figs. 1, 2, 3 and 4 show the scattering curves obtained for the elements Fe, Ni, Cu and C using the several detectors as shown. The form of the curves is such that they rise rapidly out of the origin and eventually reach a saturation value. This form of curve can be explained on greatly simplified assumptions as follows. Assuming that a plane parallel beam of neutrons falls on a scatterer of thickness x, then the fraction of neutrons scattered back to the detector will be, if one assumes a combination of single scattering and capture,

$$\frac{n}{n_0}=\frac{Na\sigma_s}{2Nb(\sigma_s+\sigma_c)}\left[1-e^{-2Nb(\sigma_s+\sigma_c)x}\right],$$

where N is the number of atoms/cm^3 of the scatterer, σ_s and σ_c the scattering and capture cross sections, respectively, and a and b quantities which come in because of the solid angles involved. The quantity $N(\sigma_s+\sigma_c)$ is the usual absorption coefficient, and the factor 2 arises since the neutrons traverse the scatterer twice. Such a simple picture does not, of course, correspond to the facts since the source does not give a plane parallel beam of neutrons, and integration over the various angles involved will eventually have to be carried out. The calculation does show, however, that the slope of the curve for small thicknesses is proportional to $N\sigma_s$ and the saturation value is governed by

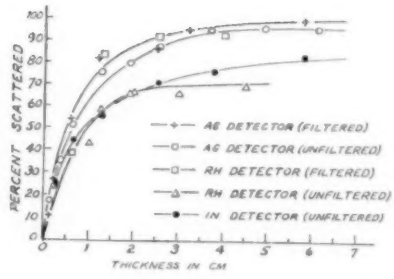

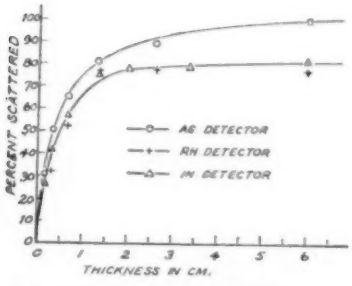

FIG. 1. (*upper*) Scattering of neutrons from iron.
FIG. 2. (*lower*) Scattering of neutrons from nickel.

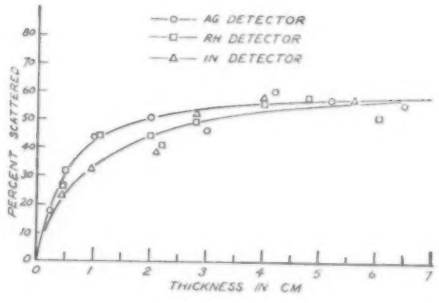

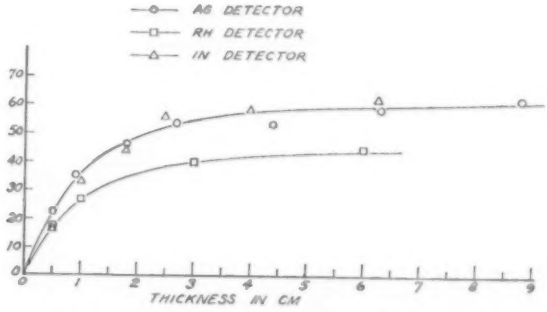

FIG. 3. (*upper*) Scattering of neutrons from copper.
FIG. 4. (*lower*) Scattering of neutrons from carbon.

$\sigma_s/(\sigma_s+\sigma_c)$. Thus the relative scattering cross section can be obtained and some idea as to the ratio of scattering cross section to total cross section. The values of the scattering cross sections of various scatterers, obtained with a Ag detector, together with the saturation value of the curve is given in Table II.

The curves of Fig. 1 show the scattering by Fe with Ag, In and Rh detectors with and without filtering through Cd. The curves for neutrons filtered through 0.218 g/cm² of Cd should represent the scattering of the *A* and *B* neutrons (Ag detector) and the *D* neutrons (Rh detector). It will be seen that these groups are scattered equally well from the iron. The curves for the unfiltered neutrons lie below those obtained when Cd filtering was employed and in the order of the number of C neutrons detected—Ag (50 percent C, 25 percent A, 25 percent B), In (60 percent C, 40 percent D), Rh (72 percent C, 25 percent D). This seems to indicate that the *C* neutrons have a somewhat smaller ratio of scattering cross section to total cross section in iron than do the other groups. The above explanation holds, of course, only in the case that the velocity distribution of the neutrons is not changed on scattering from the iron. Such an effect in Fe does not appear to occur to any appreciable extent.[1]

The curves for the scattering from Ni (Fig. 2) show that the results with Rh and In detectors are the same, whereas the curve for the silver detector shows greater scattering. In the case of scattering by Cu (Fig. 3) the curves for Ag, Rh

TABLE II. *Relative scattering cross section of various elements for slow neutrons (Ag detector).*

ELEMENT	AT. NO.	$\sigma_s \times 10^{-24}$ cm²	MAX. % SCATTERING
C	6	3.4	61
Mg	12	3.0	37 (at 6 cm)
Al	13	1.0	21 (at 6 cm)
S	16	0.9	18 (at 6 cm)
Cr	24	1.4	13
Mn	25	2.2	17
Fe	26	10.6	95
Ni	28	18	100
Cu	29	8.3	59
Zn	30	3.7	40
Ag	47	6.3	9
Cd	48	(1.2)	(2.4 at 4 mm)
Sn	50	4.1	34
Hg	80	4.7	21
Pb	82	7.7	56
Bi	83	10.2	43

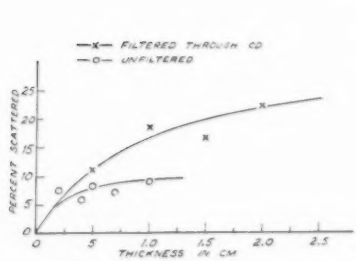

FIG. 5. Scattering of neutrons from silver. (Ag detector.)

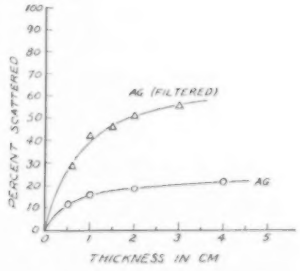

FIG. 6. Scattering of neutrons from mercury.

and In detectors give approximately the same results. For the experiments on the scattering by *C*, the curves for the Ag and In detectors are the same whereas the scattering curve using a Rh detector lies lower. No definite explanation of the differences in these scattering curves can at present be given on account of the complicated nature of the phenomena. Collisions with carbon atoms are known to cause a change in the velocity distribution of the neutrons,[9] and this will probably be the governing factor in the explanation.

The scattering from Ag and Hg present interesting cases. Both of these metals are good absorbers of "slow" neutrons. The cross sections for absorption in the whole range of the "slow region" have been found to be[10] for Ag 55×10^{-24} cm^{-2}, and for Hg 380×10^{-24} cm^{-2}. Furthermore, it is known that Ag shows marked selective absorption.

We have measured the scattering from Ag with an Ag detector with and without filtering through 0.218 g/cm^{-2} Cd. The curves are shown in Fig. 5. It will be seen that when no filter is used the scattering is small, about 9 percent, and the curve reaches saturation quickly. This indicates that the ratio of scattering to total cross section is small, most of the neutrons being absorbed in the scatterer before getting back to the detector. When the Cd filter is employed, on the other hand, the maximum observed scattering is 25 percent and the slope of the curve indicates a larger ratio of scattering to total cross section. The neutrons responsible for this scattering are probably the *B* group since the *C* group is absorbed in the Cd and the *A* group in the Ag scatterer.

The scattering from Hg with an Ag detector with and without filtering is shown in Fig. 6. When no filtering is employed the maximum scattering is 20 percent showing that a large fraction of the neutrons are absorbed in the scatterer. For those neutrons which have been filtered through Cd, however, a marked difference in the form of the curve exists. The maximum observed scattering is 55 percent and the curve is still rising at this point. The curve shows that the ratio of scattering to absorption cross section is larger in the case of the filtered neutrons (presumably groups *A* and *B*) than for the unfiltered. It is apparent, therefore, that the absorption coefficient is large in the region of thermal velocities (*C* region) and is not so large at those points in the higher energy region which correspond to the *A* and *B* group. This does not mean, of course, that the absorption may not be large in some other region of the spectrum not registered by a silver detector.

4. Temperature Effect for the Neutrons Which Effect Indium

We have measured the temperature effect on the neutrons which effect In by the method of Moon and Tillman[7] and Rasetti and Fink.[8] A block of paraffin 22 cm in diameter and 15 cm high was hollowed out so that a Dewar flask could be placed along the axis of the block. Inside of the Dewar there was located a cylinder of paraffin of 1 cm wall thickness, on the inside of which a cylindrical In detector could be placed. Arrangements were also made to interpose a cylinder of Cd (0.410 g/cm^{-2}) between the detector and the small paraffin cylinder of paraffin. The neutron source was embedded in

[9] E. U. Condon and G. Breit, Phys. Rev. **49**, 229 (1936). G. A. Fink, J. R. Dunning and G. B. Pegram, Phys. Rev. **49**, 340 (1936).

[10] J. R. Dunning, G. B. Pegram, G. A. Fink and D. P. Mitchell, Phys. Rev. **48**, 265 (1935).

TABLE III. *Effect of liquid air temperatures.*

ARRANGEMENT	COUNTS
Liquid air, no Cd.	52,816
Liquid air, Cd filter	8,027
No liquid air, no Cd	44,309
No liquid air, Cd filter	7,473

the large block 9 cm off the axis so that the thickness of paraffin in a direct line between the source and the Dewar was 4 cm. The detector was activated when the inner paraffin cylinder was at liquid air temperature and when it was at room temperature, with and without the Cd filter. The In was irradiated 45 min. and counting was carried out from the fifth to the eightieth minute after irradiation. The results are shown in Table III.

Dividing the results obtained at liquid air temperature by those obtained at room temperature, when the Cd filter was present, gives the temperature ratio for the *D* group. This value turns out to be 1.08, and is the same as that obtained by Rasetti and Fink using Rh as a detector. The differences between the counts obtained with and without the Cd filter give that part of the activity due to the *C* group. The ratio of the activities due to the *C* group is 1.21.

Recently Rasetti, Fink, Goldsmith and Mitchell[11] have determined the energy of the various groups of neutrons with boron absorption. They showed that the energy of the *D* group activating Rh is approximately 0.6 ev, while the energy of those neutrons accounting for that part of the activity of In which is not effected by Cd filtering is about 0.35 ev. This small difference in energy between the two classes of neutrons would presumably now show up in the measurement of the temperature effect.

The authors are indebted to Mr. L. M. Langer for help with the readings and to Mr. C. B. Braestrup of the Physical Laboratory of the Department of Hospitals of the City of New York for many favors.

Note Added with the Proof. R. Fleischmann[12] has recently published experiments in which he obtains much lower results for the scattering of slow neutrons from Fe and Cu than we do, and criticizes our results on the following grounds. He supposes that in our neutron beam there are a considerable number of fast neutrons which do not affect a silver detector on their way from source to scatterer. These fast neutrons are then supposed to be scattered in the Fe or Cu, return through the detector to the paraffin, and there suffer reflection with a loss of velocity which makes them capable of activating the silver detector on their second trip toward the scatterer. That this effect is playing no predominant role in our experiments can be shown by several experiments which we have already published but which we shall discuss again, in more detail, to allay this criticism.

In a group of experiments, described in our first communication,[13] we showed that, using an Ag detector, 4.3 cm of Cu as scatterer caused an increase of 52 percent in the activity of the detector. In a second experiment, a sheet of Cd 1 mm thick (0.86 g/cm²) shielded the neutron source from the detector. With this arrangement about 25 percent as many counts were obtained with Cd as without. A thickness of 4.3 cm of Cu caused an increase of about 50 percent in the count.

In another series of experiments the Ag foil was not shielded by Cd from the source, but a sheet of Cd 1 mm thick was placed on top of the foil. With this arrangement no change of activity of the detector was noted. With 4.3 cm of Cu placed above the Ag and Cd there was only an 11 percent increase instead of the 52 percent obtained without Cd. To be explicit we can use the following figures, taken directly from experiment, calculating the activity of the detector to be 1000 (the actual count was 1043):

Arrangement	Activity	Percent Scattering
Source, Ag	1000	—
Source, Ag, 4.3 cm Cu	1540	54
Source, Cd, Ag	253	—
Source, Cd, Ag, 4.3 cm Cu	392	55
Source, Ag, Cd	1000	—
Source, Ag, Cd, 4.3 cm Cu	1100	11

From the results of the experiments with and without the Cd between source and detector, one can calculate the result to be expected if the Cd is placed between detector and scatterer, assuming that the second reflection in the paraffin is negligible. It has been shown that, for those neutrons which activate Ag, the fraction transmitted by Cd is constant beyond 0.3 g/cm²,[6, 1] so that the only absorption to be considered takes place when the neutrons pass through the Cd on their way to the scatterer. The absorption on the way back to the detector may be neglected. Using the figures given above one would expect an activity of 1000+139=1139 for the arrangement (source, Ag, Cd, Cu), or an increase of 12.5 percent in substantial agreement with experiment.[14] If, on the other hand, a large number of fast neutrons were scattered from the Cu, returned to the paraffin, and were reflected back to the detector at a lower velocity, one would expect a much greater activity for the above arrangement than was actually found.

[11] F. Rasetti, G. A. Fink, H. H. Goldsmith and D. P. Mitchell, Washington meeting, Phys. Rev. **49**, 869A (1936).

[12] R. Fleischmann, Zeits. f. Physik **100**, 307 (1936).

[13] A. C. G. Mitchell and E. J. Murphy, Phys. Rev. **47**, 881 (1935).

[14] That no appreciable change of velocity takes place on scattering by Cu has been shown by us. (See ref. 1, p. 655.)

Inelastic Scattering of Electrons from Solids

ERIK RUDBERG, *Massachusetts Institute of Technology*

(Received May 9, 1936)

The energy distribution of electrons scattered inelastically from solid targets has been studied for primary energies from 50 to 400 volts, using a method of magnetic deflection. Target surfaces of Cu, Ag and Au were deposited by evaporation in vacuum immediately before the measurements were made. For certain values of the energy loss suffered by the scattered electron the curves exhibit maxima, which are characteristic of the material of the target and independent of the primary voltage in the range studied. All three metals have two maxima below 10 volts, the most pronounced one being that for Ag at 3.9 volts. These maxima appear to correspond roughly to the regions of high optical absorption for the same substance. An estimate of the depth of penetration of the scattered electron was obtained from energy distribution measurements on films of Ca, CaO, Ba and BaO of known thickness, deposited on Ag. The results indicate, that the inelastic scattering is determined by the first few atomic layers near the surface. The fresh deposits of Ca and Ba show a very high rate of oxidation, even when the total pressure is $<10^{-7}$ mm; the distribution curves for the oxide are entirely different from those for the parent metal and exhibit a rather complicated structure. Measurements of the energy distribution of scattered electrons should in some cases prove a sensitive tool for the study of surfaces. A deposit of 5×10^{14} atoms/cm^2 of Ca on CaO—less than a monatomic layer in the Ca-crystal—is easily detected by this method.

IT is a well-known fact that when the molecules of a gas are bombarded by electrons of sufficient energy, there is a re-emission of electrons from the gas which can be regarded as composed of three different parts: Elastically reflected electrons, inelastically scattered electrons and low energy secondary electrons, resulting from ionizing collisions. Since the pioneer work of Franck and Hertz the energy distribution of the inelastically scattered electrons has been studied with the object of securing information about the energy states of the molecules in question, and the transitions between such states. In the same way the secondary emission from a bombarded solid may be described as consisting of elastically reflected electrons, inelastically scattered electrons and secondary electrons proper. Some years ago it was shown[1–3] that the energy distribution of the inelastically scattered electrons exhibited a structure of maxima and minima, characteristic of the solid surface under bombardment. These occurred at a constant distance from the peak caused by reflected electrons on the energy scale, independent of the primary voltage. If the zero of the energy scale is determined by the position of this reflection peak, the curves evidently represent the distribution of the energy losses suffered by the bombarding electrons. Such curves were obtained[4] from velocity distribution measurements by three different methods, employing focusing magnetic fields, a combination of magnetic and electric fields as well as focusing electrostatic fields. The targets studied were Cu, Ag, Au, Pt and the oxides MgO, CaO, SrO and BaO; some unpublished results have also been obtained for Ni. Later Haworth[5] has reported similar results for well outgassed Mo. As in the case of a gas, the maxima in these curves were regarded as indicating that definite excitation processes were taking place in the bombarded substance, the position of a maximum representing the energy involved in that particular excitation.

A possible way of accounting for these structures theoretically was indicated in some work by Kronig and Penney[6] and in the general theory of metals by Bloch;[7] certain general results which can be derived from Bloch's work were used by Fröhlich[8] in connection with a special model in a theory of secondary emission. The theory of inelastic collisions in solids is discussed in a following paper[9] by Professor Slater and the present writer.

[1] Brown and Whiddington, Leeds Phil. and Lit. Soc. Proc. **1**, 162 (1927).
[2] Whiddington, Leeds Phil. and Lit. Soc. Proc. **1**, 242 (1928).
[3] Rudberg, K. Svenska Vet. Akad. Handl. **7**, No. 1 (1929).
[4] Rudberg, Proc. Roy. Soc. **A127**, 111 (1930).
[5] Haworth, Phys. Rev. **48**, 88 (1935); see also **37**, 93 (1931); **42**, 906 (1932).
[6] Kronig and Penney, Proc. Roy. Soc. **A130**, 499 (1931).
[7] Bloch, Zeits. f. Physik **52**, 555 (1928).
[8] Fröhlich, Ann. d. Physik **13**, 229 (1932).
[9] Slater and Rudberg, Phys. Rev., following article.

The early experimental work[4] was unsatisfactory because of the presence of vapor from a waxed joint in the tube; in order to keep the bombarded surface clean it was held at incandescence during the measurements. It now appears that this method, while successful in the case of the oxides, did not always give a well-defined surface in the case of metal targets. The present paper is a report on some work during the last few years, in which the distribution curves for Cu, Ag and Au have been remeasured under more satisfactory vacuum conditions.[10] In connection with the problem of the depth of penetration for inelastically scattered electrons, the scattering from films of Ca, Ba, CaO and BaO on Ag has also been studied.

Apparatus and Methods

The essential features of the apparatus are indicated in Fig. 1. Most metal parts are made of sheet copper. A beam of electrons of nearly uniform speed, obtained from an electron gun G, is allowed to fall on the target T in question under an angle of incidence of about 45°. The target is surrounded by a cylindrical shield S to retain the bulk of the secondary emission. The total current to T and S thus measures the bombarding current and is kept constant during a run. A narrow beam of the re-emitted electrons from T escapes through a small opening in S, in a direction at right angles to the primary beam. Through a narrow slit it enters the deflection box B, where the energy distribution in the beam is analyzed. The entrance slit and two other slits in the box define a circular path, which electrons of the proper speed are made to follow by means of a magnetic field, perpendicular to the path. Two extra partitions with slits serve to trap electrons scattered from the walls of the box. The electrons emerging from the third slit are caught by the collector C. With this arrangement, the energy distribution can be measured in two different ways. In the first, the box is kept at the same potential as T and S, and the current i received by C is measured as a function of the magnetizing current I in the Helmholtz coils. The energy distribution is then given by i/I^2 *vs.* I^2, except for constant factors. In the second method, the magnetic field is kept constant at a suitable value, and i is measured as a function of a variable voltage v applied between the target and shield unit and the box. The disadvantage with the second method, which yields results on an energy scale directly, is that the effective volume within which the electron trajectories must fall inside S in order that the electrons may reach C, varies both in shape and size with the applied voltage v, in a way which is difficult to correct for. This is most serious for low bombarding voltages V, when the range over which v is varied is not negligible compared with V. Hence the first method has been used except for a few measurements on Ag, where small parts of the energy distribution were studied with a variable accelerating voltage v.

The primary voltage V, the primary current drawn by T and S, as well as the magnetizing current in the second method, were kept sensibly constant during each run, the constancy being checked by compensating devices with galva-

[10] The material in this part of the paper was presented before the Washington Meeting of the Am. Phys. Soc., April 28, 1934. Phys. Rev. **45**, 764 (1934).

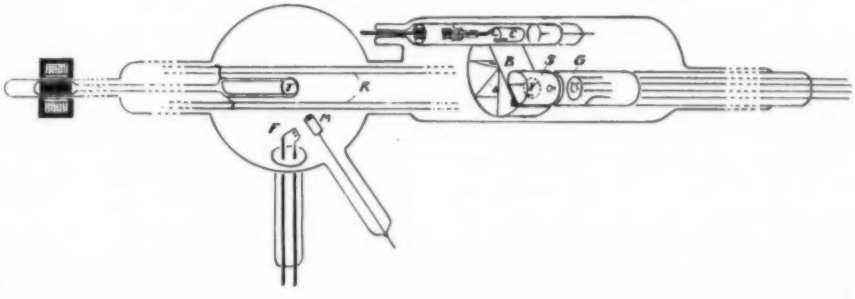

Fig. 1. Apparatus.

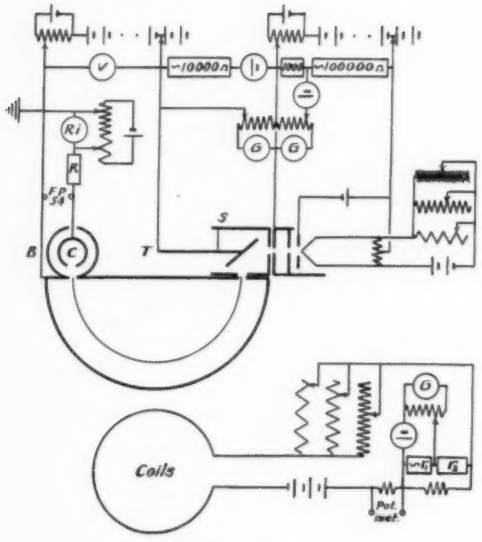

FIG. 2. Wiring diagram.

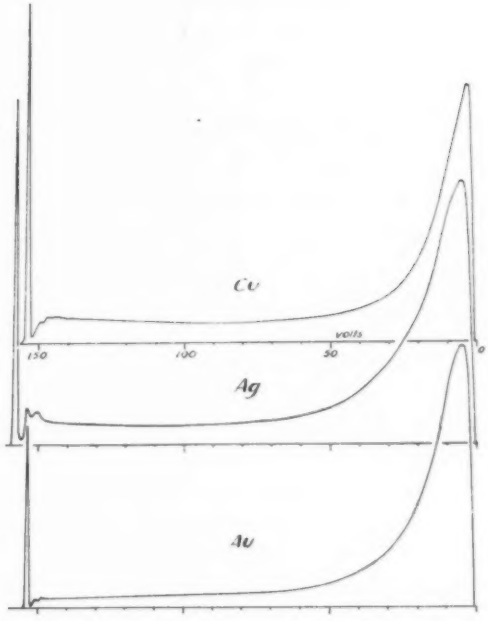

FIG. 3. Energy distribution of scattered electrons.

nometers. In the first method, I was measured with a potentiometer. The collector current i was determined by compensation of the drop produced in a high resistance R, with an FP-54 electrometer tube serving as null instrument. The electrical connections are shown in Fig. 2.

PREPARATION OF TARGET SURFACES

All the targets studied were prepared by evaporation in vacuum directly in the tube. A small disk T of sheet molybdenum is attached to a magnetically operated slider, Fig. 1, one end of which is resting on a track of glass rod R. Thus T can be withdrawn from the position for measurement inside S into the bulb to the left, where it can be outgassed by bombardment from the filament F or covered with a fresh evaporated layer of the metal to be studied. In the case of Cu, Ag and Au the metal is contained in a molybdenum crucible M, which can be heated by bombardment from F. Two such crucibles are provided.[11] The films obtained in this way were sufficiently thick, so that no effect of the backing substance could be detected. As a matter of fact the backing material soon became quite complex, since a new surface was frequently formed by evaporation and surfaces of different metals were often studied alternatingly. In one case such a target with alternate layers of Cu and Ag was heated to incandescence, so that a reaction took place. The resulting surface upon cooling gave distribution curves quite different from those for Cu and for Ag.

Ca and Ba were evaporated at accurately controlled temperatures from small molybdenum furnaces of a type described in connection with the measurement of the vapor pressures for these metals.[12, 13] The rate at which the material was deposited could therefore be computed from the geometrical arrangement and the known vapor pressure.

The apparatus was subjected to the customary outgassing by baking at 400°C and high frequency induction heating for the metal parts. It was pumped continuously. The pressure with the tube operating did not exceed the order of 1×10^{-7} mm, as measured with an ionization gauge, calibrated for air.

[11] I am much indebted to Dr. H. W. B. Skinner and Dr. H. M. O'Bryan for valuable suggestions in regard to crucible design.

[12] Rudberg, Phys. Rev. **46**, 763 (1934).

[13] Rudberg and Lempert, J. Chem. Phys. **3**, 627 (1935).

Results for Cu, Ag and Au

Typical distribution curves for Cu, Ag and Au are shown in Fig. 3, for a primary energy of about 150 volts. The sharp peak to the left in each curve represents the elastic scattering. This serves to locate the zero of energy loss in the subsequent curves. The primaries themselves have a distribution, due to temperature and filament drop, about 0.5 volt wide (Halbwertsbreite). The width of the reflection peak is satisfactorily accounted for by this original distribution and the finite resolving power of the analyzer which corresponds to a width $\Delta V = 0.008V$ on an energy scale. It is evident that the bulk of the emission is made up of low energy secondaries which exhibit the broad maximum to the right for low energies. It is possible that a closer examination of this low energy part might reveal a structure such as has recently been reported by Haworth in the case of molybdenum after prolonged heat treatment.[5] Inelastic collisions are indicated by the part of the curve immediately to the right of the reflection peak. When the primary voltage is changed this part shifts bodily, whereas the low energy side of the curve remains essentially the same. In the following Figs. 4, 5 and 6 attention is confined to the inelastically scattered electrons. As may be inferred from Fig. 3 the top of the reflection peak would fall well outside the figures on this scale; this peak, although not indicated, was always measured in order to locate the zero position on the energy loss axis.

For reasons which are not quite clear it appears to be more difficult to obtain well-reproducible

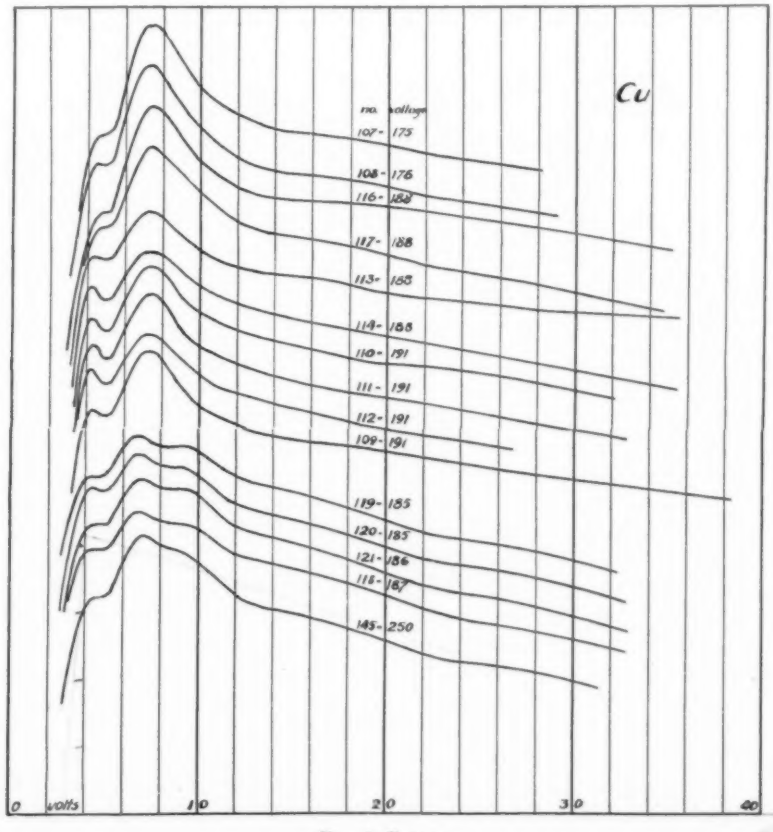

Fig. 4. Copper.

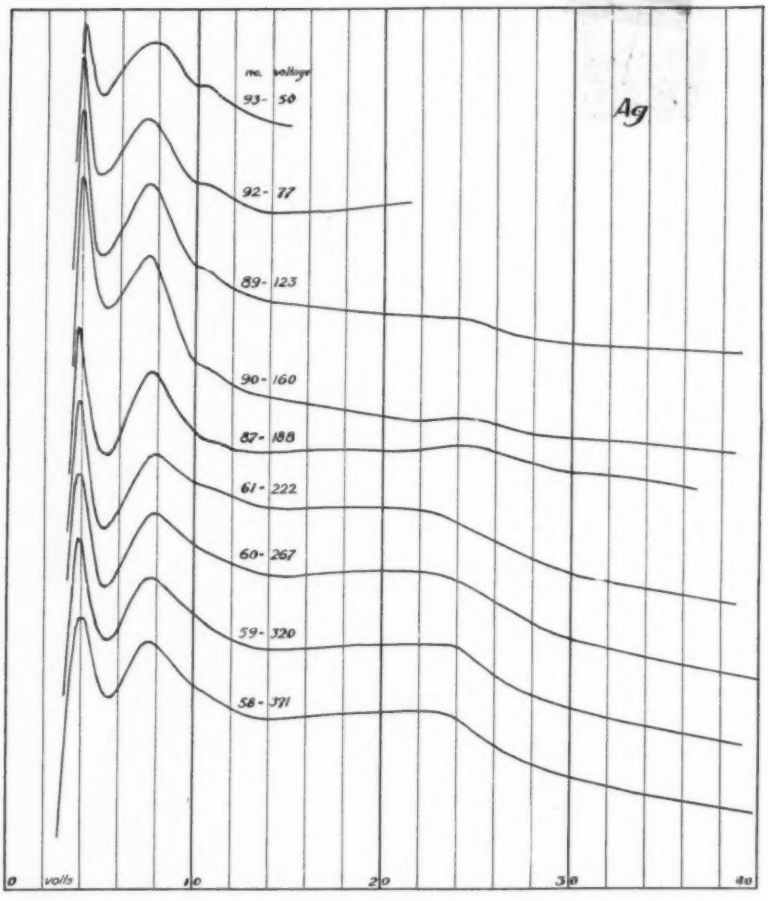

FIG. 5. Silver.

curves with copper than with the other metals, but Fig. 4 gives a fair representation of the results. The curves are labeled by the serial number and the primary voltage, the latter increasing downward. The base metal is silver, molybdenum or gold. The first hump is always present, the second is present but varies in importance and in some curves, like the group at the bottom of the figure, there is a third hump, which in the earlier stages of evaporation actually rose above the second maximum. This may possibly indicate that it is characteristic of some impurity distilling over with the metal.

Curves for silver are shown in Fig. 5. They exhibit the sharpest maximum found so far at 3.90 volts, and a broader maximum at about 7.8 volts. The range of primary voltage is from 50 to 370 volts. The broadening of the peak for higher voltages is of course due to the decreasing resolution of the velocity analyzer for higher energies.

In the case of gold, Fig. 6, there are again two main maxima, the first one for an energy loss of 3.05 volts. For this metal there is also a very broad hump around 24 volts. The relative proportion of higher energy losses is greater than for copper and silver. For high primary voltage, however, the gold curves bend down in this region like the others. The yield per primary, in the direction studied and for the voltage range employed, is less than for Cu and Ag by a factor of 2 to 4.

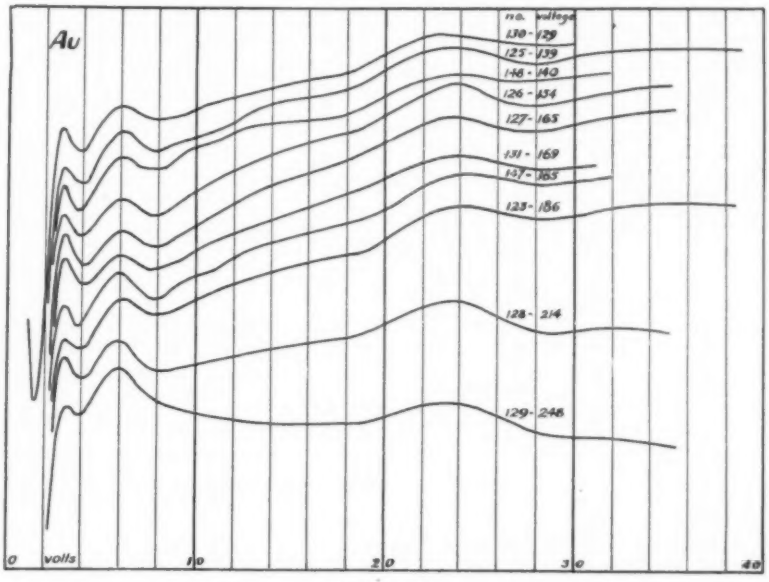

FIG. 6. Gold.

Typical curves for all three metals are collected in Fig. 7, which also illustrates the spacing of experimental points. Those for Cu and Ag have been shifted upwards by amounts indicated to the left. It will be seen that the curves for these three metals are similar in that there is a deep valley next to the reflection peak, which indicates the absence of inelastic collisions with small energy losses; this is followed by two main maxima. The positions of these in the case of Ag and Au are such that the second maximum could result from two of the processes giving rise to the first; however, the wide difference in shape, at least in the case of Ag, makes it very unlikely that this is the sole cause of the second maximum.

The fact that the position of these maxima is independent (in the range investigated) of primary voltage, of the potentials of other parts of the tube such as the electron gun, and of whether they are measured by a varied accelerating voltage or by a varied magnetic field—should prove conclusively, that these maxima are connected with characteristic transitions in the target. A separate experiment showed that the sharp silver maximum could be reproduced within 40 seconds after a fresh surface had been formed by distillation. At a pressure of 1×10^{-7} mm the formation of a monomolecular layer by the residual gas requires at least that time if every

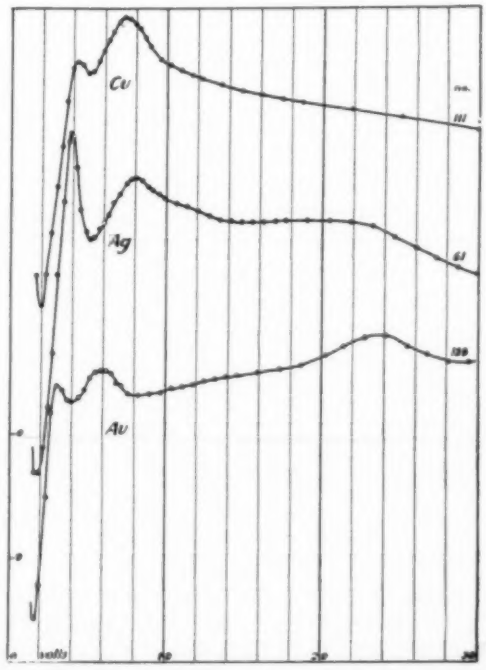

FIG. 7. Distribution of energy losses for Cu, Ag and Au.

TABLE I. *Values of the energy loss for the first maximum in silver and in gold.*

Target Ag			Target Au		
SER. NO.	VOLTAGE	ENERGY LOSS (volts)	SER. NO.	VOLTAGE	ENERGY LOSS (volts)
93	50	3.95	130	127	2.95
92	77	3.85	125	139	3.00
63	109	3.65	148	140	2.95
89	123	3.85	126	154	3.10
62	141	3.75	133	154	3.15
90	160	3.95	132	164	3.15
212	175	3.85	127	165	3.05
252	175	3.90	131	169	2.95
87	188	3.80	122	183	2.90
56*	194	3.80	144	185	3.10
57	194	3.75	123	186	2.95
64*	196	3.90	128	214	3.05
65*	196	3.90	124	217	2.95
66*	196	3.90	129	248	3.15
67*	196	3.85			
68*	196	3.90			
61	222	3.85			
232	250	4.10			
173	250	4.00			
174	250	4.05			
60	267	3.80			
88	296	4.10			
59	320	3.80			
58	371	3.90			
mean of 24 values		3.88 or 3.90	mean of 14 values		3.03 or 3.05
probable error in mean		±0.05 volt			

* Measured by method of variable accelerating voltage.

hitting molecule sticks. Even granting that the pressure of residual gases during evaporation might have been somewhat higher than 10^{-7} mm this result makes it difficult to ascribe the maximum to adsorbed gases.

The values obtained for the position of the first maximum for silver and for gold are summarized in Table I.

COMPARISON WITH OPTICAL DATA

In a given system showing linear absorption, the number of transitions per second in unit frequency range at a frequency ν may be written as $T_\nu \overline{E_\nu^2}$ and the rate of absorption of energy as $h\nu T_\nu \overline{E_\nu^2}$, if E_ν is the electric vector of the radiation field. If the complex refractive index of the substance for this particular frequency is $n-ik$, the current density for the component in phase with the field is $\nu nk E_\nu$, so that the rate of absorption of energy per unit volume is $\nu nk\overline{E_\nu^2}$. Hence T_ν is proportional to the product nk. Kronig[14] and others have shown, in the case of

[14] Kronig, Proc. Roy. Soc. **A124**, 409 (1929).

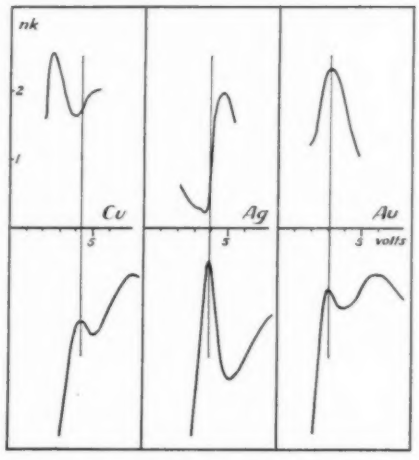

FIG. 8. Distribution of optical transitions (upper) and of electron energy losses (lower).

the Bloch-Sommerfeld model of a metal, that there exists a selection rule for the electronic transitions which can be produced by absorption of radiation. According to this rule, which results from the space periodicity of the lattice and therefore holds for crystalline solids in general, transitions can only take place between states having the same (3-fold) momentum quantum number: $\mathbf{k}_0' = \mathbf{k}_0$. The probability of such a transition is proportional to $L^2\overline{E_\nu^2}$, where L is the moment $\int \psi \tau \psi' * d\tau$ for the two states ψ and ψ' in question. Thus $T_\nu = \text{Const} \cdot \sum L^2$. It can be shown that, when the energy loss is very small compared with the energy of the bombarding electron, a similar selection rule should be approached for the case of excitation by electron impact, and that the probability of excitation is determined by L^2 also in this case.[9] Thus one would expect the curve for nk as a function of the energy $h\nu$ to be similar to the distribution curve for small energy losses for the same substance, at least when the bombarding voltage is high. Fig. 8 shows a comparison of nk and the energy loss curves for Cu, Ag and Au, the frequency being measured in equivalent electron volts. The constants used are those given by Minor[15] (Cu, Ag) and Meier[16] (Au), in all cases measured in air. It is known that optical constants vary considerably with the surface condi-

[15] Minor, Ann. d. Physik **10**, 581 (1903).
[16] Meier, Ann. d. Physik **31**, 1017 (1910).

tions, which probably accounts for the conflicting results often found by different observers. It is possible, therefore, that the constants used could refer to a material quite different from that for which the distribution of energy losses has been measured. This is more likely to be the case with copper than with the other two; the *nk*-curve given for this metal in Fig. 8 may actually be the curve for cuprous oxide. The other two metals show a fair agreement as to the position of the main peak, although the optical maximum appears shifted to higher energies for Ag. The optical measurements by Pfestorf[17] show for Au a maximum at a somewhat higher energy than that given by Meier's data, but his points are considerably more scattered. Pfestorf's data for Cu give indication of the minimum in the *nk*-curve of Fig. 8, but do not show the maximum.

Experiments with Films of Calcium and Barium and Their Oxides

The theory of these collision processes, which is given in a following paper, is based on the model of the inside of a metal infinite in extent. In the experiments, however, electrons are shot into the metal (and escape from it to be measured) through the surface. It is therefore conceivable that the collisions take place in a region at the surface, where the wave functions are quite different from those in the interior of the metal. No satisfactory theory is available for this region at present.

In order to obtain some information about the depth of penetration, it was planned to cover a substance of well-defined energy loss characteristics, such as silver, with some other material, and study the changes in the energy loss curve as a function of the thickness of the latter. The cover substances chosen were calcium and barium, since the useful part of their vapor pressure curves appeared to fall in a range available for controlled evaporation, yet high enough so that one might expect the reflection from a clean, cold surface to be negligible. Special long exposure tests with the target withdrawn to such a position, that it could be reached by atoms reflected from the walls but not by the direct beam, actually indicated that such reflection was negligible. In the case of calcium, the target rested against the flat bottom of a reentrant tube (not shown in Fig. 1) during exposure to the atomic beam from the gun. Some of the films were deposited while this tube was cooled by CO_2-ice and acetone, others with the tube at room temperature. No difference could be detected.

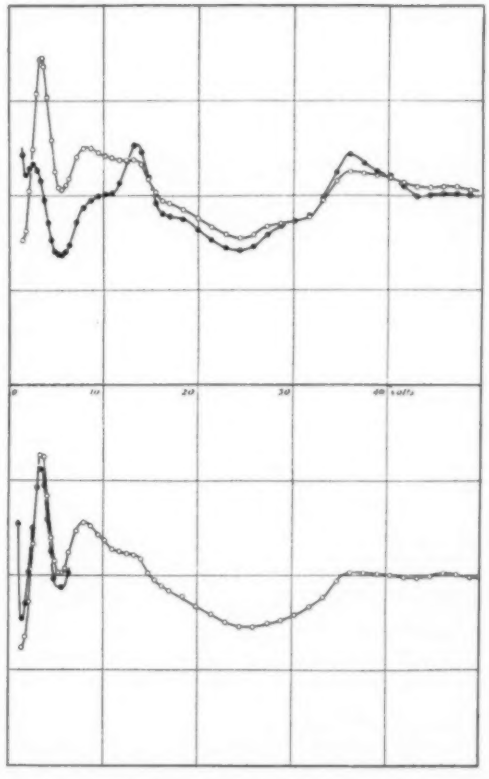

Fig. 9. Showing "aging" of Ca-deposits. White circles: fresh deposit, black: 30 minutes old. Lower curves with continuous Ca-evaporation.

For convenience the amount of metal per unit area has been expressed as the number of single layers to which it would correspond, if arranged as in the planes of closest packing in that particular metal, the (111)-planes for the face-centered Ca, the (110)-planes for Ba. It is not supposed that this is the actual arrangement of the deposits, the structure of which is as unknown as that of the underlying substance.

[17] Pfestorf, Ann. d. Physik **81**, 906 (1926).

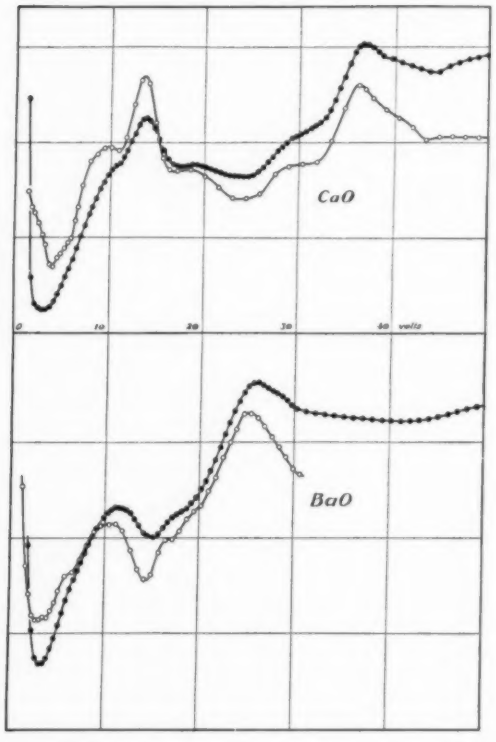

FIG. 10. Distribution curves for "aged" Ca- and Ba-deposits (white circles) compared with old data for CaO and BaO (black).

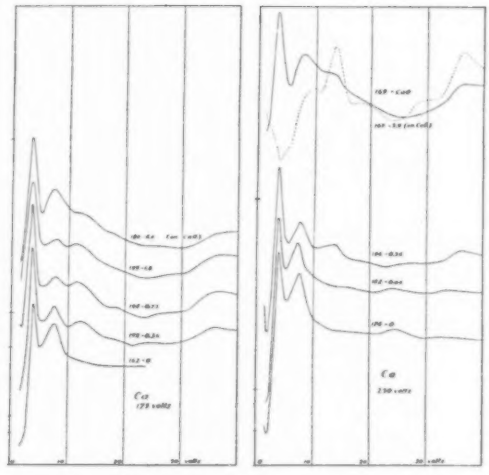

FIG. 11. Calcium on silver.

It was found both in the case of calcium and barium, that a fresh deposit gave a distribution curve quite different from that obtained from the same target after a few hours standing in a high vacuum. The change was quite noticeable even in the time (about 30 min.) required for a run; the curve obtained from a deposit a few hours old could be reproduced a week later, if no further evaporation took place. This behavior was suspected to be due to a reaction between the freshly distilled Ca- or Ba-metal and some constituent of the residual gas in the tube, at a pressure $\leq 10^{-7}$ mm, the distribution curve after "aging" being due to a compound. The following facts substantiate this hypothesis and are believed to prove that the compound formed is the oxide.

Fig. 9 shows two pairs of curves for deposits of Ca. The white circles represent measurements immediately after the film was formed, starting with low energy losses. The black points were measured 30 min. later, also from left to right. Conditions in the case of the upper pair were the same as when the lower pair was measured, except that in the latter case the Ca-gun was left on in the evaporation chamber during the measurement. In this way the walls of the chamber were continuously being covered with a fresh coating of Ca, which acted as a getter removing the active gas from the tube. This evidently greatly increased the "lifetime" of the first high peak, which is the most characteristic feature of the pure calcium curve. Several years ago energy distribution curves for CaO and BaO were measured with a different apparatus.[4] The nitrates were deposited on platinum, by evaporation of the water from aqueous solutions, and these converted into the oxides by further heating in air. Fig. 10 shows a comparison of the present measurements (white circles) on "aged" deposits of Ca and Ba and the old curves (black circles) for the corresponding oxides. The latter ones were measured according to the second method described (with an accelerating voltage v), which accounts for the gradual rise with increasing energy loss. Evidently every important feature of the old curves reappears in the present measurements on the "aged" deposits. These will therefore be called oxides.

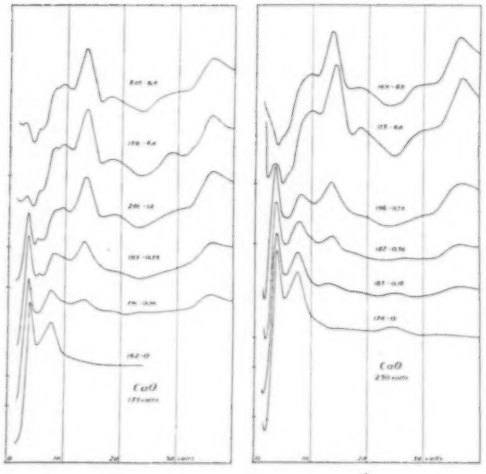

a *b*

FIG. 12. Calcium oxide on silver.

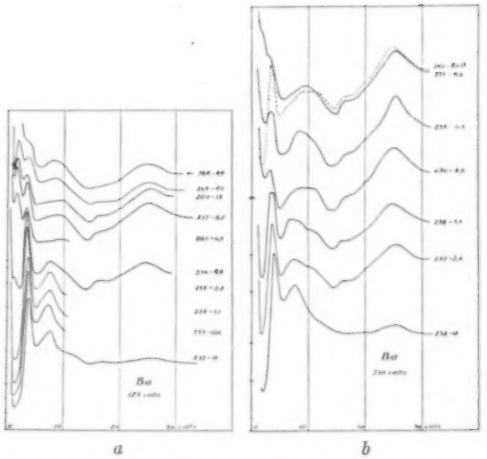

a *b*

FIG. 13. Barium on silver.

In the measurements on Ca- and Ba-films the gun was usually kept at evaporation temperature to slow down the rate of reaction, and the curves were taken as fast as possible, starting, as a rule, from the end of low energy losses, where the peaks are sharper. In this way the distribution for higher energy loss will exhibit, to some degree, features characteristic of the oxide. These can be distinguished from those of the metal itself by measuring each particular part of the curve separately, immediately after evaporation. In a new apparatus, now under construction, it will be possible to have the target sprayed continuously with the metal during the measurements.

Fig. 11 shows results for Ca-films at two voltages. The curves are labeled by their serial number and the thickness of the film in the unit defined above (thickness $1=7.46\times10^{14}$ atoms/cm^2). The backing is freshly distilled Ag, except in the top curve in *a*, where the film is backed by an old oxidized Ca-deposit. The dotted curve No. 169 shows the result of "aging" on the film which yielded No. 168 immediately after evaporation. Evidently the strongest oxide peaks are already beginning to appear in the curve for the fresh deposit. It will be seen that Ca has a strong peak very near the position of the sharp Ag-maximum and a broader hump in the region of the second maximum for silver. This makes it impossible to state at what thickness the Ag-characteristics are obscured by the Ca-deposit, but it is evident that the film affects the distribution curve already for a thickness less than 1.

Energy loss curves for CaO on Ag are given in Fig. 12. The thickness values refer to the Ca-film before oxidation. In each case the deposit was allowed to "age" for a sufficiently long time before measurement, so that no further change in the curve would take place. The oxide maxima begin to appear for a thickness less than 0.5, but the sharp silver peak is not completely obscured by a thickness 10 times greater than this.

The results for Ba-films on Ag are shown in Fig. 13 (thickness $1=5.63\times10^{14}$ atoms/cm^2). These films appear to oxidize even more rapidly than the Ca-deposits. Thus the BaO-features appear in all the curves at higher energy losses. The curves were measured from left to right, so that the part for small energy losses, in which the characteristic features of Ba fall, is representative of Ba-metal. A thick deposit of Ba, or a film of Ba on BaO, shows no maximum near the silver peak, although thin films of Ba on Ag seem to enhance that peak. Ba has a low energy maximum at 1.7 volts; this is so close to the reflection peak, that the maximum is only resolved at low primary voltage. At 250 volts it is suppressed by overlapping from the strong reflection peak, except in the top curve, although its presence is indicated in the other curves by the trend in this

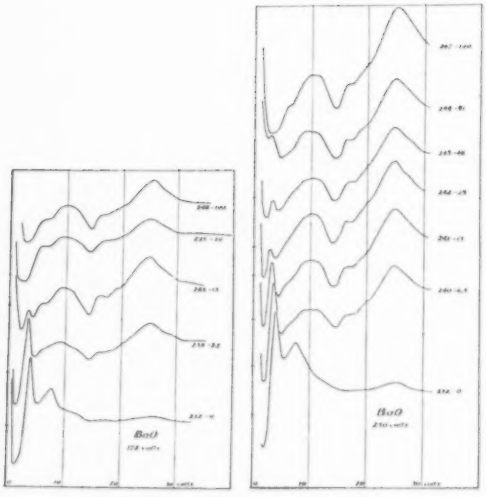

a *b*

FIG. 14. Barium oxide on silver.

TABLE II. *Measured energy losses corresponding to the top of Ag peak for Ca and Ba films on silver.*

THICKNESS	SER. NO.	VOLTAGE	ENERGY LOSS (volts)
	Ca film		
0.04	182	250	3.95
0.04	183	250	4.10
0.15	184	250	3.90
0.36	186	250	3.85
0.36	190	90	3.75
0.36	192	175	3.75
0.73	194	175	3.60
0.73	198	90	3.60
0.83	163	250	3.65
1.3	164	250	3.50
1.8	199	175	3.60
2.2	166	250	3.65
3.9	168	250	3.50
4.4	170	250	3.55
4.4	179	90	3.35
4.4	180	175	3.55
mean of 10 values			3.56
		or	3.55
	CaO film		
0.18	185	250	3.95
0.36	187	250	3.80
0.36	188	175	3.75
0.36	189	90	3.60
0.73	195	175	3.50
0.73	196	250	3.60
0.73	197	90	3.45
1.8	200	175	3.50
1.8	201	175	3.50
2.2	165	250	3.40
4.4	175	250	3.60
mean of 7 values			3.51
		or	3.50

THICKNESS	SER. NO.	VOLTAGE	ENERGY LOSS (volts)
	Ba film		
0.6	253	175	3.85
0.8	213	175	3.60
1.1	254	175	3.90
2.2	255	175	3.85
2.4	214	175	3.45
2.4	237	250	3.65
3.3	217	175	3.50
3.5	238	250	3.75
4.1	219	175	3.10
4.4	256	175	3.60
4.9	215	175	3.05
4.9	220	175	3.20
4.9	233	250	3.60
4.9	236	250	3.40
6.5	239	250	3.45
6.5	259	175	3.40
6.5	261	175	3.35
6.8	217	175	3.50
8.7	257	175	3.55
13	260	175	3.40
mean of 16 values			3.43
		or	3.45
	BaO film		
4.9	216	175	3.05
6.5	240	250	3.45
8.7	258	175	3.35
13	241	250	3.30
13	265	175	3.45
23	242	250	3.05
46	243	250	3.40
91	244	250	3.15
mean of 8 values			3.28
		or	3.30

TABLE III. *Energy losses for Ba targets.*

TARGET	THICKNESS	SER. NO.	VOLTAGE	ENERGY LOSS (volts)
Ba	4.1	219	175	1.80
	4.4	256	175	1.45
	4.9	215	175	1.75
	4.9	220	175	1.65
on BaO	6.5	249	175	1.70
	6.5	261	175	1.65
	8.7	257	175	1.70
on BaO	9.8	269	175	1.60
	13	260	175	1.75
	20	221	175	1.80
	49	263	175	1.45
	202	266	175	1.85
	202	267	175	1.50
		mean of 14 values		1.68
			or	1.70

region. The dotted curve shows the "aging" effect on the deposit of No. 239 and the extent to which BaO-maxima appear in the Ba-curves for higher energy loss. The Ag-peak shows up more strongly in No. 240 than in No. 239, indicating that the deposit becomes less opaque to the electrons when it is oxidized. Definite Ba-characteristics appear at a thickness about 4, although the enhancement of the Ag-peak can probably be noticed at a thickness of 2.

Fig. 14 shows energy loss curves for BaO on Ag. The oxide maxima appear for thicknesses less than the smallest one shown here.

The measured energy losses corresponding to the top of the Ag-peak and the peaks for Ca and Ba are collected in Table II and III.

DISCUSSION

In the cases where sharp maxima do not overlap, CaO, Ba and BaO on Ag, the results indicate that the excitation process responsible for the Ag-peak still takes place when the exciting (and scattered) electron has to penetrate a layer several atoms deep. If the penetration is of the same order in other materials as in these three substances, the distribution of small energy losses can not be determined entirely by the surface atoms, but must depend on the structure of the solid below. In that case a theory of these processes, based on the electronic model for the interior of a large crystal, would be expected to give a reasonable approximation to the actual situation.

It takes several layers of Ba before the 1.7-volt peak appears. The maxima for CaO are present

in their proper places for a thickness <1 and show no appreciable change (other than a gain in strength) as the thickness is increased. These maxima, however, occur for higher values of energy loss and they are rather broad, though distinct. Thus they are possibly chiefly determined by the nature of the atom or molecule in question, and only to a lesser degree by the forces from neighboring elements in the structure; the shifts in energy due to changes in the latter are probably unimportant compared to the width of these maxima. The situation appears to be different in the case of Ca. For a thickness <1 of this metal on CaO the sharp peak, which in Fig. 11 is superposed on the prominent Ag-maximum, shows up in the same position as for thick films. This may indicate, that a backing of CaO happens to act in just the same way on a single layer of Ca, as a backing of metallic Ca. If the distribution of energy losses results from the cooperation of several atom layers below the surface, one would in general expect a difference between the curve for a single layer and that for the thick metal. However, if we imagine a solid of N^3 atoms gradually built up from free atoms, so that first N atoms are brought together to form a string, then N of these strings lined up to make a layer and finally N layers piled up in the proper way—then the greatest change in the electronic energy levels would be expected to take place in the first step, and a relatively small change in the last.

That the surface layer in general influences the position of the energy loss peak for the underlying substance is evident from Table II. In each case, all the values for films above a certain thickness (as indicated by a horizontal line) were included in the mean. The spread of the individual values is fairly wide, but the shift from the pure Ag-value of 3.90 volts is evidently much larger than the probable error in the mean, which is of the order ± 0.05 volt. Since at least part of the peak with Ca-films represents a characteristic energy loss for this substance, there is definite evidence of the effect in question only for films of CaO, Ba and BaO, where the shift is of the same magnitude, but increasing in this order. It is believed that this represents a general shift in the energy levels of the underlying silver target, due to the forces exerted by the adsorbed film. This may be in the nature of a general change of the potential field in the target, or may result from a change in the interatomic distances, produced by the presence of the film. For "nearly free" electrons in a crystal the energy associated with a given set of quantum numbers, and therefore the energy difference for two states of given quantum numbers, is inversely proportional to the square of the lattice spacing. If the energy shift of 10–15 percent for the Ag-peak is to be accounted for in this latter way, it would indicate a linear expansion of 5–8 percent. A calculation by Lennard-Jones and Dent[18] for ionic crystals shows that the lattice spacing at the free surface should be smaller than that in the interior by an amount of the order of 5 percent. It is possible that a contraction of the same order exists at the surface of a metal. When this is covered by some other substance, so that it is no longer free, the lattice at the surface may effectively approach an interior lattice, with a corresponding increase in spacing.

In the preceding discussion it was assumed, that the evaporated deposits are spread uniformly over an area comparable with the apparent surface area of the target. This must certainly be true at the moment the deposits are formed, since there is no reflection. It is conceivable that patches of high concentration, separated by large bare regions, are subsequently formed by the process of surface migration. While this can not be disproved, it does not appear likely in view of some of the experimental results. Thus it is hard to understand the high yield of CaO-collisions with deposits <1, if the greater part of the surface is bare. The rate of migration over a bare surface can not be high at the temperature used. In some experiments the back of the target was exposed to the metal gun, so that a deposit several units thick should have been formed. The front side, however, when tested always gave the curve characteristic of Ag, showing the absence of migration round the edge. On the other hand the apparent electron

[18] Lennard-Jones and Dent, Proc. Roy. Soc. **A121**, 247 (1928).

transmission through thick BaO-deposits (Table II) may indicate the presence of thin regions, formed in the process of oxidation of thick Ba-films. That these regions are not bare is evidenced by the shift of the Ag-peak.

The distribution of energy losses appears to offer a new, sensitive tool for the study of surfaces and surface layers. If the substance of the film has a distribution curve reasonably different from that of the backing material, layers only a few atoms thick can be detected. This test appears to be somewhat more sensitive, and less likely to alter the conditions studied, than present electron diffraction methods employing high voltages.[19] In the case of Ca, the metal can be detected in a thickness decidedly <1 on a backing of the oxide. This is now being used to study the surfaces of thermionic emitters made from CaO and BaO. For the detection of small amounts of foreign material on a surface this method is probably never as sensitive as thermionic measurements, but in favorable cases it has one great advantage compared with these: it not only detects, it identifies.

[19] The diffraction beams obtained with single crystals at low bombarding voltages appear to be even more sensitive than the energy loss distribution to a small coverage of foreign material on the surface: Farnsworth, Phys. Rev. **49**, 605 (1936).

JULY 15, 1936 PHYSICAL REVIEW VOLUME 50

Theory of Inelastic Scattering of Electrons from Solids

E. RUDBERG AND J. C. SLATER, *Massachusetts Institute of Technology*

(Received May 9, 1936)

The general properties of the single electron wave functions for a crystal are discussed, and an expression derived for the probability of excitation by electron bombardment as a function of the two electronic levels involved in the transition. When the excitation energy is small compared with the energy of the bombarding electron, the relative transitions probabilities approach those for excitation by radiation. A detailed calculation has been carried out for the case of solid copper, for which the energy levels are now known from other work. Approximate wave functions —of the atomic type for the lower state, free-electron-like for the upper state—were used to evaluate the transition integrals. The calculated distribution curve for the inelastically scattered electrons is in fair agreement with the experimental curve in the region of small energy losses: the rapid rise from small values and the following two maxima exhibited by the experimental curve are all reproduced in their proper positions. The departures for higher losses are attributed to the fact that the free-electron-like wave functions used are not a proper approximation to the actual functions in this region.

THE problem of inelastic scattering of electrons in matter, early discussed for relatively fast electrons by Thomson[1] and others as a problem of atomic scattering, was treated very completely by Bohr[2] on the basis of classical electron theory. More recently, quantum theory has been applied particularly to the scattering by free atoms. Fröhlich[3] has given a wave-mechanical treatment of the inelastic scattering from metals, using a special Bloch-Sommerfeld model for the metal. He was able to deduce from this the characteristic features exhibited by the distribution of the low energy secondary electrons. In the present paper we consider the transition probabilities for electronic excitation on the basis of the general electron theory of solids. In experiments on inelastic collisions, the target is usually bombarded by a nearly parallel, homogeneous beam of electrons and the energy distribution is measured for those electrons which are scattered into a small solid angle about a definite fixed direction with respect to the target and the incident beam. Tests with polycrystalline targets have shown the energy distribution to be essentially independent of both this latter direction and of the angle of incidence. For this reason we have calculated the total probability of all

[1] J. J. Thomson, *Conduction of Electricity through Gases*, 343 (1903).
[2] N. Bohr, Phil. Mag. **25**, 10 (1913); **30**, 581 (1915).
[3] H. Fröhlich, Ann. d. Physik **13**, 229 (1932).

transitions with a given energy loss and arbitrary direction of the scattered electron, assuming an isotropic distribution in direction of the primary particles. It seems likely that the isotropic distribution of primary and scattered electrons here involved is actually nearly established inside the target as a result of the frequent processes of elastic scattering by the massive ions in the lattice.

While most experimental work in this field, for technical reasons, has been done on metallic conductors, the theory applies to solids in general. The present discussion divides into three main parts. In the first the wave functions and their properties are reviewed; in the second the general expressions for the transition probabilities are developed. In the third part approximate calculations are carried out for the case of copper, for which the energy levels are now known and approximate wave functions available, and the results are compared with experimental data.

1.

We wish to consider a collision in which a fast and a slow electron collide, the fast one losing a little energy and the slow one gaining it. The unperturbed problem is that in which each electron moves through a periodic potential field, representing the crystal, unaffected by the particular motions of other electrons. Each electron in this approximation is represented by a modulated periodic function of the type well known in the theory of metallic lattices:

$$\psi_{ak_0}(\mathbf{r}) = \exp\left[i\mathbf{k}_0\cdot\mathbf{r}\right]u_{ak_0}(\mathbf{r}), \tag{1}$$

u_{ak_0} having the periodicity of the potential field. We shall often use the equivalent Fourier resolution:

$$\psi_{ak_0}(\mathbf{r}) = \sum_p a(\mathbf{k}_0+\mathbf{K}_p)\exp\left[i(\mathbf{k}_0+\mathbf{K}_p)\cdot\mathbf{r}\right]. \tag{1a}$$

The stationary states are divided into a number of bands, and the index a represents a particular band. The vector $\mathbf{k}_0$ is different for the various states within a band. To satisfy Bloch's condition of periodicity,[4] the vectors $\mathbf{K}_p$ must form a discrete set, constituting what is called the reciprocal lattice in the $\mathbf{k}$-space. This reciprocal lattice is determined by the crystal structure, and is face-centered cubic for a body-centered cubic crystal, and *vice versa*. We can conveniently set up polyhedral cells in the $\mathbf{k}$-space, one surrounding each point of the reciprocal lattice, and of such a shape that they fill the $\mathbf{k}$-space completely without overlapping. We may imagine $a(\mathbf{k}_0+\mathbf{K}_p)=a(\mathbf{k})$ as a single-valued function of the continuous variable $\mathbf{k}$ in the $\mathbf{k}$-space; then the Fourier coefficients of a particular state $\mathbf{k}_0$ of the band a will be the values of a at the appropriate points $\mathbf{k}$ of the various cells, points reached from $\mathbf{k}_0$ by the translations $\mathbf{K}_p$. It can be shown that the square of the magnitude of one of these a's is proportional to the probability that the electron in question have a momentum $(h/2\pi)\mathbf{k}=(h/2\pi)(\mathbf{k}_0+\mathbf{K}_p)$, when in the state $(a, \mathbf{k}_0)$. For this reason the a's are sometimes called momentum eigenfunctions. It is evident that ψ_{ak_0} is a periodic function of $\mathbf{k}_0$; for if $\mathbf{k}_0$ is increased by one of the vectors of the reciprocal lattice, say $\mathbf{K}_q$, the whole lattice of points $\mathbf{k}_0+\mathbf{K}_p$ will be shifted back into itself. The same Fourier coefficients must then be chosen, leading to the same function as before, since by arranging the states according to bands we have made ψ a single-valued function of $\mathbf{k}_0$ within each band. At the same time the energy of this state will return to its initial value, so that the energy within a band may be regarded as a periodic function of the continuous variable $\mathbf{k}_0$ (or $\mathbf{k}$). Often, on account of this periodicity, it is convenient to restrict $\mathbf{k}_0$ to the central polyhedron of $\mathbf{k}$ space, but this is not always desirable.

If in particular the state a represents a free electron, its wave function is a plane wave, a constant times $\exp\left[i\mathbf{k}_1\cdot\mathbf{r}\right]$ (where $\mathbf{k}_1$ need not be in the central polyhedron in $\mathbf{k}$ space), so that only one a is different from zero. The energy of the free electron is $p^2/2m$, where p is its momentum. If we express energy in Rydberg units, distances in atomic units, this becomes simply k_1^2, where k_1 is proportional to the momentum. For the sake of uniformity, it is often convenient to represent the state of a free electron by a function in $\mathbf{k}$ space, and to make this single-valued one must break up the free electron states arbitrarily into bands. We could do this by deciding to group together all those states for which $\mathbf{k}_1$ was in a particular polyhedron in $\mathbf{k}$ space. For this particular band, $a(\mathbf{k}_0+\mathbf{K}_p)$,

[4] F. Bloch, Zeits. f. Physik **52**, 555 (1928).

regarded as a function $a(\mathbf{k})$ of the continuous variable $\mathbf{k}=\mathbf{k}_0+\mathbf{K}_p$, would be zero outside this polyhedron, constant within it. The energy, within the polyhedron, would be given by k_1^2, and by the periodicity property this would be repeated in every other polyhedron. This particular assignment, however, is not very reasonable when there is a small periodic perturbative potential. In this case, the wave function and energy will be slightly perturbed, and it can be shown that the periodic energy function which we have just discussed would be distorted by the introduction of certain planes of discontinuity, across which the energy would change discontinuously. Brillouin has shown[5] that it is much better to take unperturbed functions by setting up certain zones in $\mathbf{k}$ space. Such a zone is formed from parts of many polyhedrons, all having about the same energy and $|\mathbf{k}_1|$ value, but spread more or less uniformly about the surface of a sphere. These parts of polyhedrons are so chosen that they could be fitted together, by pure translations $\mathbf{K}_q$, to form a single polyhedron. We now assume a single energy band of the free electron to be one in which $a(\mathbf{k})$ is constant within one Brillouin zone, zero outside it. The energy within the Brillouin zone is given by k_1^2, and outside the zone it is a periodic function of $\mathbf{k}$, coming back to the same value at corresponding points of each polyhedral cell. The Brillouin zone is chosen in such a way that this determines the energy at each point of $\mathbf{k}$ space uniquely. The energy, however, is a rather complicated function of $\mathbf{k}$ within an individual polyhedron. The polyhedron, as we have said, can be divided into parts which could be displaced by $\mathbf{K}_q$ to form the zone, and within each of these parts the energy is represented by $|\mathbf{k}+\mathbf{K}_q|^2$, a parabolic function of $\mathbf{k}$; but this function changes from one part of the polyhedron to another, since the proper translation vector $\mathbf{K}_q$ is different for different parts. Because of this, the slope or gradient of the energy as a function of $\mathbf{k}$ changes discontinuously from one part of the polyhedron to another, though the function itself is continuous. This is because the direction of the vector $\mathbf{k}_1$ for the free electron, but not its magnitude or k_1^2, changes discontinuously with $\mathbf{k}$ in going from one part to another. When small perturbations appear, however, the discontinuous changes of slope are rounded off, and the energy function is a smooth one. It is this property that leads one to say that the Brillouin zone is the correct zone to use for describing the free electrons. The resulting type of function is the sort actually found in the wave functions of fast electrons in real lattices.

We shall have occasion to consider the orthogonality and normalization of our wave functions. The vector $\mathbf{k}$ as a matter of fact cannot take on arbitrary values in the $\mathbf{k}$ space, but only a discrete set lying on a sublattice much more closely spaced than the reciprocal lattice, such that the number of points within a single polyhedron of the latter equals the number of atoms in the crystal. Each state is capable of holding two electrons, one of each spin, so that each band can accommodate two electrons for every atom of the crystal. This sublattice has the property that, if $\mathbf{k}$ and $\mathbf{k}'$ are any two points of it, $\int \exp[i(\mathbf{k}-\mathbf{k}')\cdot\mathbf{r}]d\tau=0$, if the integration is carried over the whole crystal, unless $\mathbf{k}=\mathbf{k}'$, in which case the integral of course is V_0, the volume of the crystal. Now consider two wave functions, ψ_{ak_0} and $\psi_{bk_0'}$. The normalization and orthogonality conditions demand that

$$\int \sum_p \sum_q a^*(\mathbf{k}_0+\mathbf{K}_p)b(\mathbf{k}_0'+\mathbf{K}_q) \times \exp[-i(\mathbf{k}_0+\mathbf{K}_p-\mathbf{k}_0'-\mathbf{K}_q)\cdot\mathbf{r}]d\tau = \begin{cases} 1, \text{ if } a=b, \mathbf{k}_0=\mathbf{k}_0' \\ 0, \text{ otherwise.} \end{cases}$$

If $\mathbf{k}_0\neq\mathbf{k}_0'$, the property of the sublattice mentioned above immediately shows that the integral is zero, so that the only remaining case is that in which $\mathbf{k}_0=\mathbf{k}_0'$. This yields the conditions

$$\sum_p a^*(\mathbf{k}_0+\mathbf{K}_p)b(\mathbf{k}_0+\mathbf{K}_p) = \begin{cases} 0 \text{ if } a\neq b \\ 1/V_0 \text{ if } a=b. \end{cases} \quad (2)$$

For a plane wave, when only one a is different from zero, we at once see that the wave function is $V_0^{-\frac{1}{2}}\exp[i\mathbf{k}_1\cdot\mathbf{r}]$.

2.

Returning now to our problem, we assume the fast electron both before and after collision to

[5] L. Brillouin, *Quantenstatistik* (1931).

be moving fast enough so that it can be represented by a plane wave. If it has values $\mathbf{K}$ and $\mathbf{K}'$ before and after collision, its wave functions will be $V_0^{-\frac{1}{2}}\exp[i\mathbf{K}\cdot\mathbf{r}]$ and $V_0^{-\frac{1}{2}}\exp[i\mathbf{K}'\cdot\mathbf{r}]$. It is immaterial whether these happen to belong to the same Brillouin band or not. We assume the slow electron to have wave functions ψ_{ak_0} and $\psi_{a'k_0'}$ before and after collision, described by the Fourier components $a(\mathbf{k}_0+\mathbf{K}_p)$, $a'(\mathbf{k}_0'+\mathbf{K}_q)$, respectively. Let the total energy of the two electrons before collision be W, afterwards W', where $W=W'$ if conservation of energy holds. The unperturbed wave function of the two electrons together will be the product of the separate functions. Thus before collision, the function, including its time variation, is

$$e^{-2\pi iWt/h}\frac{1}{V_0^{\frac{1}{2}}}\exp[i\mathbf{K}\cdot\mathbf{r}_2]\psi_{a,\,k_0}(\mathbf{r}_1), \qquad (3)$$

where $\mathbf{r}_1$ is the coordinate of the slow electron, $\mathbf{r}_2$ that of the fast one. We treat the collision by the perturbation method of variation of constants. At time $t=0$ we assume that the Coulomb interaction $e^2/|\mathbf{r}_2-\mathbf{r}_1|$ commences to act. The solution of the time-dependent Schrödinger equation can then be expanded as a sum of terms

$$\sum_{a'k_0'K'} c(a'\mathbf{k}_0'\mathbf{K}'t)e^{-2\pi iW't/h}\times\frac{1}{V_0^{\frac{1}{2}}}\exp[i\mathbf{K}'\cdot\mathbf{r}_2]\psi_{a'k_0'}(\mathbf{r}_1). \qquad (4)$$

If we assume that at $t=0$ the only one of the coefficients c different from zero is the one multiplying the function (3), and that this is unity, perturbation theory leads to the value

$$c(a'\mathbf{k}_0'\mathbf{K}'t)=w^{-1}(1-e^{2\pi iwt/h})I, \qquad (5)$$

where $w=W'-W$, the difference in energy between the final and initial states, and

$$I=\frac{1}{V_0}\int\int\frac{e^2}{|\mathbf{r}_2-\mathbf{r}_1|}\exp[i(\mathbf{K}-\mathbf{K}')\cdot\mathbf{r}_2]\times\psi_{ak_0}(\mathbf{r}_1)\psi^*_{a'k_0'}(\mathbf{r}_1)d\tau_1 d\tau_2. \qquad (6)$$

The square of the modulus of $c(a'\mathbf{k}_0'\mathbf{K}'t)$ measures the probability of finding the system in the state $(a'\mathbf{k}_0'\mathbf{K}')$ at time t; for large values of t this will have appreciable values only near $w=0$, representing conservation of energy. $(\partial/\partial t)|c|^2$ measures the transition probability.

Let us consider first the interaction integral (6). Following Bethe,[6] we perform the integration first over the coordinates of the fast particle. Letting $\Delta\mathbf{K}=\mathbf{K}-\mathbf{K}'$, $\mathbf{r}=\mathbf{r}_2-\mathbf{r}_1$ and $\Delta\mathbf{K}\cdot\mathbf{r}=\Delta Kr\cos\theta$, we have

$$\int\frac{\exp[i\Delta\mathbf{K}\cdot\mathbf{r}_2]}{|\mathbf{r}_2-\mathbf{r}_1|}d\tau_2=\exp[i\Delta\mathbf{K}\cdot\mathbf{r}_1]\times\int_0^\infty\int_0^\pi r^{-1}e^{i\Delta Kr\cos\theta}2\pi r^2\sin\theta d\theta dr$$
$$=\exp[i\Delta\mathbf{K}\cdot\mathbf{r}_1]\cdot\frac{4\pi}{\Delta K}\int_0^\infty\sin(\Delta Kr)dr.$$

The last integral does not converge. To avoid this difficulty, Bethe averages over a small range in ΔK, and after integration makes this range approach zero. Another method is to replace the exact Coulomb potential $1/r$ by $e^{-\alpha r}/r$, perform the integration, and then let $\alpha\to 0$. Both methods give for the integral the value $1/\Delta K$. Hence

$$I=\frac{4\pi e^2}{(\Delta K)^2V_0}\int\psi_{ak_0}(\mathbf{r}_1)\exp[i\Delta\mathbf{K}\cdot\mathbf{r}_1]\psi^*_{a'k_0'}(\mathbf{r}_1)d\tau_1$$
$$=\frac{4\pi e^2}{(\Delta K)^2V_0}\sum_{p,q}a(\mathbf{k}_0+\mathbf{K}_p)a'^*(\mathbf{k}_0'+\mathbf{K}_q)\times\int\exp[i(\mathbf{k}_0+\mathbf{K}_p-\mathbf{k}_0'-\mathbf{K}_q+\Delta\mathbf{K})\cdot\mathbf{r}_1]d\tau_1. \qquad (7)$$

As mentioned above, the integral is zero unless $\mathbf{k}_0+\mathbf{K}_p-\mathbf{k}_0'-\mathbf{K}_q+\Delta\mathbf{K}=0$, or $\mathbf{k}_0'+\mathbf{K}_q-(\mathbf{k}_0+\mathbf{K}_p)=\Delta\mathbf{K}$, in which case it is V_0. If this condition is satisfied, we have

$$I=\frac{4\pi e^2}{(\Delta K)^2}\sum_p a(\mathbf{k}_0'+\mathbf{K}_p-\Delta\mathbf{K})a'^*(\mathbf{k}_0'+\mathbf{K}_p) \qquad (8)$$

or

$$I=\frac{4\pi e^2}{(\Delta K)^2}\frac{1}{V_0}\int_{V_0}\psi_{ak_0}(\mathbf{r}_1)\exp[i\Delta\mathbf{K}\cdot\mathbf{r}_1]\times\psi^*_{a'k_0'}(\mathbf{r}_1)d\tau_1=\frac{4\pi e^2}{(\Delta K)^2}\cdot\frac{1}{v_0}\int_{v_0}\psi_{ak_0}(\mathbf{r})\times\exp[i\Delta\mathbf{K}\cdot\mathbf{r}]\psi^*_{a'k_0'}(\mathbf{r})d\tau, \qquad (8a)$$

where v_0 is the volume of one lattice cell of the

[6] H. Bethe, Ann. d. Physik **5**, 325 (1930).

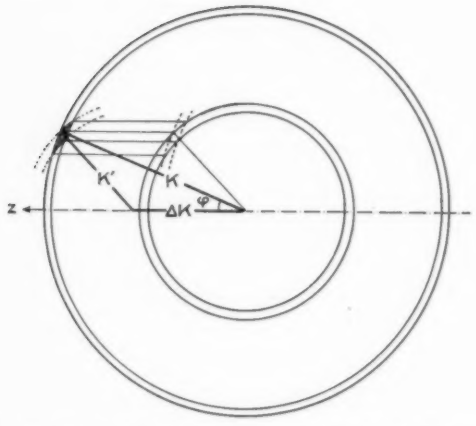

FIG. 1. Illustrating the possible transitions in the K space of the fast electron.

crystal and the last integration is over such a cell. The last step depends on the space periodicity of the wave functions (1). In (8) the quantity I, whose square determines the transition probability, is written as a sum of terms, of which each one represents a transition of the fast electron from momentum $\mathbf{K}$ to a value $\mathbf{K}-\mathbf{\Delta K}$, and an equal and opposite transition of the slow electron to momentum $\mathbf{k}'=\mathbf{k}_0'+\mathbf{K}_p$ from a value $\mathbf{k}'-\mathbf{\Delta K}$. This term has in the numerator the product of the amplitudes of the probabilities of finding the slow electron initially with momentum $\mathbf{k}'-\mathbf{\Delta K}$, when in the state $(a, \mathbf{k}_0'-\mathbf{\Delta K})$, finally with momentum $\mathbf{k}'$, when in the state $(a', \mathbf{k}_0')$, and in the denominator the square of the momentum change ΔK.

We are now ready to return to expression (5), giving the rate of transition from the initial to the final state. We really are not considering a single transition, however, but all possible transitions for which the fast electron originally has approximately a definite energy, but arbitrary direction, and the bound electron changes from state $(a\,\mathbf{k}_0)$ to state $(a'\mathbf{k}_0')$, gaining an amount of energy ϵ; we wish to compute $(\partial/\partial t)\sum|c|^2$ for all these transitions. Let Fig. 1 represent a plane section through $\mathbf{k}$ space (the reciprocal lattice and the sublattice are not shown) parallel to the vector $\mathbf{\Delta K}$, the z axis lying along the direction of $\mathbf{\Delta K}$. The points $\mathbf{K}$ where the incident electrons have nonvanishing Fourier components are assumed to lie in a spherical shell of thickness δK and radius K. This shell will not in general be entirely in one Brillouin zone, but will include parts of several zones. It contains a stationary state for each point of the sublattice, so that it is populated to a uniform density ρ. These incident electrons all have approximately the same energy K^2. A second shell, inside the first, includes all vectors $\mathbf{K}'$ for such states that the net energy increase of the system is between w and $w+dw$. Thus $K'^2+\epsilon=K^2+w$, and the thickness of the shell is $dw/2K'$. From the figure it will be seen that the number of primary electron states which can give rise to transitions in the range dw is $dn=\rho dv$, where dv is the volume generated by the small shaded area upon rotation around the z axis. Each of these states gives rise to one single transition. With the notations of Fig. 1,

$$dv=2\pi K\sin\varphi\delta K K d\varphi=\pi K\delta K d(-2K\cos\varphi)$$

and from the triangle

$$K^2+\Delta K^2-2\Delta K K\cos\varphi=K'^2$$

so that

$$d(-2K\cos\varphi)=(1/\Delta K)d(K'^2)=(1/\Delta K)dw$$

and

$$dn=\rho\pi K\delta K(1/\Delta K)dw. \tag{9}$$

The probability of all the specified transitions with a given ΔK is then

$$\frac{\partial}{\partial t}\left\{I^2\int_{-\infty}^{\infty}\left|\frac{1-e^{2\pi i w t/h}}{w}\right|^2\frac{\rho\pi K\delta K dw}{\Delta K}\right\}$$

$$=\frac{\partial}{dt}\left\{I^2\frac{\rho\pi K\delta K}{\Delta K}\frac{\pi^2 t}{h}\right\}=\frac{A}{\Delta K^5}J^2(\mathbf{k}_0',\mathbf{\Delta K}), \tag{10}$$

where $A=16\pi^5e^4\rho K\delta K/h$ and

$$J(\mathbf{k}_0',\mathbf{\Delta K})=\frac{1}{V_0}\int_{V_0}\psi_{ak_0}(\mathbf{r})\exp\left[i\mathbf{\Delta K}\cdot\mathbf{r}\right]\times\psi^*_{a'k_0'}(\mathbf{r})d\tau \tag{11}$$

or

$$J(\mathbf{k}_0',\mathbf{\Delta K})=\sum_p a(\mathbf{k}_0'+\mathbf{K}_p-\mathbf{\Delta K})a'^*(\mathbf{k}_0'+\mathbf{K}_p). \tag{11a}$$

This holds provided this type of transition is possible at all. From Fig. 1 it can be seen that transitions are possible only if

$$2K-\epsilon/2K>\Delta K>\epsilon/2K=\Delta K_m. \tag{12}$$

In the experiments on inelastic scattering from solids, the lower limit ΔK_m in (12) is usually

quite small compared with the spacing of the reciprocal lattice. For small values of ΔK the exponential factor in (11) can be expanded and higher terms than the second neglected, giving

$$J(\mathbf{k}_0', \Delta\mathbf{K}) = \frac{1}{V_0}\int_{V_0} \psi_{ak_0}(\mathbf{r})\psi^*_{a'k_0'}(\mathbf{r})\{1+i\Delta\mathbf{K}\cdot\mathbf{r}\}d\tau$$

$$= \frac{1}{V_0}\int_{V_0} \psi_{ak_0}(\mathbf{r})\psi^*_{a'k_0'}(\mathbf{r})d\tau + \frac{i}{V_0}\Delta\mathbf{K}\cdot\mathbf{L}$$

$$= \frac{i}{V_0}\Delta KL\cos(\Delta K, L), \quad (13)$$

the first term vanishing on account of orthogonality. Here

$$\mathbf{L} = \int_{V_0} \psi_{ak_0}(\mathbf{r})\mathbf{r}\psi^*_{a'k_0'}(\mathbf{r})d\tau, \quad (14)$$

the linear moment for this pair of states.

Given the upper state $(a', \mathbf{k}_0')$ there will be a number of lower states a from which transitions to this state can take place with a change of momentum of magnitude between ΔK and $\Delta K + d\Delta K$ and direction (of $\Delta\mathbf{K}$) within the solid angle element $d\omega$. This number is proportional to $\Delta K^2 d\Delta K d\omega$; each transition has a probability (10). The total probability of transition to the state $(a', \mathbf{k}_0')$ will therefore be proportional to

$$\int\int \frac{J^2(\mathbf{k}_0', \Delta\mathbf{K})}{\Delta K^3} d(\Delta K)d\omega, \quad (15)$$

the limits of integration being determined by the condition (12).

It turns out that, when small values of $\epsilon/2K$ are possible, the greater part of all transitions to the state $(a', \mathbf{k}_0')$ comes from those terms in the probability sum (15) for which ΔK is very near its minimum value ΔK_m. In that region we can use the expression (13) for J. We should therefore obtain a fairly good approximation to the actual distribution of small energy losses of the scattered primary electrons, by allowing each $\mathbf{k}_0'$ of an unoccupied state to receive transitions only from the occupied lower state with $\mathbf{k}_0 = \mathbf{k}_0'$, assigning to each such transition a probability proportional to

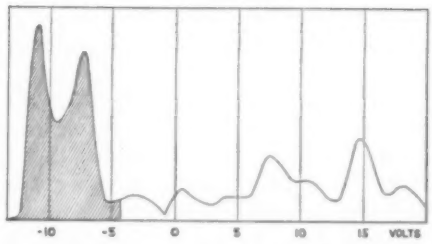

FIG. 2. Distribution in energy of the higher electronic levels in solid copper.

$$\int_0^{4\pi}\int_{\Delta K_m}^{\infty} \frac{L^2\cos^2(\Delta K, L)}{\Delta K} d(\Delta K)d\omega$$

$$= \tfrac{1}{3}\overline{L^2}\cdot\ln(2K/\epsilon) \quad (16)$$

or proportional to $\overline{L^2}$ for very high K where $\epsilon =$ the energy difference between the two states. This approximation must be restricted to the region of small energy losses. When ϵ is large, the approximation would introduce a considerable error, except for very fast primary electrons, because ΔK_m would not be small. The effect in the region of small losses is essentially to make the peaks and valleys in the calculated energy distribution appear sharper than they should be, because of the sharp selection rule by which we have replaced the distribution of transition probabilities in the sum (15). For high K and small energy losses, where the selection is quite strong, the transition probabilities for electronic excitation become practically proportional to those for optical absorption, both being determined by the square of the moment L.

3.

We shall apply the method outlined in the preceding section to the calculation of the energy losses on scattering from solid copper. The transitions involved in this case are from the partly occupied band deriving from the $3d$ of the free atom to the unoccupied states above it, of which the nearest ones correspond to the atomic $4s$. Fig. 2 shows the distribution in energy of the electronic states for solid copper;[7] the shaded area represents the part normally

[7] From an extension of the work by H. Krutter, Phys. Rev. **48**, 664 (1935); see also J. C. Slater, Phys. Rev. **49**, 537 (1936).

occupied by electrons. Since the energy levels are known for the different states of all the bands in question, the energy required for each particular "vertical" transition, $\mathbf{k}_0=\mathbf{k}_0'$, can be found. To calculate L from (14), however, and hence the weight $\overline{L^2}$ to be attached to each such transition, we have to find approximate wave functions for the lower and upper states involved.

The lower states a constitute a band of essentially bound electrons. If the solid is imagined as formed by bringing the free atoms together, the overlapping of neighboring atomic $3d$ functions will therefore be small for this band and Bloch's approximation to the wave functions can be used. From the general properties of the Bloch function it can readily be shown that its introduction to represent the lower state in (11) and (14) results in replacing ψ_{ak_0} in these equations by $(V_0/v_0)^{\frac{1}{2}}\psi_a$, where ψ_a is the corresponding atomic wave function, in this case $3d$. Thus for a given $\mathbf{k}_0'$, L is independent of ΔK, and $\overline{L^2}=L^2$. The integral over the finite volume V_0 of the entire crystal can then be replaced by an integral over all space, since the atomic function $\psi_a(\mathbf{r})$ has appreciable values only in a very small region of $\mathbf{r}$.

Actually the $3d$ band is 5-fold, as is the atomic d state, and accommodates 10 electrons per atom like the atomic state. This multiplicity arises from the five possible m values, 2, 1, 0, -1, -2 for a d state; in general, however, a single member of the band does not correspond to one particular m, but to a linear combination of all five. We shall only need the average L for all five components. To a good approximation the wave function for the mth component state of the $3d$ in copper may be written[8] as the product of a radial function $R(r)$ and the tesseral harmonic $T_l^m(\varphi, \theta)$ in the polar angles of $\mathbf{r}$ for $l=2$, each normalized to unity for the entire range of the variables:

$$\psi_a=R(r)\cdot\left\{\frac{(l-|m|)!}{(l+|m|)!}\right\}^{\frac{1}{2}}e^{im\varphi}P_l^{|m|}(\cos\theta) \quad (17)$$

with

$$R(r)=r^2(75.8e^{-6.29r}+4.236e^{-2.65r}+0.1185e^{-1.15r}). \quad (18)$$

The unoccupied upper states behave much like states of free electrons, at least those immediately above the $3d$ band, which may be said to derive from the atomic $4s$. One might therefore try to represent such a state by a free electron wave function $V_0^{-\frac{1}{2}}\exp[i\mathbf{k}_1\cdot\mathbf{r}]$, where k_1 could be determined by the condition that k_1^2 should equal the energy of the state in question, measured from a suitable zero, fixed by the location (in energy) of the lowest $4s$ level. This choice of function, however, does not satisfy the condition of orthogonality, and therefore makes (13) invalid; for the same reason it does not make J vanish for $\Delta K=0$, as the proper function should according to (11). To represent the upper state $(a', \mathbf{k}_0')$ one would therefore have to set up a function ψ_{k_1}, which is orthogonal to the atomic function ψ_a and yet which resembles the plane wave $V_0^{-\frac{1}{2}}\exp[i\mathbf{k}_1\cdot\mathbf{r}]$. Such a function can be found by using the expansion for a plane wave in a series of spherical harmonics, corresponding to s, p, d, f, $\cdots$ components, and by assuming that the function ψ_{k_1} equals the plane wave, without the d spherical harmonic:

$$\psi_{k_1}(r)=\frac{1}{V_0^{\frac{1}{2}}}\left(\frac{2\pi}{k_1r}\right)^{\frac{1}{2}}\sum_{\substack{l=0\\ l\neq 2}}^{\infty}(l+\tfrac{1}{2})i^lJ_{l+\frac{1}{2}}(k_1r)\times P_l(\cos\theta). \quad (19)$$

Here r, θ are spherical polar (zonal) coordinates, the polar axis being the direction of $\mathbf{k}_1$. Since the other harmonics are orthogonal to the atomic d function (17), this removes the difficulty of nonorthogonality. As far as the calculation of L is concerned, it really makes no difference whether we use the simple plane wave or the expression (19), since the contribution of the omitted d term to the moment is zero. Of course (19) is not quite correctly normalized for a crystal of finite size, because of the omission of the d term; we have ignored this. The resulting function resembles a plane wave in the region where the atomic function is appreciable, but is distorted particularly for fairly small values of r where the d spherical harmonic is relatively large. This is the type of behavior actually shown by the wave function for one of the higher states in the metal in the neighborhood of the lattice points. In $\mathbf{k}$ space the simple plane wave has a single component for its Fourier resolution at $\mathbf{k}=\mathbf{k}_1$.

[8] J. C. Slater, Phys. Rev. **42**, 33 (1932).

Actually, with the d term missing, the Fourier resolution of (19) will still have a large component at the point $\mathbf{k}_1$, but in addition there will be fairly small components at all possible points $\mathbf{k}_1+\mathbf{K}_q$ in $\mathbf{k}$ space. This in general is true of the correct wave functions of electrons in crystals, since they are never exactly plane waves. Of course our approximation is not very good. The correct function can be represented as a sum of s, p, d, $\cdots$ components, which are not very well approximated by the Bessel's functions, and the coefficients multiplying them are not well given by the coefficients in the plane wave expansion. Nevertheless, the general features are fairly well given by our assumption, in particular the way in which the wave-length of the oscillations of the function changes with energy, and this is the determining feature in the variation of $\overline{L^2}$ for different upper states, which is the fundamental thing we shall get from our calculations. In the approximation adopted here the atomic d state is degenerate, the five m values all corresponding to the same energy. We are therefore free to choose any orientation of the coordinate system in (17); we shall take a polar axis that coincides with the axis used in (19), the direction of $\mathbf{k}_1$. With this choice, the vector $\mathbf{L}$ is most conveniently determined from the matrix elements of $r\cos\theta$, $r\sin\theta e^{i\varphi}$, $r\sin\theta e^{-i\varphi}$, representing the three components of the vector $\mathbf{r}$, rather than x, y, z. The only terms in (19) which contribute anything to the moment are the p and f terms for $l=1$, 3, according to the same selection rules which apply for atoms. Furthermore, only the functions (17) for $m=\pm1$, 0 contribute anything, again in agreement with the selection rule for atomic transitions. For a case $m=0$, the only component of $\mathbf{L}$ different from zero is that of $r\cos\theta$; for $m=1$, that of $r\sin\theta e^{i\varphi}$, and for $m=-1$, $r\sin\theta e^{-i\varphi}$. The components have the following values:

$m=0$,

$$L_{r\cos\theta}=V_0^{-\frac{1}{2}}((4\pi i/5)M_p+(6\pi i/5)M_f),$$

$m=\pm1$,

$$L_{r\sin\theta e^{\pm i\varphi}}=V_0^{-\frac{1}{2}}(2\pi i\sqrt{6}/5)(M_p+M_f), \qquad (20)$$

where

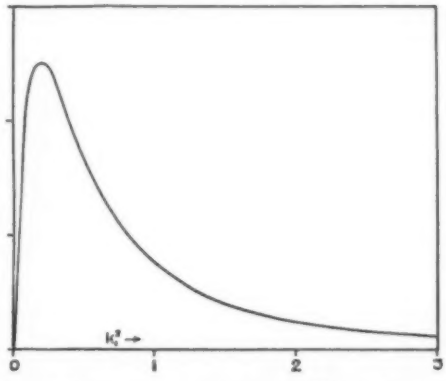

FIG. 3. The average square moment $\overline{L^2}$ as a function of the energy k_1^2 for the upper state.

$$M_p=\int_0^\infty r^3R(r)\left(\frac{2\pi}{k_1r}\right)^{\frac{1}{2}}J_{3/2}(k_1r)dr$$

$$=k_1\left\{0.0933\frac{1-0.01516k_1^2}{(1+0.0253k_1^2)^5}+2.218\right.$$
$$\left.\times\frac{1-0.0856k_1^2}{(1+0.1425k_1^2)^5}+21.35\frac{1-0.4545k_1^2}{(1+0.757k_1^2)^5}\right\}$$

and (21)

$$M_f=\int_0^\infty r^3R(r)\left(\frac{2\pi}{k_1r}\right)^{\frac{1}{2}}J_{7/2}(k_1r)dr$$

$$=k_1^3\left\{\frac{0.00378}{(1+0.0253k_1^2)^5}+\frac{0.5050}{(1+0.1425k_1^2)^5}\right.$$
$$\left.+\frac{25.85}{(1+0.757k_1^2)^5}\right\}.$$

To obtain $\overline{L^2}$ we square the L value for each m, add and divide by 5, since all five m values occur with the same weight in the band of d functions. The result is that

$$\overline{L^2}=\text{Const.}\,(M_p^2+\tfrac{3}{4}M_pM_f+(21/16)M_f^2). \qquad (22)$$

In Fig. 3, $\overline{L^2}$ is shown as a function of the energy k_1^2 of the upper state.

To construct the energy loss curve to be expected on this theory, we now proceed as follows. The energy range in question is divided into elements of the same size, $\Delta\epsilon$—in this case $\Delta\epsilon=0.01$ atomic unit. The transition probability $\overline{L^2}$ is evaluated for each one of a series of upper states, picked with a uniform spacing as regards $\mathbf{k}_0'$. The energy involved in the corresponding

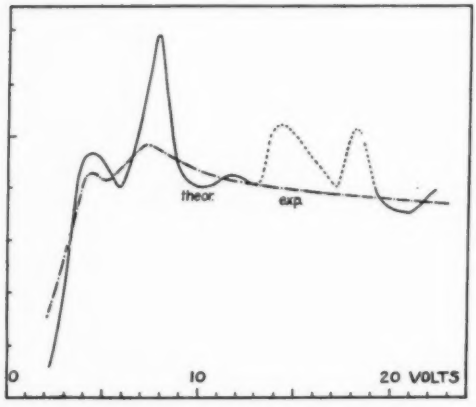

FIG. 4. Comparison of calculated and experimental distribution curves for the energy losses in solid copper.

vertical transition is determined from the tabulated energy levels for the different bands, and the $\overline{L^2}$ value listed in the column for the corresponding element $\Delta\epsilon$. The distribution curve for the energy losses is obtained by adding the $\overline{L^2}$ contributions in each such column. The result is shown in Fig. 4 together with the experimental curve,[9] which is given for comparison. The agreement in general is not unsatisfactory. Both curves start with low values for zero energy loss. In the theoretical case this arises from the small number of possible transitions with small energy losses. The curves then rise rapidly, each one coming to a peak at about 7 volts, preceded by a subsidiary peak at about 4.3 volts. At higher voltages both curves fall off. The agreement here, however, is less satisfactory, since the experimental curve falls off smoothly, while the theoretical one shows marked further peaks. In regard to these differences one may make the following comments. Our calculation of the number of transitions for a given energy difference has been based on actual calculations of energy levels, and should be fairly reliable. It takes account of the distribution of density within the band of *d* electrons and of the deviation of the excited electrons from free electrons. It is this part of the calculations in which the peaks are introduced. Those at 4.7 and 7 volts arise in a rather fundamental way: the band of *d* electrons shows specially large concentration of states at its two extreme energies, about 3 volts apart, and it is roughly these two concentrations which result in the two peaks. The two maxima at 14 and 18 volts also arise from these two concentrations, but here combined with peculiarities in the excited electron bands, about which there is much more uncertainty, on the basis of independent evidence. These peculiarities are connected with an especial concentration of excited *d* components in the stationary states for these bands. But in calculating the transition probability $\overline{L^2}$ we have represented the upper state by a free electron function without the *d* component. If, as it happens in this region, a large part of the correct wave function is actually *d*, our method must give too big values for $\overline{L^2}$, since *d*–*d* transitions should not occur. One thus infers that the proper transition probability to be used in this case should be small, which would tend to counteract the high concentration of transitions, thus reducing the violence of the fluctuations in this range. No such feature is present with the peaks at 4.7 and 7 volts. Of course our approximation to consider the transitions as vertical becomes increasingly poor for higher energy losses. Apart from this, one must bear in mind that there is no direct way of distinguishing between the effects produced by single and multiple impacts in the experimental curves. A fast electron may have two or more inelastic impacts before escaping from the metal. Since it tends to lose only a few volts on one impact, it would then emerge with something like double the energy loss in a single collision, tending to raise the number escaping with a moderate energy loss. Since the experimental distribution curves show very few electrons for quite small energy losses, however, it is fairly certain that the first two peaks represent single inelastic impacts.

[9] E. Rudberg, Phys. Rev., preceding paper.

Ionization of Gases by Collisions of Their Own Accelerated Atoms

ROBERT N. VARNEY, *University of California, Berkeley*

(Received May 7, 1936)

Neutral atom beans of noble gases of energies between 20 and 400 volts were produced by accelerating ionized atoms and then neutralizing the charges. The minimum energies which these neutral atom beams needed in order to ionize gas atoms by collision were determined. Neon, argon, krypton and xenon were found to ionize their own gases at energies about three times the actual ionization potentials. Attempts to observe ionization of one gas by neutrals of another have as yet given no results.

INVESTIGATION of the minimum energies necessary for ionization of noble gases by collisions of positive alkali ions[1] showed three significant results. If we remember that a singly charged positive alkali ion has identically the same number of electrons and electron structure as the noble gas atom next beneath it in the periodic table, the results were as follows: First, the experimentally observed ionizing energies had to be multiplied by a factor $m_a/(m_a+m_i)$, this factor being the fraction of the incident ion energy available for outside work after deduction of the amount necessary for the conservation of momentum (m_a and m_i are the masses of the gas atom and alkali ion, respectively). The reduced energy thus obtained for an ionizing collision between an ion having A electrons and an atom with B electrons was almost identical with that obtained when the ion had the B electrons and the atom had the A electrons. Secondly, the reduced ionizing energy was less when an ion and an atom had the same number of electrons than when they had different numbers. Thirdly, if other gases than the noble gases were ionized at all by positive alkali ions, the ionization could not have greatly exceeded one percent of the efficiency of K^+ in A.

The results of Beeck[2] and of Rostagni[3] on ionization efficiencies of noble gases by their own accelerated neutral atoms indicated that the determination of the actual inset energies for these processes might also yield valuable information, so the same method used for the alkali ion experiments was adapted to this problem.

The apparatus is illustrated in Fig. 1. Gas flows from a reservoir over the heated tungsten filament through a deep, narrow slit, 3 mm×0.5 mm (×4 mm depth), into a mercury pump. Electrons are accelerated from the filament toward the slit. If they produce any ions by collision in the field-free space inside the slit, these ions will be swept out at gas kinetic velocities by the flow through the slit. These ions are accelerated, as soon as they emerge from the slit, toward the negatively charged slit lying directly in line with slit one, and any electrons emerging from the first slit are stopped by this same potential.[4] Gas is allowed to stream out of slit number two into the pump orifice. The positive ions which were formed and accelerated before reaching slit two are now allowed to pass through the field-free space between slit two and aperture three. This region contains gas at about 10^{-2} mm Hg pressure. In these experiments, the same gas is used on both sides of the apparatus, so the positive ions are now traveling through their own gas. Kallmann and Rosen[5] first observed the fact that when ions, particularly noble gas ions, travel thus through their own gas, they are extremely efficient in picking off electrons from the relatively stationary neutral atoms, proceeding without change of velocity (speed or direction) as neutral atoms, and leaving behing a very slow positive ion which may be removed by a weak cross field. Beeck[6] has reported observing, under similar conditions to those described above, a beam of neutral atoms

[1] R. N. Varney, Phys. Rev. **47**, 483 (1935).
[2] O. Beeck, Ann. d. Physik **19**, 129 (1934).
[3] A. Rostagni, N. Cimento **11**, 34 (1934).

[4] This method appears to be due to Goldmann, Ann. d. Physik **10**, 460 (1931). It is obviously an excellent source of intense, monochromatic, positive gas ion beams. For details of the efficiency of this source see the reference above.
[5] Kallmann and Rosen, Zeits. f. Physik **61**, 61 (1930).
[6] O. Beeck, Ann. d. Physik **19**, 129 (1934).

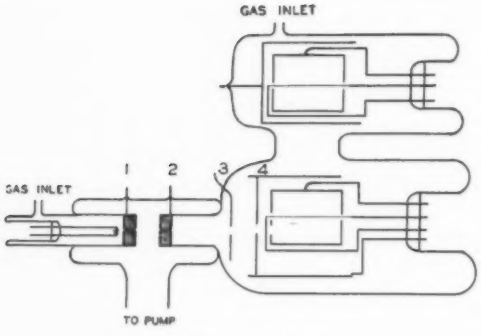

FIG. 1. Diagram of tube.

having 60 percent of the intensity of the original positive ion beam. No investigation was made in the present experiments to check the efficiency of neutralization, other than to observe that the intensity of positive ions emerging from the field-free space between slits two and three dropped off considerably when the gas was admitted. A final aperture number four having a large positive potential assured the stopping of any unneutralized positive ions emerging from aperture three, but this potential obviously has no effect on the neutral atom beam.

The neutral atoms, which are traveling with the energy they obtained as positive ions before neutralization, are now allowed to enter one of the space charge cylinders described at length in reference 1. Between this cylinder as anode and a heated tungsten filament as cathode flows a space-charge-limited electron current. If the neutral atom beam ionizes any gas atoms inside this cylinder, the positive ions thus produced are extremely effective in neutralizing the electron space charge, primarily because of their slower speed and more circuitous path. One positive ion has been observed to produce a space-charge effect equivalent to that of about 50,000 electrons.[1] The increased electron current reaching the anode as a result of this ionization by neutral atoms is measured by balancing out the ordinary electron current against that from a similar cylinder and filament arrangement outside of the path of the neutral atom beam.

The neon, krypton, and xenon used in these experiments were purchased in Pyrex flasks as 100 percent pure. The argon used was taken from a cylinder. Spectroscopic investigations at Berkeley indicated that impurities in argon from this tank did not exceed one percent, so aside from a liquid-air trap to remove water and mercury vapors, no further purification was attempted. In these experiments where the effect observed was large, traces of impurities are quite unimportant since the effects of impurities fall off directly with the pressure.

The ionization of each of these four gases by its own neutral atoms has been observed. The energies in electron volts at which ionization was observed to set in are given in column 1 of Table I.

These results are probably correct to within ± 2 volts except for Ne for which ± 4 volts is more accurate. Repeating the measurements under varying conditions, e.g., different pressures, different potential between filament and slit one, gave the same results usually well within the limits given above. The errors are only estimated and are based chiefly on possible doubts of the exact speed of the beam ions at the time of their neutralization.

Helium and nitrogen have been tried in this apparatus. Up to 400 volts no ionization was observed in either gas. Absolute measurements of ionization efficiency cannot be made with the space charge method, but it is estimated from the size of galvanometer readings that if the ionization of He in He had been five percent of that for A in A it could have been observed. In the case of N_2, it is possible that the experiments are confused by the fact that N^+ may have been formed rather than N_2^+ in the ion source, that N^+ might not neutralize very well in going through N_2 gas, and that barring the latter the N neutrals might not ionize N_2 by collision as well as N_2 neutrals might. A mass spectrograph is needed for further investigation of nitrogen ionization.

TABLE I. *Observed and reduced energies at which various gases are ionized by neutral atoms.*

	OBSERVED	REDUCED
Ne in Ne	74 volts	37 volts
A in A	48	24
Kr in Kr	40	20
Xe in Xe	35	17.5

The reduction factor mentioned above to correct the experimentally observed energies for energy losses in conserving momentum must also be applied in these cases. The factor is just one-half for all the cases in the table because the masses of the target and bullet atoms are equal. The resulting reduced values are given in column 2 of Table I.

These values are surprisingly low, being in each case only a few volts above the actual ionization potentials of the gases. The difference between these reduced potentials and the ionization potentials range from 16 volts for Ne to 6 volts for Xe. The results are almost half those for the alkali ions in the noble gases. This is not surprising because the previous results indicated the importance of electron configurations in this process. A collision, for example, between K^+ and A should be the same as between A and A except for the initially greater energy of the former combination with its positive charge which should make it more difficult to remove the electron.

The result for A in A agrees quite well with that obtained by Rostagni[7] at about 55 volts. Rostagni observed ionization of He by He neutrals, the efficiency being about ten percent that of A in A. Some doubt falls upon these results with helium, however, because ionization was indicated in the published curves at energies less than twice the electron ionization potential of He. Because of the conservation of momentum, which it seems certain must occur, only one-half of the energy of the incident atom at most is available in a collision between two such atoms of equal mass. Ionization by this mechanism should certainly cease therefore at a minimum value of twice the ionization potential. If the ordinates of Rostagni's He curve be multiplied by ten, the He curve coincides almost exactly with his A curve. This implies that the helium may have been contaminated with argon.

Further experiments have been conducted with a view to observing the ionization of one gas by the neutral atoms of another gas. Such experiments require one additional gas-filled chamber. In the present experiments the ions were neutralized in the same part of the tube in which they later ionized the gas. To observe the ionization of one gas by another, the ions must be neutralized in a chamber containing their own gas and then pass into one containing the different gas. Such an apparatus has been built and preliminary measurements made. So far, no ionization has been observed by argon neutrals in Kr or Xe up to 250 volts. The experiments are not final, however, because the complications in forming ions in one gas, accelerating them in vacuum, neutralizing them in more of the gas, and finally passing them into another gas result in such a drop in intensity as to cause some doubts over the sensitivity of the method. A in A was tested in the new arrangement and positive results were obtained. The efficiencies of A in Kr or Xe should thus not exceed 10 to 20 percent of those for A in A. Further experiments on ionization of one gas by accelerated neutral atoms of another may be reported at a later date.

[7] A. Rostagni, N. Cimento **11**, 34 (1934).

The Total Ionization of Nitrogen by Electron Collisions

GLADYS A. ANSLOW AND MADELEINE DEBLOIS WATSON, *Smith College*

(Received February 14, 1936)

Measurements of the total ionization produced in nitrogen by beams of electrons, whose homogeneity of velocity had been tested, have been taken for electron energies up to 1500 volts. The ionization was found to increase rapidly up to 75 volts, then less rapidly but linearly to 375 volts, for which there is a break in the ionization curve, indicating the onset of K electron ionization; the ionization again increases rapidly near 750 volts and after 1200 volts is found to increase less rapidly but linearly with increased electron energies. From determinations of the critical pressures for some of the electron energies used, the mean effective ranges, the thicknesses of the absorbing gas layer, have been measured and found nearly to obey the equation, $R_e = 0.07 + 1.88 \times 10^{-6} V^2$ cm at 1 mm pressure. By dividing the total ionization produced by electrons by their effective ranges as determined above the average total ionization per cm of absorbing gas layer has been calculated: the results show a maximum above 100 volts in the region found for primary ionization per cm by Compton and Van Voorhis and by Tate and Smith. The authors' curves show a second maximum at 750 volts, twice the ionization potential of the K electrons of nitrogen, these characteristics being similar to those discovered by the senior author in an earlier study of the total ionization produced in air. None of these curves agree with the results of Lehmann and Osgoode in the same field, the discrepancies being ascribed to differences in the shapes of the ionization chambers used and in the fields within them.

SINCE the publication by the senior author[1] of determinations of the total ionization produced in air by electron collisions involving energies up to 2250 volts, a limited number of experiments in the same field and involving the same range of electron energies have been reported, principally those of Lehmann and Osgoode,[2] who used a method nearly equivalent to that of Anslow[1] and accelerating voltages up to 1000 volts, and those of Langmuir and Jones,[3] who used an entirely different method and voltages up to 100 volts. The best known experiments with voltages in excess of 1000 volts are those of Eisl[4] and Buchmann,[5] in which the total ionization produced by swiftly moving electrons was measured, and those carried out by Williams and Terroux,[6] who examined tracks of fast β particles in a Wilson cloud chamber.

In general, ionization measurements have dealt with that portion of the ionization produced in the first fraction of the path of the moving electron, in which there is little chance of secondary collisions, some of the most outstanding measurements being those of Hughes and Klein,[7] Compton and Van Voorhis,[8] Smyth,[9] Bleakney,[10] and Tate and Smith.[11] Attention has been focused on this type of measurement largely because in comparisons of experimental results with the predictions of the collision theories of classical theory[12] and of wave mechanics[13] it has been difficult to evaluate the amount of energy lost in secondary and further collisions.

The necessity of examining the homogeneity of the velocity of the electron beam used in ionization experiments was pointed out and the homogeneity examined by Lehmann and Osgoode,[14] and later by Lawrence.[15] In the experiments, reported by the senior author[16] at the Washington meeting of the American Physical Society in April, 1934 and described in the present article, the homogeneity of the

[1] Anslow, Phys. Rev. **25**, 484 (1925).
[2] Lehmann and Osgoode, Proc. Roy. Soc. **A115**, 609 (1927); Lehmann, Proc. Roy. Soc. **A115**, 634 (1927).
[3] Langmuir and Jones, Phys. Rev. **31**, 357 (1928).
[4] Eisl, Ann. d. Physik **3**, 277 (1929).
[5] Buchmann, Ann. d. Physik **87**, 509 (1928).
[6] Williams, Mem. Man. Phil. Soc. **71**, 23 (1927); Proc. Camb. Phil. Soc. **24**, 315 (1928); Proc. Roy. Soc. **A125**, 420 (1929); **A128**, 459 (1930); **A130**, 310, 328 (1931); **A135**, 108 (1932); Williams and Terroux, Proc. Roy. Soc. **A126**, 289 (1930).
[7] Hughes and Klein, Phys. Rev. **23**, 111, 450 (1924).
[8] Compton and Van Voorhis, Phys. Rev. **26**, 436 (1925); **27**, 724 (1926).
[9] Smyth, Phys. Rev. **35**, 472, 478 (1930).
[10] Bleakney, Phys. Rev. **35**, 139 (1930); **36**, 1303 (1930).
[11] Smith, Phys. Rev. **36**, 1293 (1930); Tate and Smith, Phys. Rev. **39**, 270 (1932); **46**, 773 (1934).
[12] J. J. Thomson, Phil. Mag. **23**, 449 (1912); Bohr, Phil. Mag. **25**, 1 (1913); **30**, 581 (1915); Henderson, Phil. Mag. **44**, 690 (1922); Fowler, Proc. Camb. Phil. Soc. **21**, 521, 531 (1923); Phil. Mag. **47**, 257 (1924).
[13] Bethe, Ann. d. Physik **5**, 325 (1930); Massey and Mohr, Proc. Roy. Soc. **A132**, 605 (1931); **A139**, 187 (1933); **A140**, 613 (1933).
[14] Lehmann and Osgoode, Proc. Camb. Phil. Soc. **22**, 731 (1925).
[15] Lawrence, Proc. Nat. Acad. Sci. **12**, 29 (1926).
[16] Anslow, Phys. Rev. **45**, 750 (1934).

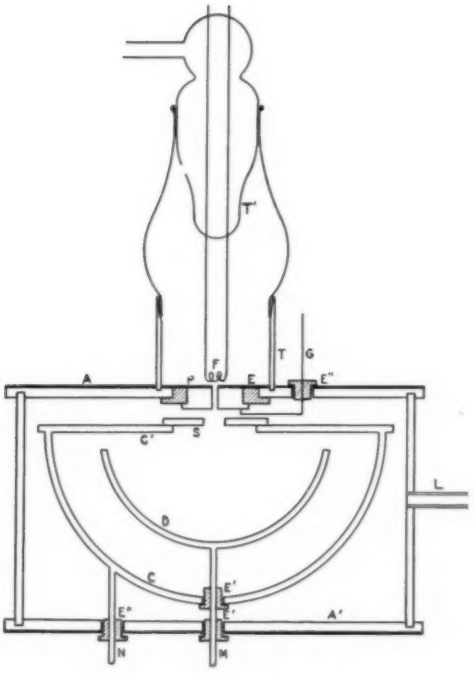

FIG. 1. The filament tube and ionization chamber.

electron beam was tested at various voltages and measurements taken of the total ionization in nitrogen produced by electron collisions with energies up to 1500 electron volts.

EXPERIMENTAL PROCEDURE

The pure nitrogen used in the experiment was produced according to the method of Waran,[17] by the action of dilute bromine water on dilute ammonium hydroxide, and was stored over phosphorus pentoxide, being allowed to leak through a capillary into the ionization chamber at a rate which maintained a nearly constant pressure in the chamber.

The filament tube and ionization chamber are shown in Fig. 1, being the same as described in the earlier paper[1] with one alteration, necessary for the measurements of the homogeneity of the beam; the opening at the center of the hemispherical ionization chamber was decreased to 4 mm by attaching to its lid an aluminum plate, *s*, with this circular opening, taking care to center the aperture opposite the end of the capillary of the anode through which the accelerated electrons passed just before they entered the ionization chamber. The capillary was 1.1 cm long and 0.2 mm in diameter and the distance between the lid of the chamber and the anode was adjusted to 2 mm.

The ionization measurements were also taken according to the compensation method described in the first experiment, the accelerating potential applied to the electrons being taken in all cases as that between the midpoint of the filament and the anode.

The homogeneity of the beam

To test the homogeneity of the electron beam the fraction of the electrons entering the ionization chamber with a velocity corresponding to the full drop of potential between the filament and the anode was determined by applying a retarding potential between the anode and the plate, *s*, of the ionization chamber, the pressure in the chamber being maintained by diffusion pumps at less than 10^{-4} mm before starting a run. In spite of the previous outgassing of the metal parts, the pressure usually rose during a run to about 2×10^{-4} mm with a consequent production of ions, which had to be considered in the interpretation of the measurements. The fraction of the electrons emitted by the hot filament and accelerated to the anode, which enter the chamber through the aperture, *s*, with velocities equivalent to the full drop of potential, was determined in the following manner, the electrical connections being shown in Fig. 2. Connecting the rods and chamber together and

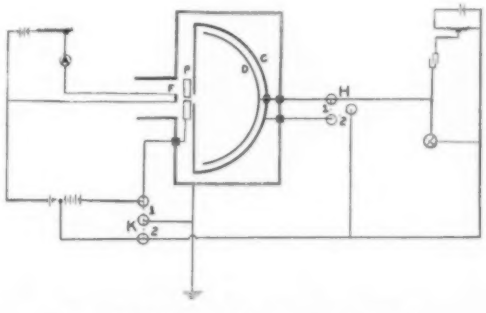

FIG. 2. Circuit used in homogeneity and ionization measurements.

[17] Waran, Phil. Mag. **42**, 246 (1921).

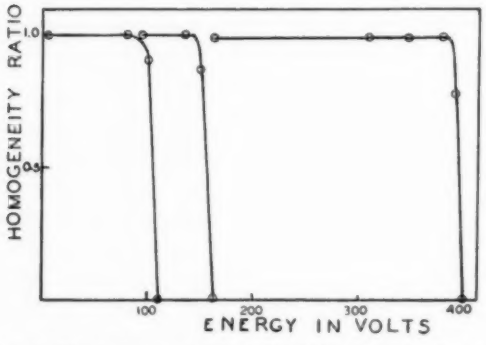

FIG. 3. The homogeneity ratio for 108, 165 and 400-volt electron beams.

to one pair of the quadrants of the electrometer by using the switch H in the position 1 shown in the diagram, and applying an accelerating potential between the filament and the anode while the shielding cylinder and anode were connected to earth by switch K, used in position 1, the number of electrons reaching the rods and chamber in a given time interval was measured by the rate of charging of the electrometer. Then, with switches K and H in positions 2 and 1, respectively, a retarding potential was applied between the anode and the chamber by keeping the anode at a positive potential and connecting the chamber and the rods to earth through the electrometer; the latter collected both the total number of electrons which entered the chamber with velocities in excess of that corresponding to the retarding potential and also the positive ions produced by collisions with molecules of the gas in the chamber; the negative ions and any secondary electrons emitted by the walls of the chamber were attracted to the anode. Finally, with switches K and H in positions 1 and 2, respectively, an equal retarding potential was applied between the anode and the chamber with the anode connected to earth and a negative potential on the chamber which had been disconnected from the rods. The rods, connected to earth through the electrometer, collected the electrons which entered the chamber, the negative ions formed, and the secondary electrons produced, while the positive ions flowed to the chamber.

The Townsend null method was used in taking the measurements, by balancing in turn the currents flowing to the electrometer by opposing currents from a potentiometer system, which charged a standard air condenser shunted to the

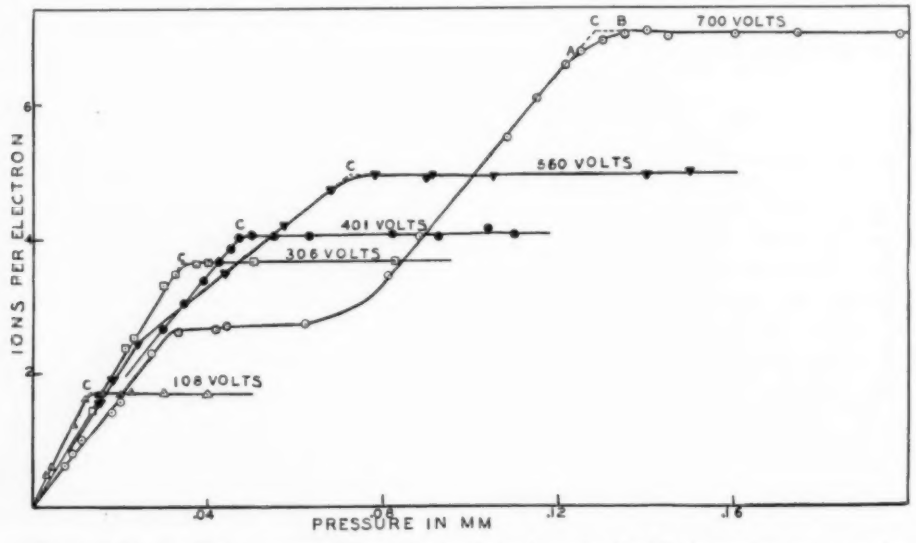

FIG. 4. Typical ionization-pressure curves. The ionization is proportional to the pressure up to a region of critical pressures, for which the thickness of the absorbing gas layer is nearly equal to the radius of the chamber. The pressure at C in a curve is used to calculate the mean effective range of the electrons. Total ionization values for a given energy are taken as the mean of the values on the horizontal part of the curve.

TABLE I. *Test of homogeneity of electron beams.*

Accelerating Potential	400 volts			165 volts		
Retarding Potential	310 volts			152 volts		
Pressure (10^{-4} mm)	1.2	0.8	1.5	1.8	1.1	2.0
r_1	0.74	0.97	0.60	0.59	0.61	0.67
r_2	1.24	1.00	1.44	1.17	1.16	1.06
Homogeneity ratio	0.99	0.98	1.02	0.88	0.88	0.86
	mean 1.00			mean 0.87		

electrometer. Since the pressure on the chamber side of the anode rose slightly and the electron beam varied somewhat in intensity during a set of readings, the three measurements to be made were taken in order and then the first and the second repeated in reverse order. If r_1 represents the ratio of the current due to the retarded electrons and the positive ions within the chamber to the unretarded electron current, and r_2 the ratio of the current due to the retarded electrons, the negative ions and the secondary electrons to the same unretarded electron current, the homogeneity ratio may be taken as the mean of r_1 and r_2. Two sample sets of results are given in Table I, and the values of the homogeneity ratios for different retarding potentials are shown graphically in Fig. 3 for 108, 165 and 400-volt electrons. It is evident that these electron beams possessed a high degree of homogeneity.

Ionization measurements

The ionization produced by electrons of a definite energy was measured exactly as in the previous experiment. For a number of voltages the ionization was determined for a series of gas pressures: typical ionization-pressure curves are shown in Fig. 4, and indicate that for small pressures a linear increase in ionization occurs with increasing pressure up to a region of critical pressures, for which the radius of the chamber is comparable with the mean thickness of the absorbing gas layer traversed; for still higher pressures the ionization is constant, this constant value giving the total ionization measurement. Determinations of the total ionization produced were made at frequent voltage intervals; the values obtained are given in the first two columns of Table II, and the results are shown in Fig. 5.

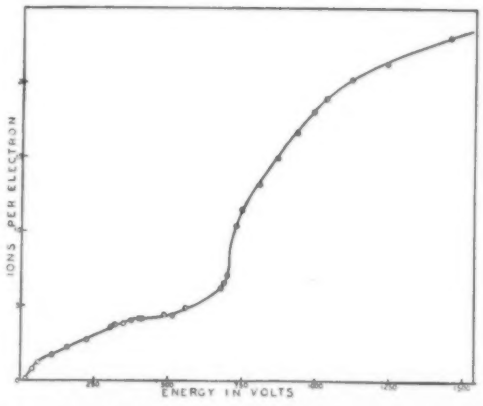

FIG. 5. Total ionization curve for electrons with energies ranging from 0–1500 volts.

It is evident that the total ionization produced is not a linear function of the energy of the colliding electron for energies less than 1000

TABLE II. *Measurements of total ionization produced by electrons of various energies in nitrogen.*

Energy (volts)	Ions Per Electron	Effective Range at 1 mm Pressure	Ions Per Electron Per cm of Effective Range at 1 mm Pressure
22	0.11	*0.071	1.55
42	0.73	0.073	9.95
60	1.20	0.077	14.2
108	1.72	*0.092	18.7
165	2.25	*0.123	18.3
225	2.78	0.165	16.9
306	3.59	*0.241	14.6
321	3.78	0.264	14.3
350	3.85	0.316	12.3
376	4.06	0.335	12.1
386	4.18	0.350	11.9
401	4.17	*0.372	11.2
412	4.20	0.398	10.5
487	4.46	*0.513	8.6
514	4.39	0.574	7.65
560	4.88	*0.640	7.40
680	6.20	0.939	6.60
690	6.52	0.960	6.79
700	7.05	*0.975	7.23
732	10.4	1.097	9.66
754	11.5	1.110	10.40
804	13.2	1.255	10.52
870	15.1	*1.470	10.17
935	17.1	1.693	10.10
990	18.3	*1.880	9.65
1030	19.2	2.053	9.36
1100	19.5	2.275	8.54
1120	20.0	2.348	8.52
1240	21.2	*2.732	7.71
1460	23.1	*3.618	6.36

Note. The values of the effective range marked * were obtained from the ionization-pressure curves, the others by interpolation from the range curve in Fig. 8.

volts, contrary to the results of Lehmann and Osgoode;[2] it is believed that this lack of agreement can be attributed to two important differences in the experimental conditions. Firstly, Lehmann and Osgoode used a cylindrical rather than a hemispherical ionization chamber. In the former type of chamber the electrons deflected in primary collisions may hit the sides of the vessel before their energy is exhausted, since their ranges at the pressures used are greater than the radius, though less than the length of the cylindrical vessel. In the hemispherical type of chamber these deflected electrons spend all their energy in collisions before reaching the sides of the chamber. Secondly, in the experiments of the authors the anode was kept at earth potential, thus maintaining a field free region within the ionization chamber; whereas, in the other experiments the filament was at earth potential and the anode at a positive potential, thus causing a retarding field between the anode and the ionization chamber, which decreased the energy of the electrons passing through it. It is believed that these variations in the shape of the ionization chamber and in the field within it are mainly responsible for the discrepancies between the total ionization and the range curves here reported and those of Lehmann and Osgoode.

Fig. 5 indicates that the ionization of nitrogen sets in at about 17 volts, the ionization potential of the nitrogen molecule,[18] increases rapidly to about 75 volts, then less rapidly but linearly up to 375 volts, the ionization potential of the K electrons[19] of nitrogen, at which there is a sudden decrease in the number of ions produced because of the large amount of energy expended in releasing one of the K electrons, leaving less energy available for the secondary collisions. The fact that a bend in the ionization curve is to be expected has been emphasized by Darrow,[20] and probably is more evident in total ionization measurements, which include the effects of secondary collisions, than in primary ionization experiments, in which these are eliminated. The break has never been recognized in any of the latter experiments.

[18] Smyth, Proc. Roy. Soc. **A104**, 121 (1923).
[19] Mohler and Foote, Sci. Papers Bur. Standards **17**, 471 (1922).
[20] Darrow, *Electrical Phenomena in Gases* (1932), p. 43.

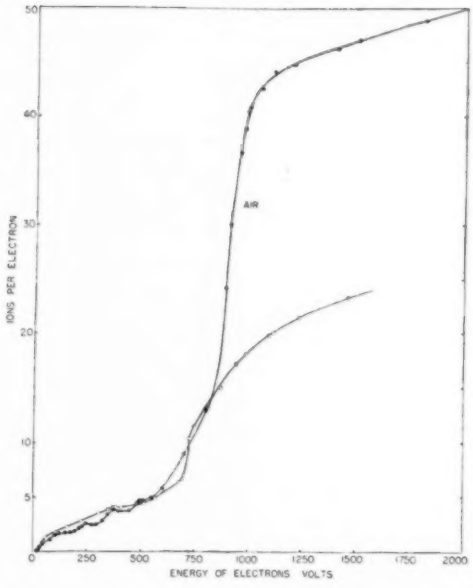

FIG. 6. Total ionization curve for nitrogen and air. Both show breaks at 375 volts and similar rapid increases in ionization near 750 volts.

As the energy of the accelerated electron approaches that equal to twice the ionization energy of the K electrons, the probability of this type of ionization increases rapidly, and finally a second linearity is approached at and beyond 1200 volts.

It is interesting to note that these features were some of the characteristics of the total ionization curve for air given in the previous paper, and which is shown with the nitrogen curve in Fig. 6; the breaks at 250, 375, and 495 volts in the air curve were attributed to argon, nitrogen, and oxygen, respectively, since these are their ionization potentials.[21, 19, 22] The rapid increase in the ionization of air near 1000 volts was attributed in the earlier paper to the ionization of oxygen.

Range calculations

Since the path of an electron which has suffered multiple collisions is tortuous and in three dimensions, the mean depth of the absorbing gas layer, known as the effective range, is consider-

[21] Int. Crit. Tab. **6**, 71–72 (1929).
[22] Kurth, Phys. Rev. **18**, 461 (1921).

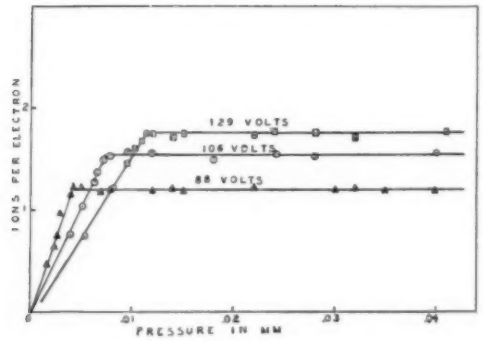

FIG. 7. Ionization-pressure curves for small energy electrons in air.

ably smaller than the actual length of path traversed by the electron. In a separate paper the senior author[23] has given the derivation of a formula relating these quantities, and reported numerical calculations of the actual ranges, made by suitably choosing constants which appear in Bethe's[13] equations for the scattering of electrons in both elastic and inelastic collisions.

In this experiment a mean value of the effective range of the electrons may be obtained from an examination of the region of critical pressures in their ionization-pressure curve. Those electrons, for which the fraction of energy lost in collisions is consistently large, are scattered most; when the pressure in the ionization chamber is such as that at the point A in the curve for the 700-volt electrons in Fig. 4, the ends of their paths must be on the surface of the ionization chamber and the radius of the chamber will equal the effective range of these electrons. Similarly, the point B on the same curve represents a pressure for which the radius of the vessel is very nearly equal to the effective range of those electrons and for which scattering is a minimum and straggling a maximum. For some intervening pressure the radius of the chamber must equal the mean value of the effective range of the electrons in the beam, such that half the electrons have effective ranges in excess of this value and the others less. Since the region of critical pressures is very narrow for the lower energy electrons and amounts to less than ten percent of the mean pressure within the critical region for the highest energy electrons used, a mean value of the effective range of the electrons in a beam may be obtained by calculating the pressure, C, at which the linear portions of its ionization-pressure curve intersect: multiplying this pressure in mm by the radius of the chamber gives the effective range in cm at 1 mm pressure. The error involved in such a determination cannot be large for energies somewhat in excess of those used in this experiment, for an inspection of the

[23] Anslow, Phys. Rev. **49**, 480A (1936).

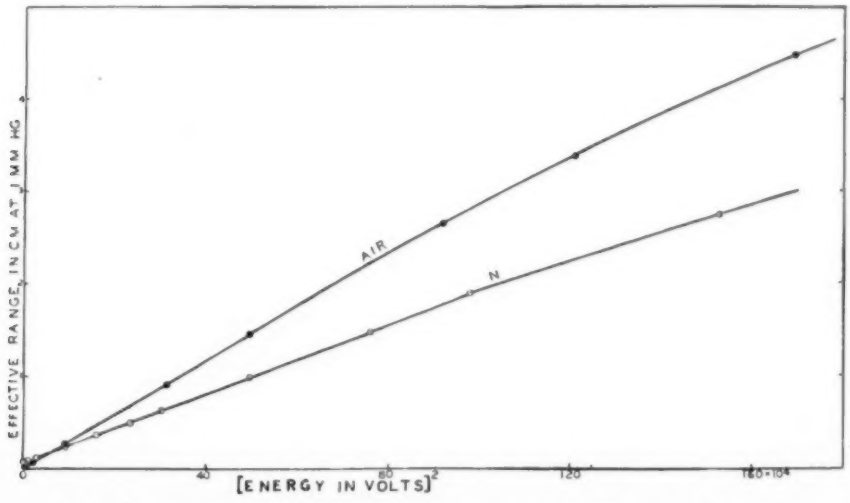

FIG. 8. Effective range *vs.* voltage relation for energies up to 1500 volts in N_2 and air.

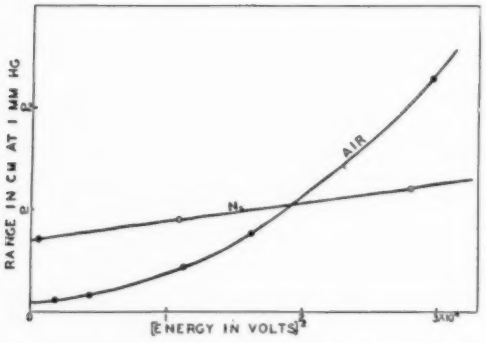

FIG. 9. Effective range *vs.* voltage relation for energies up to 175 volts in N_2 and air.

similar curves obtained by Buchmann[5] for electrons with energies from 4–13 kv and by Eisl[4] for energies from 9.8–3.6 kv indicate that the region of critical pressures remains narrow up to at least 20,000 volts. The region narrows down to practically a single pressure for beams with energies less than 150 volts, as can be seen in Fig. 7, where are plotted three of a series of curves obtained in a detailed study of the range of such electrons in air, measured since the publication of the previous paper. Since electrons with these energies have ranges scarcely twice the mean free path of electrons in the gas, they participate in only one or two collisions and those in a single beam must suffer practically equal scattering. Hence for these low energy electrons a single critical pressure should be anticipated.

The effective ranges thus obtained were plotted against the square of their energy in volts for energies up to 1500 volts, the results being shown in Fig. 8, together with the similar result obtained in the previous experiment for air. In Fig. 9 the same is shown for energies less than 175 volts. It is evident that there is a fair linear relation between the effective range of the colliding electron and the square of the energy expended for ranges less than 2 cm at 1 mm pressure, with a slight falling off in the range values for higher energies, and that there is a deviation from this linearity for small energy collisions in air. The empirical equation, derived from the lower portion of the curve in Fig. 8, between the mean effective range, R_e, measured in cm at 1 mm pressure, and the electron energies, measured in electron volts, V, is for nitrogen

$$R_e = 0.07 + 1.88 \times 10^{-6} V^2. \qquad (1)$$

The slope of this curve, 1.88×10^{-6}, decreases with the higher energies, and probably approaches the value obtained by Williams[24] for slow β-

[24] Williams, Phil. Mag. 2, 1109 (1926).

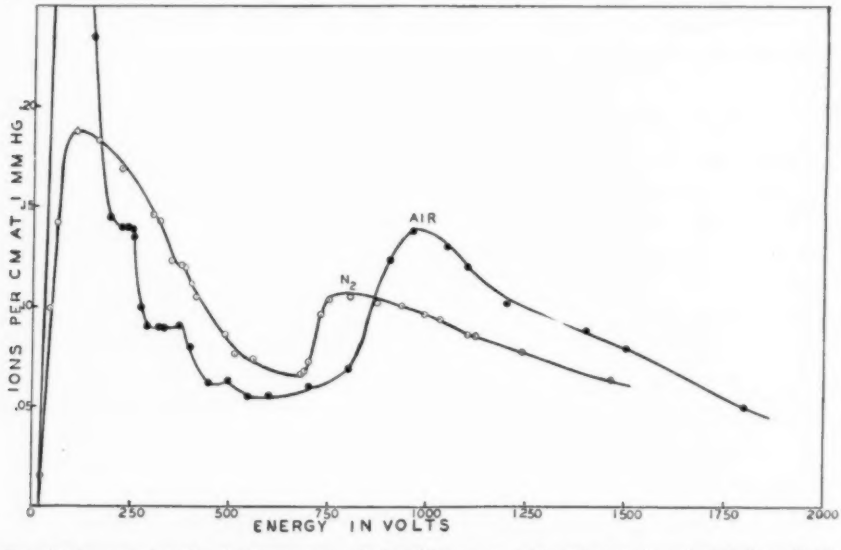

FIG. 10. Average total ionization per cm of absorbing gas layer for N_2 and air, calculated by dividing total ionization measurements by the mean effective range of the ionizing electron.

particles in nitrogen, which reduced to 1 mm pressure, is 1.54×10^{-6}. The effective ranges of the various electron beams, estimated from this curve, are given in the third column of Table II.

Ionization per cm of absorbing gas layer

The average ionization produced per cm of the absorbing gas layer was obtained by dividing the experimentally determined value of the total ionization by the effective range of the colliding electron. The values obtained are given in the last column of Table II and plotted against the energy of the accelerated electrons in volts in Fig. 10, together with the same for air as given in the first paper, the results for small voltages having been calculated from the later determinations of the range in air. It is seen that in the curve for nitrogen a maximum value of the average ionization per cm of the effective range occurs between 100 and 150 volts, a break at 375 volts, and a second maximum at 750 volts, this latter maximum being at twice the ionization potential of the K electrons of nitrogen. In the air curve this maximum came at twice the K ionization potential of oxygen.[1]

In Fig. 11 the characteristics of the nitrogen curve are compared with the well-known curves for primary ionization per cm of Compton and Van Voorhis[8] and of Tate and Smith.[25] At the low pressure used in these experiments not more than one collision is probable in the electron path, and the thickness of the absorbing gas layer is identical with the actual distance traversed by the electron. In the figure there are also given graphs of the results obtained in Kossel's[26] early experiment and values calculated by the present authors from the total ionization and range curves published by Lehmann and Osgoode.[2] It is evident that both total and primary ionization measurements indicate a

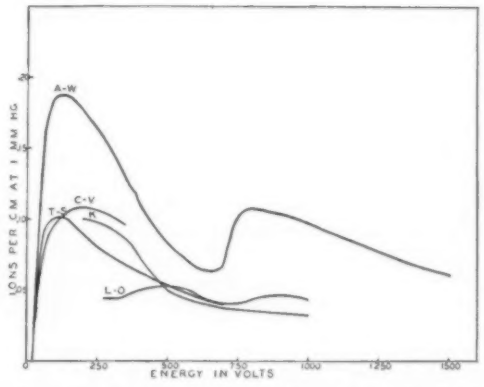

FIG. 11. Average total ionization per cm of effective range compared with primary ionization per cm results for actual range of Compton and Van Voorhis (C–V), Tate and Smith (T–S), Kossel (K), and average total ionization per cm of effective range calculated from Lehmann and Osgoode's determinations (L–O).

maximum probability of ionization for energies slightly in excess of 100 volts, but that the second maximum at 750 volts does not appear in any of the curves except that of the authors. In the experiments of von Hippel[27] with mercury and Funk[28] with sodium and potassium similar maxima have been located at approximately twice the ionization potentials involved. The form of the Lehmann and Osgoode curve is at almost complete variance with the general type of curve obtained in these experiments, and strengthens the belief of the authors that the Lehmann and Osgoode results were seriously affected by the shape and the field within their ionization chamber.

A reduction of the authors' results to the ionization per cm of the actual range, together with a comparison with the values predicted by Bethe's theory may be presented in a future communication by the senior author.

[25] Tate and Smith, Phys. Rev. **39**, 270 (1932).
[26] Kossel, Ann. d. Physik **37**, 393 (1912).
[27] von Hippel, Ann. d. Physik **87**, 1035 (1928).
[28] Funk, Ann. d. Physik **4**, 149 (1930).

A Theoretical Analysis of the Operation of Ionization Chambers and Pulse Amplifiers

E. A. JOHNSON AND A. G. JOHNSON, *Department of Terrestrial Magnetism, Carnegie Institution of Washington*

(Received April 28, 1936)

The noise level of a system composed of an ionization chamber and a linear amplifier is calculated as a function of the input circuit parameters and the characteristics of the amplifier. The frequency spectrum of a pulse caused when an ionizing particle passes through the ionization chamber is also calculated as a function of the circuit parameters and the collection time. From this analysis the shape of the output pulse is calculated as a function of the frequency characteristic of the amplifier. It is concluded that the cut-off frequencies of the amplifier for optimum pulse shape and amplitude depend upon the collection time. The signal to noise ratio is calculated for the case of optimum pulse shape. By proper choice of tubes it is shown that it should be possible to count 100 ion pairs and that for a 1-cm deep chamber and fast protons the signal to noise ratio should be 38 : 1.

MOST of the information available concerning the design of ionization chambers and their associated circuit and pulse amplifier have been of a strictly empirical nature. It is the purpose of this analysis to indicate more definitely the important factors which limit the sensitivity of this type of detector in the investigation of the products of nuclear disintegrations. The problem is essentially one of determining the effect of circuit parameters and the characteristics of the amplifier used upon the signal to noise ratio.

In the design of an amplifier for the measurement of voltages whose amplitude is of the same order of magnitude as the noise of the first tube and its associated input circuit, the ratio of signal voltage to noise voltage depends upon their relative frequency spectrum and the transfer characteristics of the amplifier. In order to design an amplifier for the measurement of pulses from an ionization chamber, therefore, it is necessary to determine the frequency spectrum of a pulse, and the frequency spectrum of the noise from the input circuit and first tube. Before considering the limitations imposed in practice by tube characteristics, these two frequency spectra will be determined.

There are three principal sources of noise[1] from a circuit of the type shown in Fig. 1 which is the equivalent circuit of an ionization chamber and the first stage of the amplifier. The noise is due to thermal noise from the resistance, shot noise from the grid current in the resistance-capacity network, and the zero noise of the tube. In Fig. 1, C is the combined capacity of the ionization chamber, tube, and wiring, and R is the resistance in the grid circuit due to the internal dynamic grid resistance and any external grid resistance.

In the analysis that follows an ideal amplifier is assumed which has constant gain between the frequencies f_1 and f_2 and zero gain outside of this band, and no phase distortion in the band. Such an amplifier is difficult to obtain in practice, but the conclusions reached will be only slightly affected by the approximation.

Calculation of Noise Level

The thermal noise from the input circuit due to thermal agitation of charge in the resistance is given by

$$\overline{E_r}^2 = 4kTR\int_{f_1}^{f_2} df/(1+4\pi^2R^2C^2f^2), \qquad (1)$$

where K is Boltzmann's constant, T is the absolute temperature. By integrating

$$E_r^2 = (4kT/2\pi C)\tan^{-1} [2\pi RC(f_2-f_1)/(1+4\pi^2R^2C^2f_2f_1)]. \qquad (2)$$

The shot noise in the input circuit due to statistical fluctuations in the grid current I_g of the first tube is given by

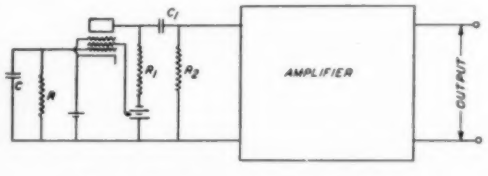

FIG. 1. Input stage of pulse amplifier.

[1] G. L. Pearson, Physics **5**, 233 (1934).

$$\overline{E_s}^2 = 2eI_gR^2\int_{f_1}^{f_2} df/(1+4\pi^2R^2C^2f^2), \quad (3)$$

$$E_s^2 = (2eI_gR/2\pi C)\tan^{-1}$$
$$[2\pi RC(f_2-f_1)/(1+4\pi^2R^2C^2f_2f_1)], \quad (4)$$

where e is the electronic charge and $I_g = |I+| + |I-|$ where $|I+|$ and $|I-|$ are the absolute magnitude of positive and negative components of grid current. From (2) and (4) we obtain the relation for $T = 300°\text{K}$,

$$\overline{E_s}^2 = (19.4I_gR)\overline{E_r}^2. \quad (5)$$

The third source of noise is due to the zero noise level in the tube itself and is given by:

$$\overline{E_t}^2 = 4kT\int_{f_1}^{f_2} R_t df \quad (6)$$

$$= 4kTR_t(f_2-f_1), \quad (7)$$

where R_t is the resistance which, if placed in the input of the first tube, would give the same reading in the output meter of the amplifier if there were no noise from the tube itself. The total mean square voltage is then given by

$$\overline{E_n}^2 = \overline{E_s}^2 + \overline{E_r}^2 + \overline{E_t}^2,$$

$$E_n^2 = 4kT\{(1/2\pi C)\tan^{-1}$$
$$[2\pi RC(f_2-f_1)/(1+4\pi^2R^2C^2f_1f_2)]$$
$$\times[1+19.4I_gR]+R_t(f_2-f_1)\}. \quad (8)$$

The case of interest to us is when $2\pi f_2RC > 2\pi f_1RC \gg 1$ and for this condition Eq. (8) reduces to

$$\overline{E_n}^2 = 4kT(f_2-f_1)$$
$$\times[R_t+(1+19.4I_gR)/RC^24\pi^2f_1f_2]. \quad (9)$$

If we plot $\overline{E_n}^2$ *vs.* R from Eq. (8) we obtain a curve of the type shown in Fig. 2 where the circuit constants assumed are: $f_1 = 500$ c.p.s., $f_2 = 5000$ c.p.s., $C = 10^{-11}$ farad, $I_g = 10^{-10}$ ampere and $R_t = 20{,}000$ ohms.

We see that when R is very small the zero noise from the tube itself predominates and determines the noise level. As R is increased the thermal noise increases and is the determining factor and would increase indefinitely except for

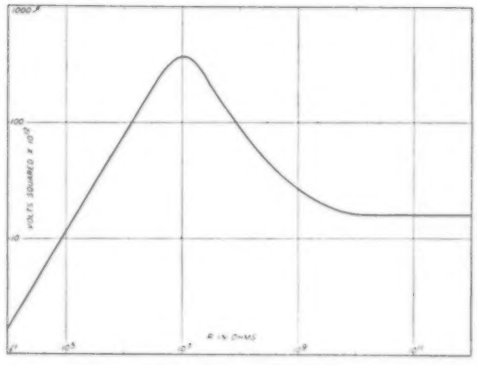

FIG. 2. Input noise as a function of input resistance.

the shunting effect of the capacity C. Because of the shunting effect of C which becomes more effective as $R\omega C$ is large compared to unity, the thermal noise decreases and the total noise would again be reduced to the noise level of the tube alone were it not for the fact that the shot noise due to the grid current becomes of importance. The shot noise decreases with an increase in R to an asymptotic value and the minimum noise is given by

$$\overline{E_n}^2 = 4kT(f_2-f_1)[R_t+19.4I_g/4\pi^2C^2f_1f_2] \quad (10)$$

and is determined only by the zero noise of the tube, by its grid current and by the parameters C, f_1, and f_2 and does not depend upon R if R is sufficiently large.

From (10) we conclude that the noise level is made a minimum by choosing a tube with as low values of grid current and of zero noise as possible and making R as large as possible. The parameters f_1, f_2, and C also determine the noise level but we shall see that they are fixed by the requirements of pulse definition.

FOURIER ANALYSIS OF PULSE

The voltage on the grid of the first tube due to the discharge of the ionization chamber is given by[2]

$$E_g = 0, \qquad -\infty < t < 0,$$
$$E_g = (Rq/\lambda)(1-\epsilon^{-t/RC}), \qquad 0 < t < \lambda, \quad (11)$$
$$E_g = (Rq/\lambda)(1-\epsilon^{-\lambda/RC})\epsilon^{-(t-\lambda)/RC}, \quad \lambda < t < +\infty,$$

[2] G. Ortner and G. Stetter, Zeits. f. Physik **54**, 449 (1929).

where q is the charge collected on the plate of the ionization chamber connected to the first stage of the amplifier, due to the passage of a single ionizing particle through the chamber, and λ is the time required to sweep the ions to the plate.

$E_g(t)$ is continuous and the integral $\int_{-\infty}^{+\infty} E_g(t)dt$ is absolutely integrable. Thus the conditions for a Fourier integral are satisfied. The spectrum of (11) is then given by

$$G(\omega)=(1/(2\pi)^{\frac{1}{2}})(Rq/\lambda)\Big[\int_0^{\lambda}\epsilon^{-j\omega t}dt - \int_0^{\lambda}\epsilon^{-(1/RC+j\omega)t}dt+\epsilon^{\lambda/RC}\int_{\lambda}^{\infty}\epsilon^{-(1/RC+j\omega)t}dt - \int_{\lambda}^{\infty}\epsilon^{-(1/RC+j\omega)t}dt.\Big] \quad (12)$$

Integrating and substituting the limits we have

$$G(\omega)=A(1-\cos\omega\lambda+j\sin\omega\lambda)/j\omega(1+j\omega RC) =A(1-\epsilon^{-j\omega\lambda})/j\omega(1+j\omega RC), \quad (13)$$

where $A=Rq/(2\pi)^{\frac{1}{2}}\lambda$.

We note that the frequency spectrum is of the oscillating type with an envelope that approaches $Rq/(2\pi)^{\frac{1}{2}}$ asymptotically at the origin. The average energy per cycle consequently falls off at the higher frequencies and it should be noted that there is no maximum in the frequency spectrum corresponding to a frequency $1/4\lambda$ as is commonly supposed. The effect of varying λ is merely to change the number of oscillations inside of the envelope of the energy spectrum within a given frequency range. The effect of changing RC is to shift the envelope to higher or lower frequencies as RC is decreased or increased.

The best means of evaluating the effect of the circuit parameters is to determine the time response in the output of the amplifier. The time response in the output of the amplifier referred to the input, i.e., divided by the gain of the amplifier, is given by

$$E(t)=A\int_{\omega_1}^{\omega_2}(1-\epsilon^{-j\omega\lambda})\epsilon^{j\omega t}d\omega/j\omega(1+j\omega RC). \quad (14)$$

It can easily be shown that the value of $E(t)$ will be a maximum when $\omega_2RC>\omega_1RC\gg1$ and (14) becomes *

$$E(t)=A(t-\lambda)/RC\int_{y_1}^{y_2}\epsilon^{jy}dy/y^2 - At/RC\int_{x_1}^{x_2}\epsilon^{jx}dx/x^2, \quad (15)$$

where $x=\omega t$ and $y=\omega(t-\lambda)$. By integrating and substituting the limits,

$$\begin{aligned}E(t)=&\{A(t-\lambda)/RC\}\{[\cos\omega_1(t-\lambda)]/\omega_1(t-\lambda)\\&-[\cos\omega_2(t-\lambda)]/\omega_2(t-\lambda)+Si\omega_1(t-\lambda)\\&-Si\omega_2(t-\lambda)\}-\{At/RC\}\{[\cos\omega_1t]/\omega_1t\\&-[\cos\omega_2t]/\omega_2t+Si\omega_1t-Si\omega_2t\}\\&+\{jA(t-\lambda)/RC\}\{[\sin\omega_1(t-\lambda)]/\omega_1(t-\lambda)\\&-[\sin\omega_2(t-\lambda)]/\omega_2(t-\lambda)-Ci\omega_1(t-\lambda)\\&+Ci\omega_2(t-\lambda)\}-\{jAt/RC\}\{[\sin\omega_1t]/\omega_1t\\&-[\sin\omega_2t]/\omega_2t-Ci\omega_1t+Ci\omega_2t\}. \quad (16)\end{aligned}$$

In any practical case the amplitude of the complex part is small and can be neglected, and (16) can be written:

$$E(t)=[q/C\lambda(2\pi)^{\frac{1}{2}}][t(X-Y)+\lambda Y] =[q/C(2\pi)^{\frac{1}{2}}]E(\lambda,t), \quad (17)$$

where

$$E(\lambda,t)=[t(X-Y)+\lambda Y]/\lambda, \quad X=X_1-X_2,$$
$$X_n=[\cos\omega_nt]/\omega_nt+Si\omega_nt,^* \quad Y=Y_1-Y_2,$$
$$Y_n=[\cos\omega_n(t-\lambda)]/\omega_n(t-\lambda)+Si\omega_n(t-\lambda).$$

Then the ratio of signal to the root-mean-square value of noise is given by

$$E(t)/E_n=qE(\lambda,t)3.14\times10^9/((f_2-f_1) \times[R_tC^2+(1+19.4I_gR)/4\pi^2Rf_1f_2])^{\frac{1}{2}}. \quad (18)$$

One of the additional requirements in counting pulses is that the amplitude of all except the first pulse in the train of output pulses due to the causal input pulse be small. This requirement is a fundamental one, since otherwise a single pulse

* The best tables of this function are found in Vol. I of the *Mathematical Tables* published by the British Association for the Advancement of Science.

might be counted more than once in the output, and the sharpness of the first output pulse is a deciding factor in the resolution of the counting system.

From a consideration of (18) we can now determine the relative noise level when all of the parameters are given. Before discussing this equation it is necessary to consider the function $E(\lambda, t)$.

$E(\lambda, t)$ depends only upon f_1, f_2, λ, and t. In order to determine its dependence upon these quantities $E(\lambda, t)$ has been plotted for a large number of different combinations of the parameters. A typical family of curves of $E(\lambda, t)$ is shown in Fig. 3 for various values of f_2 with $f_1 = 240$ c.p.s. and $\lambda = 2 \times 10^{-4}$ second. It is to be noted that only the first pulse is essentially affected by the upper band limit, the secondary and negative pulses are primarily determined by the lower band limit. This does not hold exactly

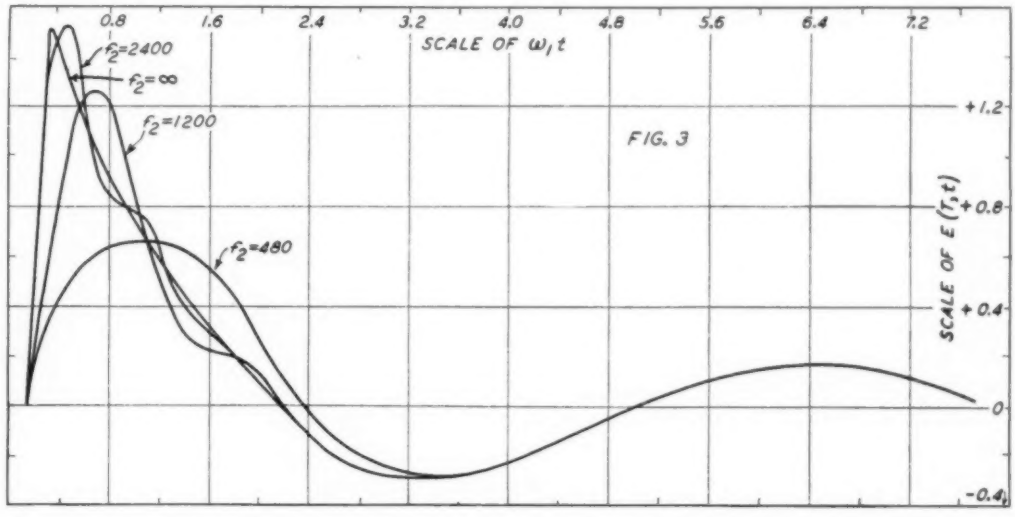

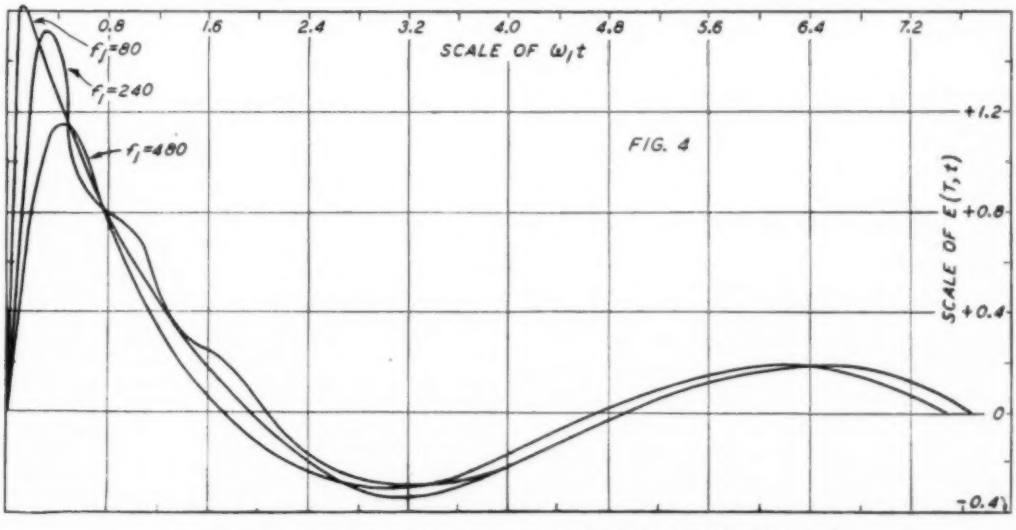

FIG. 3. Pulse shape as a function of upper cut-off ($T = 2 \times 10^{-4}$; $f_1 = 240$ c.p.s.).
FIG. 4. Pulse shape as a function of lower cut-off ($T = 2 \times 10^{-4}$; $f_2 = 2400$ c.p.s.).

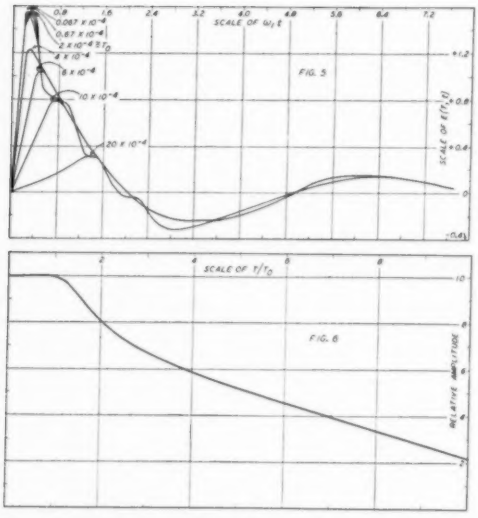

FIG. 5. Pulse shape as a function of collection time ($f_1=240$ c.p.s.; $f_2=2400$ c.p.s.).
FIG. 6. Pulse amplitude as a function of collection time ($f_2=10f_1$; $T_0=2/f_2$).

when f_2 is very near to f_1 but does for the cases in which we are interested, since from Fig. 3 it is evident that f_2 must be large compared to f_1. However, it is seen that no appreciable change occurs if f_2 is increased beyond 2400 c.p.s. in this particular case. Similar families of curves are obtained for different values of f_1 and λ and in each case the critical value of f_2 occurs at $f_2=1/2\lambda$.

Fig. 4 shows a similar family of curves of $E(\lambda, t)$ *vs.* t for various values of f_1 and with $f_2=2400$ c.p.s. and $\lambda=2\times10^{-4}$ second. From these curves and similar families we conclude that the optimum value of f_1 is obtained when f_1 equals $1/20\lambda$.

The optimum pulse shape is thus seen to be obtained when f_2 equals $10f_1$ and $f_2=1/2\lambda$. Fig. 5 is a plot of $E(\lambda, t)$ *vs.* t for various values of λ and with $f_1=240$ c.p.s. and $f_2=2400$ c.p.s., and shows the effect of variation of collection time for a fixed band width. The same data are plotted in a different way in Fig. 6 in which the maximum amplitude of $E(\lambda, t)$ is plotted against λ/λ_0 where $\lambda_0=1/2f_2$. This curve is perfectly general and it is seen that no further change in pulse amplitude occurs if λ is less than the critical collection time λ_0. From this discussion we see that if the longest collection time of the ionization chamber is known the characteristics of the amplifier are determined.

In any practical case the collection time λ is determined by the geometry and the gas of the ionization chamber as well as the collection voltage. It should be noted that the curve of Fig. 6 provides a means of determining the collection time of a chamber, for since λ can be varied by varying the collection voltage across the chamber, the voltage at which the critical collection time is obtained can be determined, and the collection time at any other voltage found from the curve.

If we assume the amplifier $f_2=10f_1$ and $f_2=1/2\lambda$ and write for $E(\lambda, t)$ its maximum value we obtain as a measure of the signal to noise ratio

$$E_m(t)/E_n=q7.3\times10^9(\lambda/[R_tC^2+\lambda^2\times(1+19.4I_gR)/0.99R])^{\frac{1}{2}}. \quad (19)$$

If we differentiate (19) with respect to λ and set equal to zero in order to find the optimum value of λ for a given set of tube and circuit parameters, we find that (19) is a maximum when λ has the value:

$$\lambda=C(0.99R_tR/(1+19.4I_gR))^{\frac{1}{2}}. \quad (20)$$

The maximum signal-to-noise ratio is then given by

$$[E_m(t)/E_n]_{\max}=N11.3\times10^{-10}\times(R/R_tC^2(1+19.4I_gR))^{\frac{1}{4}}, \quad (21)$$

where N is the equivalent number of singly charged ion pairs collected by the chamber. If we regard R_t and I_g as parameters fixed by the tube from (21) the signal-to-noise ratio is made a maximum when C is a minimum and R is large. If the tube is operated with a floating grid the factor $(R/R_tC^2(1+19.4I_gR))^{\frac{1}{4}}$ is a measure of the merit of the tube. In this particular case R is the dynamic grid resistance at the floating potential, and C is the sum of the ionization chamber capacity and the dynamic input capacity of the tube, and is given nearly enough by

$$C=C_i+C_{gf}+(1+\mu_c)C_{gp}+C_s \quad (22)$$

where:

C_i = ionization chamber capacity,
C_{gf} = grid-to-filament capacity,
C_{gp} = grid-to-plate capacity,
C_s = stray capacity to ground,
μ_e = effective voltage amplification of first stage.

In triodes R_t may be as low as 4000 ohms[1] while in pentodes the best values of R_t usually fall between 10,000 to 20,000 ohms.[1, 2] However, in triodes the value of $(1+\mu_e)C_{gp}$ is usually prohibitively large so that pentodes are to be preferred in spite of their higher values of R_t.

For example, if we assume an ionization chamber plus stray capacity of 5 mmf, the relative merit of the RCA 238, the WE 259-B and WE 262-A has been calculated from published data and is given in Table I.

The 238 and 259-B are pentodes and the 262-A is a triode. There are a large number of other types of tubes, both pentodes and triodes with factors of merit in the same range of values; and the pentodes in general have the higher values.

Since the collection time λ determines the amplifier which in turn determines the resolution, for fast counting rates it may be desirable to operate at a different value of λ than the one that gives the best noise level. For this case from (19) we see that the best ratio of signal to noise is still obtained when R_t and C are a minimum and R is large. When counting fast protons it may not be necessary to keep the secondary extremely low compared to the first pulse, and in that case the signal to noise may be improved slightly by the use of a narrower band width.

By a careful choice of tubes it may be expected that the factor of merit of the input tube may be increased beyond the values given in Table I. If the circuit of Fig. 1 is used and a tube with the constants $R_t = 10{,}000$ ohms, $C = 10^{-11}$ farad, $I_g = 10^{-13}$ ampere, and an input resistance of 10^{12} ohms is used, the factor of merit will be

TABLE I. *Relative merit of several input tubes for pulse amplifiers.*

TUBE	R_t	C $\times 10^{12}$	R $\times 10^{-10}$	I_g $\times 10^{11}$	$(R/R_tC^2(1+19.4I_gR))^{\frac{1}{2}}$ $\times 10^{-6}$
RCA 238	14000	14	5	0.2	8.9
WE 259-B	19800	11	1.2	0.8	6.5
WE 262-A	7700	28	0.8	1.8	4.3

[2] E. A. Johnson and C. Neitzert, Rev. Sci. Inst. **5**, 196 (1934).

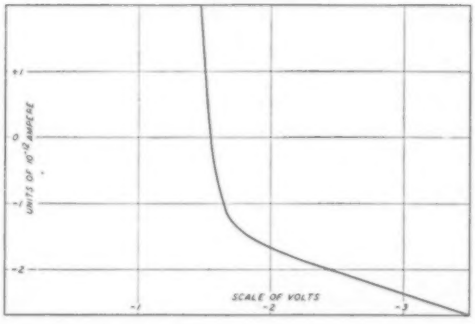

FIG. 7. Grid voltage *vs.* grid current curve of RCA type 38 tube.

24×10^6. From Eq. (21) if we assume that pulses whose amplitude is twice the mean noise level can just be detected, the minimum number of ion pairs that can be counted will be approximately 100. If we assume that fast protons produce 2000 ion pairs per centimeter of path, the signal-to-noise ratio for a one-cm deep ionization chamber will be 38 : 1 from Eq. (21) for fast protons and will be higher for slow protons and alpha-particles.

The circuit proposed in Fig. 1 has several advantages. If we consider the curve of E_g *vs.* I_g of the 238, from Fig. 7 we see that by operating at the point $E_g = -2$ volts instead of at the floating potential the grid current is reduced to about half, since the electronic component is reduced to practically zero. The resistance of the circuit is practically the external resistance at $E_g = -2$ volts since the dynamic resistance is very large. The noise level can consequently be improved slightly by the use of this circuit. It has one further advantage as is shown by the following analysis.

If RC is large and the number of impulses large, the grid will assume a voltage different from the voltage with no signal impressed. We assume first that the resistance in the grid circuit remains constant. It must be pointed out that this may be far from the actual circumstance, and may seriously affect the operating conditions.

We assume that each pulse decays as

$$E\epsilon^{-t/RC} \quad \text{where} \quad E = Rq(1-\epsilon^{-\lambda/RC})\epsilon^{\lambda/RC}/\lambda. \quad (23)$$

If the pulses occur at an average interval of $1/n$,

then the voltage of the grid at any time t will be

$$V=E[\epsilon^{-t/RC}+\epsilon^{-(t-1/n)/RC}+\epsilon^{-(t-2/n)/RC}+\cdots].$$

Assuming a large number of pulses, the grid will be driven to a voltage: $V=E/(\epsilon^{1/nRC}-1)=nRCE$ since nRC will usually be large compared to unity.

V may be of the order of 0.1 volt if the counting rate is high, when counting alpha-particles. With a floating grid, if we consider the curve of E_g *vs.* I_g of Fig. 7 it is seen that if the sense of V is such as to make the grid more negative I_g is decreased and R_g is increased. This results in an increase in V which carries the operating point still further negative, and the process continues until the grid voltage is driven so far negative that the tube becomes inoperative. For this reason the ionization chamber collection voltage is applied so that V drives the grid positive. However, this increases I_g and decreases R_g and the grid voltage is established at a new equilibrium at a more positive voltage, with I_g greater and R_g less than with no signal impressed. Both of these factors result in a decrease in the signal to noise ratio which may be quite appreciable.

The circuit of Fig. 1 can be used to prevent this condition either by manually correcting for the change in grid bias at high counting rates, or by automatically biasing the grid.

In conclusion it should again be pointed out that this analysis holds only when an amplifier which has no phase distortion is used. If unequal phase changes occur between the frequency components during amplification, they will not add in the output to give a maximum signal, but interference will take place which will result in a decreased signal. It is therefore essential that the overall characteristic of the amplifier shall contain no phase distortion.

The authors are indebted to Dr. John A. Fleming, the Director of the Department of Terrestrial Magnetism, for the opportunity to carry on this investigation, and to Dr. L. C. Van Atta and Dr. L. R. Hafstad for criticism of the manuscript.

JULY 15, 1936 PHYSICAL REVIEW VOLUME 50

Magnetization of Nickel Under Compressive Stresses and the Production of Magnetic Discontinuities

C. W. HEAPS, *Rice Institute*

(Received May 26, 1936)

When nickel is compressed its hysteresis loop approaches a rectangular shape. Several curves for stresses increasing up to the elastic limit have been obtained. At the maximum stress the steep part of the loop is still not vertical and the Barkhausen effect is not appreciably changed by the pressure. Much smaller stresses in an elastically bent wire produce large magnetic discontinuities, hence the existence of contiguous compressed and stretched regions appears to be necessary for the production of the large discontinuities.

WHEN a straight piece of nickel wire is bent into the arc of a circle large discontinuities of magnetization are found to appear in its hysteresis loop.[1] It has been supposed that a discontinuity of this kind is caused by the sudden and complete reversal of the saturated magnetization of the compressed region of the wire. The compressed nickel is believed[2] to have an approximately rectangular hysteresis loop, while the region of the wire which is under tension has an oblique loop with hardly any knee visible in the respective branches. The resultant loop for the entire wire would be obtained by superposition of the two loops.

The compressed half of the material of the wire maintains an almost constant intensity of magnetization as the field is decreased from a saturation value to zero; during this same field change the stretched part of the wire decreases its magnetization from saturation to a relatively

[1] R. Forrer, J. de physique **7**, 109 (1926); **10**, 247 (1929).
[2] M. Kersten, Zeits. f. Physik **71**, 553 (1931).

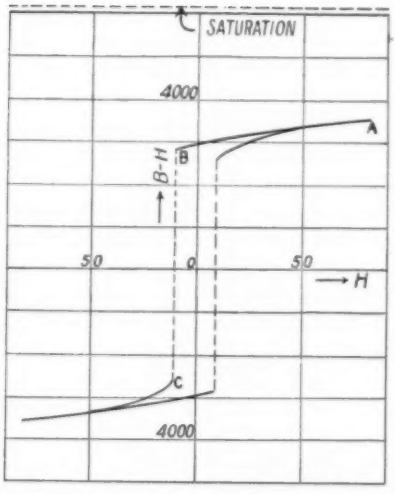

FIG. 1. Hysteresis loop of a nickel wire subjected to an elastic bending strain.

small value. The resultant effect, therefore, is that the residual magnetism for the entire wire should be about half the saturation value. Fig. 1 shows the experimental results obtained by M. Kersten for a nickel wire under bending stress. Not only does the residual magnetization have approximately the half-saturation value, as expected, but according to Kersten the part AB of the curve is quite accurately given by the theory.

In order to understand more perfectly the nature of the processes involved in the discontinuity BC it is desirable to know more about the behavior of nickel under high, purely compressive stresses. The rectangular hysteresis loop with magnetic discontinuities has not been observed experimentally. Experiments have been performed on compressed nickel bars by Ewing.[3] His data show that the loop tends towards a rectangular form as the compressive stress increases, but there are no discontinuities. However, Ewing used the method of reversals and would therefore not discover a discontinuity even if it existed. This consideration made it seem desirable to repeat Ewing's experiment.

Commercial nickel was obtained in the form of a bar, specified by the makers as "pure, grade A, annealed." It was turned down into a rod 10.0 cm long and 0.795 cm in diameter. This rod was fitted into a yoke of soft iron, the cross-sectional area of the yoke on each side of the nickel bar being 56.2 cm². Each end of the bar extended 2.5 cm into the yoke so that a length of 5 cm was available for the coils. An inner induction coil of 478 turns was used. Over this was placed a magnetizing coil of 286 turns.

A hard steel plunger was put through a hole in the yoke so as to rest on top of the vertical nickel bar, and by means of a lever resting on the steel plunger various pressures could be applied by the use of weights. The hysteresis curve was obtained by using a ballistic galvanometer and the step-by-step method. In the region where discontinuities might be expected a liquid resistance could be used to vary the current slowly and continuously.

Fig. 2 shows one branch of each of the various hysteresis loops obtained. A common saturation value of $I=450$ was obtained for all the curves in a field of about 120 gauss. No large discontinuities were detected for any of the curves. Furthermore, the use of a telephone receiver and amplifier showed that the general character of the Barkhausen effect was about the same on the steep parts of all the curves. This result is in decided contradistinction with the effect produced on the Barkhausen phenomenon by slight elastic bending of a wire. In the latter case the Barkhausen jumps are made larger and fewer, whereas pure compression appears to have no effect of this kind.

When a stress of 12.1 kg/mm² was applied to the nickel the curve obtained was not so steep as the one for a stress of 10.2 kg/mm². It appears, therefore, that plastic flow must have occurred during the adjustment of the weights for the higher stress, and the nickel had become hardened.

The presence of internal strains in the nickel initially will, of course, make the actual operative stresses somewhat different from the values listed in Fig. 2. The nickel, however, had been annealed and appeared to be quite soft, so probably it did not have large internal strains. If internal compressive strains existed they would have the effect of making the values listed in Fig. 2 smaller than the actual maximum of stress in the material.

The experiments lead to the conclusion that a

[3] J. A. Ewing, Phil. Trans. **179**, 333 (1888).

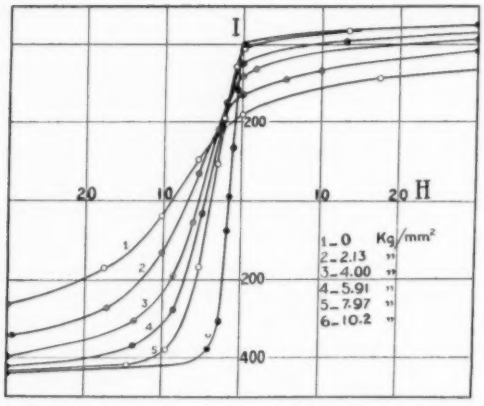

FIG. 2. Descending branches of hysteresis loops for a nickel bar subjected to various compressive stresses.

rectangular hysteresis loop in nickel cannot be obtained by compression alone, although an approximation to that shape is secured by using sufficiently high pressures. It is now of some interest to determine whether compressive stresses in bent nickel wires need to be higher than those used in this experiment with the bar before the large discontinuity of Fig. 1 appears.

In the case of a wire elastically bent into the arc of a circle the compressive stress may be calculated from the equation $\sigma_x = Ex/\rho$. Here E is Young's modulus, ρ is the radius of curvature of the arc into which the wire is bent, and σ_x is the compressive stress at a point distant x from the neutral surface where the strain is zero. The maximum compressive stress, σ_m, is obtained when $x = r$, the radius of the wire.

A wire of radius 0.006 cm was drawn down from a piece of the nickel bar and heated to redness to remove internal strains. A straight piece of this wire was then thrust into a capillary tube curved to make $\rho = 23$ cm. Taking $E = 2 \times 10^4$ kg/mm² we get $\sigma_m = 5.2$ kg/mm². The Barkhausen effect in this wire was investigated using a small coil, amplifier, and telephone receiver. Outside the tube when unstrained, the wire showed the usual large number of very small Barkhausen jumps. Inside the tube no jumps were observed until the demagnetizing field reached a sufficiently large value, when a single large discontinuity occurred. This large discontinuity was followed by a number of small ones. It appears, therefore, that large stresses are not necessary in a bent wire for the production of the large discontinuity. These discontinuities will appear even though the maximum compressive stress in the bent wire is considerably smaller than some of the compressive stresses recorded in Fig. 2, where no discontinuities are to be observed.

In explaining the jump BC of Fig. 1, therefore, it seems necessary to suppose that the stretched portion of the wire plays an important role in the production of instability. A somewhat simpler distribution of strains than is found in elastically bent wires may be obtained by the following device. A nickel bar is fitted into a nickel tube which has plugs brazed in at each end. The bar is inserted through a slot in the side of the tube and is strongly compressed by means of a heavy bolt threaded through one of the plugs. In this way the tube is strongly stretched and the bar strongly compressed. Such an assembly shows a Barkhausen effect different in no noticeable way from that observed when the strains are removed by unscrewing the bolt. A continuous lateral, mechanical connection between the stretched and compressed portions of the specimen appears necessary if the discontinuity is to be produced.

The main features involved in the production of a discontinuity are probably as follows. As the field is decreased from A towards B in Fig. 1 the compressed portion of the wire decreases its intensity of magnetization by a very small amount, the stretched portion by a much larger amount. At B, however, a certain small region of the compressed portion where strain is a maximum, will have reached and passed the knee of the loop. The magnetization of this small region will be zero although the rest of the wire still retains residual magnetism. A slight increase in the demagnetizing field will now cause this small region to acquire an increment of magnetization in the direction of the field. Whereas, previously, during the demagnetization process it had been expanding, it now begins to contract. This contraction will reduce the strain of the contiguous stretched region and allow a decrease of residual magnetism here. The net result is that the small region acts as a nucleus of instability and a wave of reversal of magnetism travels along the wire in both directions out

from the nucleus.[4] This wave of magnetic reversal will be accompanied by a wave of magnetostrictive strain, of eddy currents, and of temperature rise, so that the interaction of the various factors is decidedly complex.

In many cases the waves run completely to the ends of the wire; in other cases a magnetic wave may be blocked before it reaches the end. This blocking, or freezing, of the wave is probably due to unfavorable local strains at the point of blocking. When it occurs a magnetometer as ordinarily used cannot, of course, give an accurate picture of the magnetic state of the wire. Some device must be used to detect the existence of consequent poles,—usually moving the wire parallel to its length past the magnetometer needle serves to indicate the presence of such anomalies.

The writer is indebted to Mr. H. B. Slayback of The Metal Goods Corporation and to the Driver Harris Company for supplying the nickel used in these experiments.

[4] Raymond E. Reinhart, Phys. Rev. **46**, 483 (1934).

JULY 15, 1936 PHYSICAL REVIEW VOLUME 50

The Electrical Resistivity of Bismuth Single Crystals

ALFRED B. FOCKE AND JOHN R. HILL, *Brown University*

(Received April 18, 1936)

Measurements were made in the temperature range from −185°C to +100°C on bismuth crystals containing Pb, Sn, Sb and Te. The effects were found to be complicated but the following generalizations may be made. Decreasing temperature results in greater effectiveness of the impurity present except when the impurity concentration is such that a separation of phases occurs at low temperatures. Extremely small amounts (less than 0.03 percent) of all impurities cause a sharp increase in the resistance. The effect of larger amounts depends on the nature of the impurity. Pb and Sn continue to increase the resistance, additional Te forces the resistance to fall to lower values than that of pure Bi, additional Sb causes the initial rise of resistance to fall off and then to be slowly reestablished. More than 0.03 percent Sn and more than 0.3 percent Pb result in a negative temperature coefficient for the resistance parallel to the principal axis. In other cases the coefficient remains positive. The results may be explained on a combined theoretical and empirical basis.

INTRODUCTION

THIS study of the effect of impurities upon the electrical resistivity of single crystals of bismuth, was originally undertaken at the California Institute of Technology as a companion problem to the magnetic study reported by Goetz and Focke.[1] The data obtained at that time have not been used in the present paper, although the results obtained here are in very good agreement with the previous ones. It was considered much more satisfactory to complete the entire study using but one supply of bismuth. In this way the undetermined quantity of residual impurities would be the same for all crystals, so that direct comparisons, could be made.

Previous measurements of the electrical resistivity of bismuth single crystals by Kapitza,[2] Bridgman[3] and Goetz and Focke,[4] have clearly demonstrated the variations which may occur in different samples of "chemically pure" bismuth. These variations suggested the desirability of a quantitative investigation of the electrical resistivity of bismuth as a function of the amount and kind of impurity present.

In the magnetic problem mentioned above, the impurities which were found to cause the principal changes were lead, tin and tellurium. These metals were therefore the ones which have been used in the present work. Antimony has also been used as an impurity because it is an isomorph of bismuth and might be expected to act as a control. The case of tin is especially important because of the work of Ufford[5] on the resistance of polycrystalline alloys of the tin-

[1] A. Goetz and A. B. Focke, Phys. Rev. **45**, 170 (1934).
[2] P. Kapitza, Proc. Roy. Soc. **A119**, 358 (1928).
[3] P. W. Bridgman, Proc. Am. Acad. Sci. **63**, 351 (1928).
[4] A. Goetz and A. B. Focke, Phys. Rev. **37**, 1044 (1931).
[5] C. W. Ufford, Proc. Am. Acad. Sci. **63**, 309 (1928).

bismuth series. Jones[6] has used the results obtained by Ufford as a basis for a theoretical discussion of both the electric and magnetic properties of bismuth. Thomas and Evans[7] made measurements on the temperature coefficient of resistance of polycrystalline lead-bismuth alloys within the range from $-20°C$ to $+30°C$.

Experimental Procedure

The bismuth used was specified as "Merk, Pure 99.5 percent to 100 percent." No chemical tests were made to determine its absolute composition because preliminary tests indicated that the probable maximum total impurity was not greater than 0.01 percent to 0.02 percent. The results obtained were in agreement with this allowance. The metals used as impurities were "chemically pure." Any minute amounts of contamination in them would be entirely negligible because of the small quantities used.

The masses of metals added to the bismuth were such as to result in crystals containing atomic concentrations of 0.01, 0.03, 0.09, 0.27 and 0.81 percent of each impurity studied. Two crystals were grown from each concentration. One of these had the principal axis [111] parallel to the length of the rod, while the orientation of the other was 90° from this. In the notation introduced by Goetz,[8] these orientations are designated as P_3 and P_1, respectively.

Ten grams of bismuth was heated in a Pyrex crucible to a temperature of 500°C under an atmosphere of hydrogen, so that the oxide could be reduced. The bismuth was then cooled to about 350°C and the impurity was added. The mixture was thoroughly stirred and poured into a small steel mould which was heated to about 270°C and was also in a hydrogen atmosphere. Thus bars of all alloys were formed which had dimensions of $2\times2\times150$ millimeters. The bars were cut in half, each half later being formed into a single crystal. Magnetic tests showed no evidence of iron in the resulting samples, which is sufficient proof that no contamination of the alloys was caused by contact with the mould.

The single crystals were grown by progressive crystallization from the molten metal, the orientation being predetermined by a seed crystal. The procedure followed closely that described by Goetz and Focke[1] with the one difference that here the furnace was moved while the crystal remained at rest. Much of the trouble due to vibrations during crystallization was thus eliminated, and single crystals were obtained with practically no failures.

The electrical measurements were made by the potentiometer method of comparing the potential difference observed across a standard resistance, with that observed across the sample under test when the same current was passed through both.

Measurements were made at the temperatures of boiling liquid air ($-185°C$), carbon dioxide snow and acetone ($-77°C$), ice and water (0°C), water at room temperature (22°C) and boiling water (100°C). In all cases the crystals were placed directly into the temperature baths.

The results obtained in this manner were satisfactory with the exception of two crystals containing tin as the impurity. For these a nearly continuous change was desired between about $-150°C$ and room temperature. This was obtained by inserting the crystal being studied, into a hole drilled in a massive cylinder of brass. The brass was cooled with liquid air and covered with a thermos flask so that its temperature would increase very slowly. A thermocouple placed beside the crystal was used to determine its temperature. By this means it was possible to obtain measurements at 5° intervals from $-150°C$ to $+20°C$, the entire change requiring about two hours.

Results

A summary of the results is given in Table I.

The group of isothermal curves showing the dependence of the resistivity parallel to the principal axis (111), upon the amount of impurity present for crystals containing tin and lead is given in Fig. 1. It is evident from these curves that the effects produced by tin and lead are qualitatively the same, the principal difference being in the relative effectiveness of the different atoms. One atom of tin produces the effect of from three to five atoms of lead. Since this similarity occurs for both P_1 and P_3 orientations, further curves and discussion will treat only the case of tin.

[6] H. Jones, Proc. Roy. Soc. **A147**, 396 (1934).
[7] W. R. Thomas and E. J. Evans, Phil. Mag. **16**, 329 (1933).
[8] A. Goetz, Phys. Rev. **35**, 193 (1930).

TABLE I. *Electrical resistivity of bismuth single crystals.* All resistivities multiplied by 10^4.

Resistivity parallel to the principal axis

	−185°	−77°	0°	22°	100°
PURE BISMUTH	0.36	0.88	1.20	1.28	1.82
CRYSTALS CONTAINING ANTIMONY					
0.01%	0.57	0.86	1.19	1.28	1.67
0.03%	0.68	0.83	1.17	1.28	1.64
0.09%	0.57	0.83	1.26	1.36	1.77
0.27%	0.45	0.86	1.22	1.35	1.78
0.81%	0.47	0.86	1.23	1.35	1.76
CRYSTALS CONTAINING LEAD					
0.01%	0.77	0.98	1.32	1.41	1.88
0.03%	1.28	1.17	1.41	1.64	1.96
0.09%	4.05	2.15	1.93	1.97	2.18
0.27%	3.37	3.24	2.57	2.48	2.52
0.81%	1.79	5.25	4.10	3.62	3.14
CRYSTALS CONTAINING TIN					
0.01%	0.88	0.91	1.28	1.50	1.82
0.03%	3.14	2.10	1.96	1.94	2.10
0.09%	1.98	4.27	3.07	2.88	2.62
0.27%	1.38	5.40	5.40	4.84	3.64
0.81%	1.21	5.70	7.25	6.70	5.42
CRYSTALS CONTAINING TELLURIUM					
0.01%	0.42	0.74	1.16	1.26	1.68
0.03%	0.27	0.55	0.98	1.05	1.52
0.09%	0.25	0.53	0.82	0.92	1.40
0.27%	0.29	0.55	0.82	0.91	1.43
0.81%	0.53	0.94	1.22	1.36	1.66

Resistivity perpendicular to the principal axis

	−185°	−77°	0°	22°	100°
PURE BISMUTH	0.33	0.74	0.98	1.06	1.36
CRYSTALS CONTAINING ANTIMONY					
0.01%	0.53	0.78	1.06	1.16	1.47
0.03%	0.44	0.70	0.98	1.06	1.41
0.09%	0.41	0.66	0.96	1.05	1.40
0.27%	0.42	0.69	0.97	1.05	1.37
0.81%	0.48	0.76	1.03	1.10	1.44
CRYSTALS CONTAINING LEAD					
0.01%	0.56	0.76	1.00	1.08	1.40
0.03%	0.72	0.86	1.06	1.14	1.44
0.09%	0.94	1.05	1.16	1.22	1.44
0.27%	0.91	1.27	1.37	1.40	1.69
0.81%	0.82	1.77	1.97	2.00	2.07
CRYSTALS CONTAINING TIN					
0.01%	0.86	0.98	1.08	1.14	1.40
0.03%	0.97	1.10	1.23	1.27	1.58
0.09%	0.76	1.44	1.57	1.60	1.75
0.27%	0.56	1.68	1.99	2.05	2.11
0.81%	0.85	1.80	2.36	2.43	2.51
CRYSTALS CONTAINING TELLURIUM					
0.01%	0.48	0.72	0.96	1.04	1.37
0.03%	0.28	0.62	0.91	0.98	1.32
0.09%	0.24	0.51	0.78	0.88	1.28
0.27%	0.25	0.52	0.76	0.85	1.22
0.81%	0.38	0.69	0.95	1.04	1.41

Three important characteristics can be seen in Fig. 1: first, the tremendous effect produced by extremely small amounts of the impurities; second, the marked difference between the measurements at liquid air temperature and for those at higher temperatures; and third, the existence of a negative temperature coefficient of resistance within certain temperature ranges in the cases of some of the crystals.

These abnormal temperature coefficients are more clearly shown in Fig. 2, in which the resistivity is plotted as a function of temperature for P_3 crystals containing tin. In order to determine the true shape of these curves, measurements were taken at intervals of 5°C in the range from −150°C to +20°C in the cases of the crystals containing 0.09 percent and 0.27 percent tin.

The isothermal curves for P_3 crystals containing tellurium and antimony are given in Fig. 3. It may be seen from these that the effects produced by tellurium and antimony are very much smaller than those produced by tin and lead. Furthermore, while tin and lead increased the resistivity, tellurium tends in general to decrease it. Antimony seems to be a hybrid, which decreases the resistivity at high temperatures and increases it at low temperatures. For amounts greater than 0.09 percent antimony the changes produced are negligibly small.

Fig. 4 shows the variations produced in the resistivity perpendicular to the principal axis. In the case of tin the difference in behavior at −185°C is again apparent; otherwise the only irregularity is the initial increase in the resistivity observed both in the case of tellurium and of antimony.

The results given in Figs. 3 and 4 indicate that there is no great advantage to be gained from plotting these resistivities as a function of temperature. The temperature coefficients will be positive at all times although they would obviously be greatly increased between −185°C and 0°C for those crystals containing more than 0.03 percent tin.

DISCUSSION

A nearly complete explanation of the results may be obtained through a consideration of the theoretical work of Jones[6] together with the phase equilibrium diagram of the bismuth-tin system.

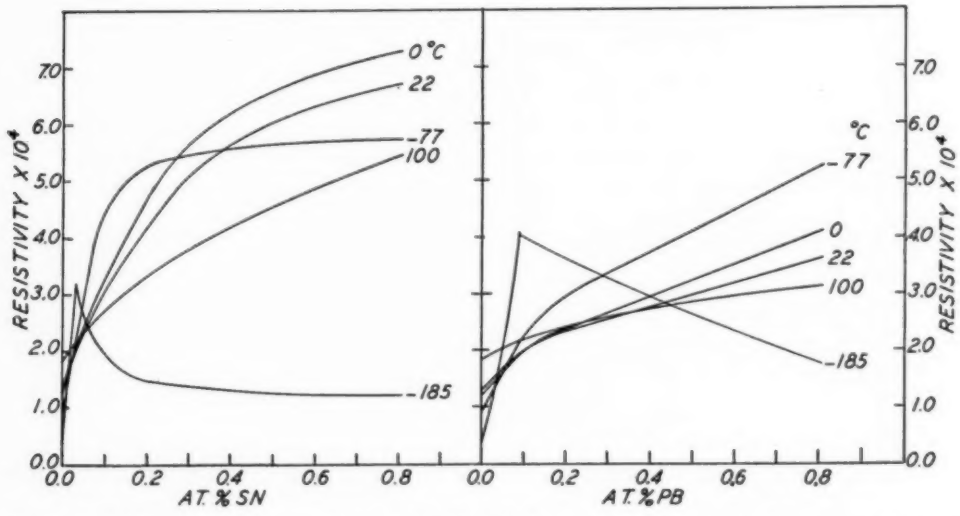

FIG. 1. Resistivity of bismuth crystals, parallel to the principal axis, as a function of the amount of tin and lead present.

Jones has attacked the problem of the electric and magnetic properties of bismuth by making use of the Bloch theory and has determined that the number of electrons within the inner Brillouin zone in the bismuth lattice is very nearly equal to five. Since the number of valence electrons for bismuth is five, this leaves, on the average, only a very small fraction of one electron per atom in the outer zone which is therefore available for participation in normal metallic conduction.

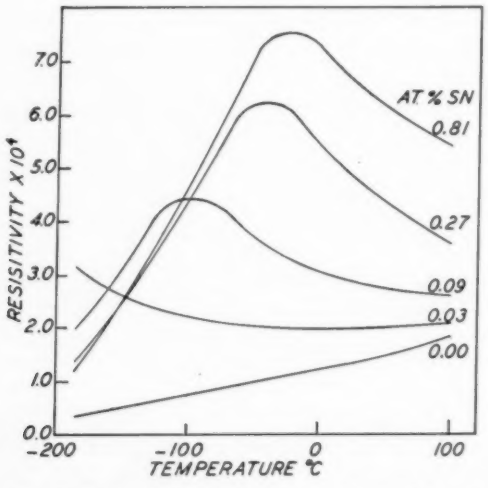

FIG. 2. Resistivity of bismuth crystals, parallel to the principal axis, as a function of temperature for bismuth crystals containing tin.

If some of the bismuth atoms are replaced by foreign atoms having a valence of four, the average number of these electrons per atom, for the whole lattice, will be reduced below five. If this is carried far enough there will be no electrons remaining in the outer zone, and ordinary metallic conduction will be replaced by one which is characterized by a negative temperature coefficient. In this way Jones has explained the results of Thomas and Evans[7] and Ufford.[5]

This same reasoning would explain the initial effects observed for all temperatures with either tin or lead as the foreign atoms. It would also explain the results obtained at temperatures above $-10°C$ for all crystals containing these impurities.

A possible explanation of the decided changes that occur at lower temperatures may be obtained from the phase equilibrium diagram for the bismuth-tin system. This is similar to the bismuth-lead system and is given in Fig. 5. The important thing to notice here is that the boundary between the single solid solution phase A, and the mixture of solid solutions $A+B$, is not a vertical line but approaches the pure bismuth axis as the temperature decreases. This indicates that a single crystal of solid solu-

tion A is not stable at all temperatures, but that if the temperature is sufficiently reduced, a recrystallization must take place so that some of the tin, together with some of the bismuth, must leave the bismuth lattice.

If this occurs, the average number of valence electrons per atom remaining in the bismuth lattice must be increased, thus forcing the resistance back toward that for the pure metal. Since this is just the type of behavior that is observed, this is probably a valid explanation of the results.

It is interesting to note here that this is also a probable explanation of the similar peaks observed in the magnetic study.[1]

The curves for antimony given in Figs. 3 and 4 cannot be explained on the basis of Jones' theory, because antimony possesses five valence electrons. Thus there can be no change made in the average number of electrons per atom by the addition of antimony. It may be that the presence of the antimony atoms increases or decreases the existing mechanical strains within the crystal, the type of change depending upon the temperature and the orientation in the crystal.

This type of distortion would probably be present regardless of the kind of impurity added

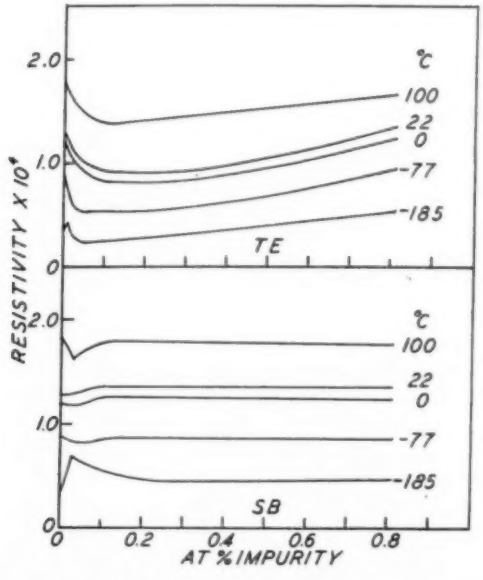

FIG. 3. Resistivity of bismuth crystals, parallel to the principal axis, as a function of the amount of tellurium and antimony present.

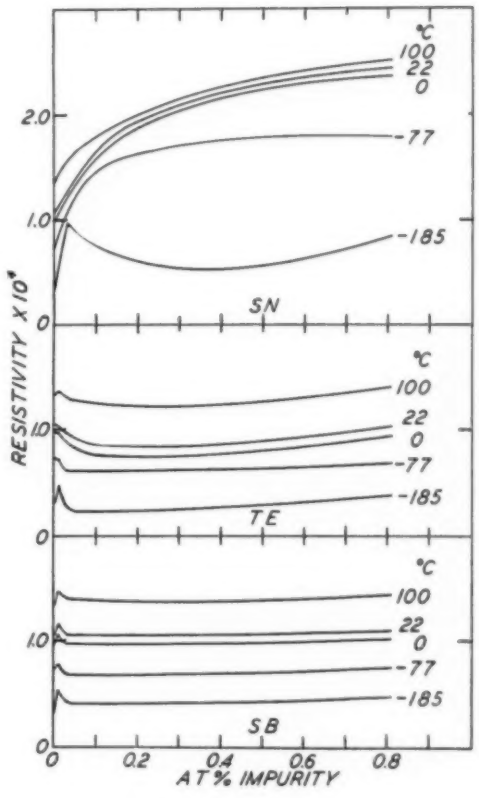

FIG. 4. Resistivity of bismuth crystals, perpendicular to the principal axis, as a function of the amount of impurity present.

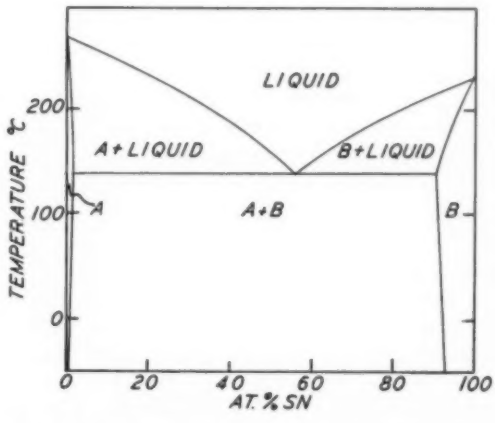

FIG. 5. The phase equilibrium diagram of the bismuth-tin system. (After Endo.)

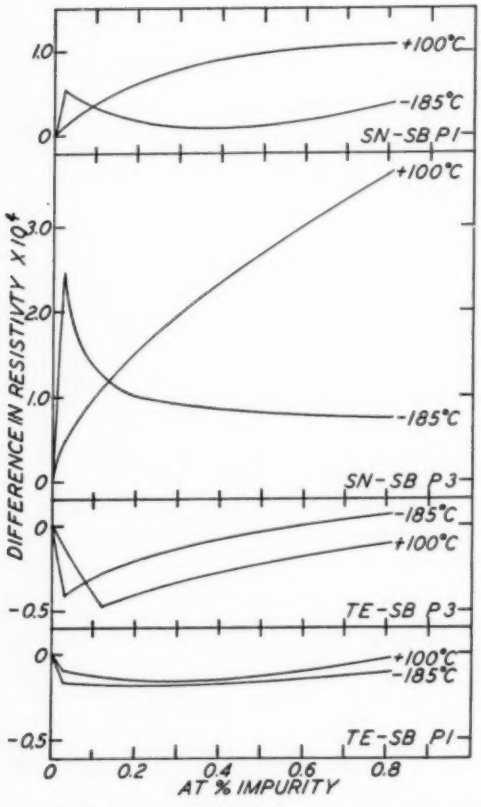

FIG. 6. The resistivity of bismuth crystals containing antimony subtracted from the resistivity of crystals containing tin and tellurium in an attempt to eliminate mechanical strain effects.

to the bismuth, so that in general the observed effect would be a combination of the mechanical and electronic disturbances in the lattice.

If the mechanical distortions due to atoms of nearly the same atomic weight can be assumed to be approximately the same, the pure electronic effect would be obtained by subtracting the observed antimony result from that of the corresponding quantity of tin or tellurium. In the case of tin such a procedure would not cause any particular change in the character of the curves obtained, but in the case of tellurium the complicated curves given in Figs. 3 and 4 would be replaced by those given in Fig. 6. These curves show the same general characteristics as the curves for tin at −185°C except that here the resistivity is decreased instead of being increased. This may be explained by the same reasoning as that given for the case of tin when the fact that tellurium has a valence of six instead of four is considered. The presence of tellurium would increase the average number of electrons per atom thus decreasing the resistivity of the crystal containing it. The sharp breaks in the curves would again be explained by recrystallization.

At first the possibility of recrystallization taking place with such small amounts of impurity seems rather questionable. The work of one of the authors,[9] however, has definitely shown that in the case of polonium, the foreign atoms are segregated into groups and are not distributed at random throughout the bismuth crystals. The recrystallization would thus take place in the regions of high impurity and there would be no question of the need of migration of foreign atoms through the solid, to permit the formation of the new lattice.

The results may be summarized as follows: The addition of tin or lead to bismuth causes a marked increase in the electrical resistivity. This increase is greater, the larger the amounts of impurity added, for all temperatures, so long as no recrystallization takes place: The addition of tellurium usually causes a decrease in the resistivity so long as no recrystallization occurs: The addition of antimony causes an increase in the resistivity except in the instance of the resistivity parallel to the principal axis [111] at temperatures of the order of 100°C.

Approximate limits of solubility of tin, lead and tellurium in solid bismuth may be estimated as follows: tin, 0.03 percent at −185°C, 0.09 percent at −95°C, 0.27 percent at −42°C and 0.81 percent at −20°C; lead, 0.09 percent at −185°C, 0.81 percent between −185°C and −77°C; tellurium, 0.03 percent at −185°C, 0.12 percent at +100°C.

The results may be explained quite well by the theoretical work of Jones[6] together with the assumption that the effects due to antimony give an indication of the changes produced by mechanical factors alone.

We wish to express our thanks to Professor Goetz of the California Institute of Technology for his suggestion of the problem and his help and interest in the early part of the work.

[9] A. B. Focke, Phys. Rev. **46**, 623 (1934).

LETTERS TO THE EDITOR

Prompt publication of brief reports of important discoveries in physics may be secured by addressing them to this department. Closing dates for this department are, for the first issue of the month, the eighteenth of the preceding month; for the second issue, the third of the month. The Board of Editors does not hold itself responsible for the opinions expressed by the correspondents.

Communications should not in general exceed 600 words in length.

Use of the Reflection Echelon for Interferometric Wave-Length Comparisons Extending into the Schumann Region

Interference patterns have been photographed which are suitable for the comparison of wave-lengths of lines in the spectrum of Cu II from 1488A to 1621A with the wave-lengths (greater than 2100A) of lines measured interferometrically by Burns and Walters.[1] A reflection echelon was used with a concave grating as shown in the plan in Fig. 1. This optical system was enclosed in a vacuum chamber. Eight wave-lengths shorter than 2100A computed by Shenstone[2] from term values for Cu II have been compared with values deduced from the patterns. The greatest discrepancy was 0.004A, and five of the values differed by less than 0.001A from the computed values. These wave-length values were based on the assumption of a zero average error in Burns and Walters' values. The precision of measurement was low because of the difficulties to be discussed below. Consequently no wave-length values based on these patterns will be published.

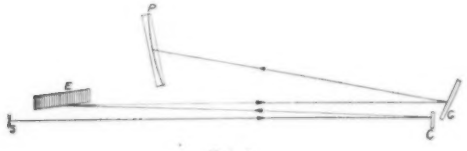

FIG. 1.

The only source found to radiate with sufficient intensity and homogeneity was the hollow cathode copper discharge in helium described by Shenstone.[2] The radiation entered the chamber through the slit, *S*. After collimation by the platinized concave mirror, *C*, the beam fell on the twenty-five plate, platinized, Hilger fused quartz reflection echelon, *E*, placed with edges of the steps vertical. The reflected beam fell on the two meter, platinized, concave, glass grating, *G*, having 30,000 lines per inch and placed with the rulings vertical. The resulting parallel dispersions were found to be advantageous in permitting long fringes without increase of overlap of adjacent patterns. The grating was rotated about a vertical axis to place various wave-length regions on the plate, *P*, whose distance from the grating and inclination to the beam from the grating could be adjusted for focus. Ilford *Q* plates five inches long were used, recording simultaneously all of the patterns within any 1000A wave-length range. The beam incident on the echelon was exactly perpendicular to the edges of the echelon steps, a necessary condition for reliable wave-length comparisons. The fiducial mirrors were used for wave-length determinations in essentially the manner described by Williams.[3] Some work was done with crossed dispersions, in which case the edges of the echelon steps were horizontal, and the center of *C* was below the line joining the centers of *E* and *G*. The stigmatic image necessary for crossed dispersions can be secured only when *P* is on the normal to the grating. The dimensions of the vacuum chamber prevented the fulfillment of this condition for wave-lengths longer than 2400A.

The most serious disadvantage of the reflection echelon is the concentration of intensity near the single order fringe position. As a consequence there are never more than two measurable fringes, and errors of measurement cannot be eliminated by averaging a number of fringes. This concentration of intensity also causes displacements of all but extremely sharp fringes toward the single order position by amounts proportional to their distance from the single order position and to their widths. The widths of the lines of the uncooled hollow cathode discharge were observed to be 0.01A, which caused displacements amounting to about twenty percent of the distances of the fringes from the single order position. The extremely high order of interference (100,000 at 1460A) in the extreme ultraviolet makes the measurement of the patterns and the identification of the order of interference increasingly difficult for shorter wave-lengths.

It can be concluded that the reflection echelon is suitable for wave-length comparisons in the Schumann region when the optical system described is used. This outline is of work fully described in a thesis submitted to the faculty of the Massachusetts Institute of Technology and performed under the direction of Professor G. R. Harrison to whom grateful acknowledgment is now made.

DAVID L. MAC ADAM

Massachusetts Institute of Technology,
June 18, 1936.

[1] Burns and Walters, Publ. Alleg. Obs. **8**, 27 (1930).
[2] A. E. Shenstone, "The First Spark Spectrum of Copper," Phil. Trans. Royal Soc. London **235**, 145 (1936).
[3] W. E. Williams, "Studies in Interferometry. II. Construction, Testing and Use of Reflection Echelons for the Visible and Ultraviolet Regions," Proc. Phys. Soc. **45**, 699 (1933).

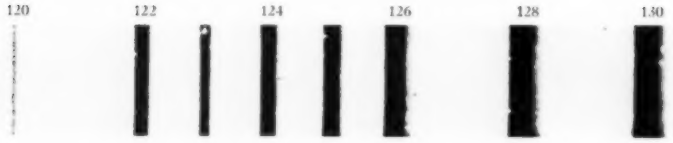

FIG. 1. Mass spectrum of tellurium.

The Isotopic Constitution of Strontium and Tellurium

In the *Physical Review* for May 15, J. P. Blewett and M. B. Sampson report the observation of a new isotope at mass 84 in strontium. I have recently confirmed this observation, the mass spectrum of the ions from a spark between a palladium and a strontium electrode showing the mass at 84 in addition to the much stronger lines at 86, 87, and 88.

Mass spectra of the charged atoms from a spark between tellurium and palladium electrodes showed a new faint isotope at mass 120. A reproduction is shown in Fig. 1. Only the four heaviest isotopes at 130, 128, 126, 125 were observed by Aston. Later Bainbridge[1] found three additional isotopes at 124, 123, and 122, and indications of an extremely faint one at 127. The present photographs show no trace of this line at 127, and it may have been due to iodine present as an impurity. The new isotope at 120 cannot be ascribed to tin as the other strong tin isotopes are not present. In a chart of the elements it extends the limit of stability of the tellurium nucleus to make it more in line with the lightest isotopes of tin, xenon, and barium.

A. J. DEMPSTER

University of Chicago,
June 23, 1936.

[1] K. T. Bainbridge, Phys. Rev. **39**, 1021 (1932).

Evidence from Efficiency Curves for the Nature of the Disintegration Process for Boron

The existence of a continuous distribution and a homogeneous group of α-particles resulting from bombarding boron with protons has been definitely established,[1, 2] and confirmed by integrated numbers-*vs.*-range curves in this laboratory.

This letter reports an investigation of the efficiency of production of α-particles from this reaction as a function of the voltage accelerating the protons. A transformer-kenetron-condenser source of high potential up to 275,000 volts with voltage measured by a high resistance voltmeter was used. The energy of the magnetically resolved proton beam could be controlled to within three kilovolts and except for collision energy losses after resolution was highly monochromatic. The α-particles emitted from the fused B_2O_3 *thick* target were observed by an ionization chamber and amplifier of the Dunning[3] type and a thyratron counter adjusted to count all α-particles reaching the ionization chamber. The apparatus gave absolute yields from a thick target of LiCl to within 10 percent of the results of the Wisconsin laboratory.[4]

The observed efficiency curves for production of all α-particles having a range greater than a given range are shown in Fig. 1. It is seen that the main group of range greater than 18 mm follows the ordinary efficiency curve with no evidence for any peculiarities of excitation. This is also true for the Li efficiency curve shown by the dotted line. However, when the majority of α-particles recorded are of the long range type, >38 mm, it is seen that the curve is not exponential but shows a decided break with the maximum of the differentiated curve (i.e., thin target) at 180 kv. The feet of these curves are of a quite different character from those of the shorter range curves, and the intermediate sections show a more rapid rise in yield with increasing voltage.

These curves suggest that the disintegration which has been proposed[1]

$$ {}_1H^1 + {}_5B^{11} \rightarrow {}_4Be^8 + {}_2He^4 $$

or any further reaction postulated to account for this long range group, is a case of resonance disintegration.

Reasons for the non-constancy of the yield from thick targets at higher voltages are: (a) the onset of further modes of disintegration; (b) the change of shape of the numbers-*vs.*-range curve so that the continuous distribution extends to greater range and is observed with increasing abundance at higher voltages. From this point of view the short range continuous distribution efficiency curve is not "regular." There is evidence for the latter suggestion from the differential curve, Fig. 5 of Cockcroft and Lewis.[2]

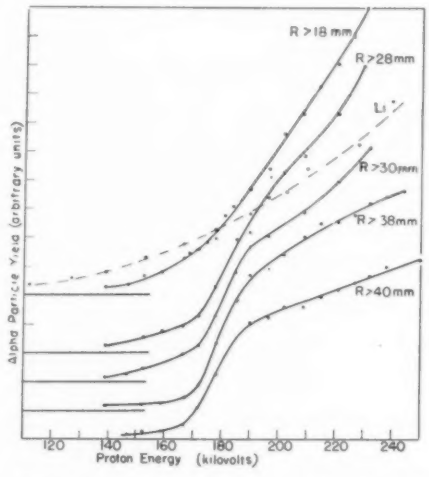

FIG. 1. Yield curves for α-particles from the disintegration of boron by protons. The yields are in arbitrary units and the zeros for the various curves are shifted vertically as indicated. For comparison purposes the yield curve for the α-particles from lithium bombarded with protons is also given.

An attempt to overcome the latter effect by working near the end of the homogeneous group range, absorber more than 45 mm, met with inherent experimental difficulties.

These observations are substantiated by the observations of Cockcroft and Lewis[2] that: "the ratios of the numbers counted at the peak of the main curve at 2 cm to the numbers at the peak of the end group at 4 cm changes from 22 : 1 at 185 kv to 90 : 1 at 360 kv."

An explanation of the observed efficiency curve for the long range homogeneous group is dependent on a satisfactory explanation of the proton-boron disintegration products, for which there have been several mechanisms devised.[5]

Qualitative results for the yield of α-particles per proton calculated for a pure boron target by multiplying the observations by 34/10 at 150, 175, 200 and 225 kv are: for range greater than 18 mm, 1.68×10^{-9}, 7.06×10^{-9}, 18.4×10^{-9}, and 32.3×10^{-9}; for range greater than 40 mm, 1.79×10^{-11}, 17.4×10^{-11}, 49.7×10^{-11} and 59.7×10^{-11}.

We wish to express our sincere thanks to Professor E. L. Hill for many stimulating discussions and to Messrs. W. G. Shepherd and R. O. Haxby for invaluable assistance with the recording apparatus. This research was supported by a grant from the Graduate School to Professor John T. Tate and the senior author.

University of Minnesota,
Minneapolis, Minnesota,
June 19, 1936.

JOHN H. WILLIAMS
WILLIAM H. WELLS

[1] Kirchner, Naturwiss. **21**, 473 (1933); Kirchner and Neuert, Physik Zeits. **34**, 897 (1933); Oliphant, Kempton and Rutherford, Proc. Roy. Soc. **A150**, 241 (1935); Neuert, Physik Zeits. **36**, 629 (1935).
[2] Cockcroft and Lewis, Proc. Roy. Soc. **A154**, 246 (1936).
[3] Dunning, Rev. Sci. Inst. **5**, 387 (1934).
[4] Herb, Parkinson and Kerst, Phys. Rev. **48**, 118 (1935); Heydenberg, Zahn and King, Phys. Rev. **49**, 100 (1936).
[5] Dee and Gilbert, Proc. Roy. Soc. **A154**, 279 (1936).

Photon Theory and Compton Effect

Recently Shankland[1] reported coincidence experiments on the Compton effect with Ra C γ-rays, which led him to the conclusion that the photon theory fails to explain such experiments. On the other hand Bothe[2] and Geiger had shown some years ago, that the Compton effect is in full agreement with this theory for x-rays of about 70 kv. This result has been carefully established and is to be considered as correct, although meanwhile there has been some progress in the experimental technique. The result of Shankland has been discussed theoretically by several authors.[3]

We have reexamined Shankland's result, to find out whether really the behavior of radiation changes so fundamentally if the frequency is altered by one order of magnitude. Our experiments do not confirm Shankland's results. We found the photon theory able to describe the scattering of hard γ-rays as well as of the x-rays.

The arrangement was similar to the one used by Shankland except some simplifications. As primary radiation we used the filtered γ-rays of Th C'' (20 mg RaTh), which have the advantage of being more homogeneous than the γ-rays of Ra C. The scatterer was a Cellophane foil 0.028 mm thick. The recoil electrons were counted by one thin-walled Geiger-Müller counter 1.2 cm in diameter, the scattered photons in most cases by two connected lead counters of the same size. The β and γ counters were mounted symmetrically on opposite sides of the primary beam at a distance of about 2.1 cm from its axis; only for the experiment number 3 the azimuth was not 180°, but 90° (designated by *j*). The foil could be moved in the direction of the primary beam. According to the photon theory coincidences were to be expected if the foil was placed in such a manner that the direction from the foil to both the recoil electron counter and the photon counters formed an angle of 30° with the primary beam.

TABLE I. *Summary of results.*

Exper. No.	Scattering and Recoil Angle	Recoil Electrons per min.	Coincidences in 14.5 Hours		
			Without Foil	With Foil	Surplus
1*	30°	40	5	25	20
2	30°	52	34	95	61
3	30°	40	30	39	9
4	21°	40	39	46	7
	30°	38		95	56
	45°	28		50	11

* Only one tube counter for scattered γ-rays.

The results of experiments are given in Table I.[4] The second column gives the angle between the primary beam and the line from the foil to each one of the counters. The third column gives the increase of β counts caused by the foil. The fourth column shows the zero effect; to obtain it the foil was removed and the counting rates of the β counter were, by means of a weak source of β-rays, adjusted to the same amount as found when the foil was present. The γ counting rates were not changed noticeably by the foil. In the fifth column the numbers of coincidences counted with the foil are shown, in column 6 the difference caused by the foil. It is seen that in the position predicted by theory the number of coincidences is far greater than the zero effect, while in every adjacent position there is only a small fraction of this effect.

These experiments show, firstly that scattered photons and recoil electrons are emitted simultaneously, and secondly that their directions are interconnected as is predicted by Compton's theory. By a more detailed discussion, which will be published elsewhere, it is seen that the observed number of coincidences is consistent with the assumption of this connection holding quantitatively.

To get a satisfactory explanation of Shankland's negative result it would be necessary to consider some more experimental data which were not contained in his paper. We believe that the inhomogeneity of the Ra C γ-rays played an important role in his experiment.

Institut für Physik
am Kaiser Wilhelm—Institut
für medizinische Forschung,
Heidelberg, June 6, 1936.

W. BOTHE
H. MAIER-LEIBNITZ

[1] R. S. Shankland, Phys. Rev. **49**, 8 (1936).
[2] W. Bothe and H. Geiger, Zeits. f. Physik **32**, 639 (1925).
[3] P. A. M. Dirac, Nature **137**, 298 (1936); E. J. Williams, Nature **137**, 614 (1936). R. Peierls, Nature **137**, 904 (1936).
[4] The experiments 1, 2, 3 have been published in Göttinger Nachrichten, No. 2, 127 (1936).

Band Spectrum of OH^+

Loomis and Brandt[1] have found that the constant A of the multiplet splitting varies from -66 to -97 cm^{-1}. This according to the authors is accounted for by the uncertainty of the energy formulae. Indeed Loomis and Brandt used the energy formulae of the molecule in the state which corresponds to the pure case a. Meanwhile the molecule OH^+ is in the state which is intermediate between a and b cases even when J is small.

Hill and Van Vleck[2] gave an exact equation of the third degree (for the computation of triplet terms) which holds true for the limiting and intermediate cases. We have solved this equation using the Cardan formula.[3] For $K=10$ and 11 and when $\alpha=A/B_v$ has values -4, -5, -6, -7, -8, we get the solutions summarized in Table I. In Table II the corresponding differences $^3\Pi_0-{}^3\Pi_1$ and $^3\Pi_1-{}^3\Pi_2$ are given. These differences are plotted against α in Fig. 1. On the other hand these differences for $K=10$ and 11 can be determined by using in the following formulae the experimental data given by Loomis and Brandt.

$$^3\Pi_2(10)-{}^3\Pi_1(10)$$
$$=[{}^PQ_{12}(11)-P_2(11)+{}^QR_{12}(10)-Q_2(10)]/2$$
$$=-22.095 \text{ cm}^{-1} \text{ (for the (1, 0) band).}$$

Similarly,

$$^3\Pi_2(11)-{}^3\Pi_1(11)$$
$$=[{}^PQ_{12}(12)-P_2(12)+{}^QR_{12}(11)-Q_2(11)]/2$$
$$=-21.475 \text{ cm}^{-1} \text{ (for the (1, 0) band).}$$

According to Loomis and Brandt $B_1'=12.381$ cm^{-1}.

TABLE I.

K / α	10			11		
	$\gamma=+1$, $J=11$	$\gamma=0$, $J=10$	$\gamma=-1$, $J=9$	$\gamma=+1$, $J=12$	$\gamma=0$, $J=11$	$\gamma=-1$, $J=10$
	$^3\Pi_2/B_v$	$^3\Pi_1/B_v$	$^3\Pi_0/B_v$	$^3\Pi_2/B_v$	$^3\Pi_1/B_v$	$^3\Pi_0/B_v$
-4	108.3323	109.1537	109.6343	130.3983	131.1295	131.5830
-5	108.0363	109.2036	109.9233	130.1166	131.1722	131.8570
-6	107.7003	109.2577	110.2730	129.8066	131.2191	132.1693
-7	107.3250	109.3155	110.0523	129.4600	131.2693	132.5190
-8	106.9043	109.3978	111.0566	129.0710	131.3414	132.8940
	$\Sigma=+1$	$\Sigma=0$	$\Sigma=-1$	$\Sigma=+1$	$\Sigma=0$	$\Sigma=-1$

TABLE II.

K / α	10		11	
	$\frac{^3\Pi_1-{}^3\Pi_2}{B_v}$	$\frac{^3\Pi_0-{}^3\Pi_1}{B_v}$	$\frac{^3\Pi_1-{}^3\Pi_2}{B_v}$	$\frac{^3\Pi_0-{}^3\Pi_1}{B_v}$
-4	0.8214	0.4806	0.7312	0.4535
-5	1.1673	0.7197	1.0556	0.6848
-6	1.5574	1.0153	1.4125	0.9502
-7	1.9905	1.3368	1.8093	1.2497
-8	2.4935	1.6588	2.2704	1.5526

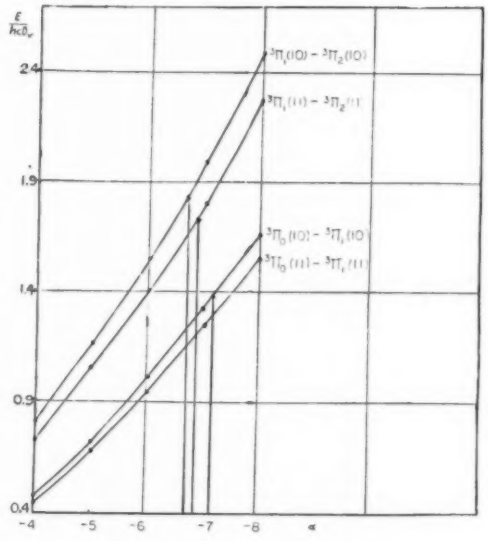

FIG. 1. Term differences plotted against α.

Therefore:

$$^3\Pi_2(10)-{}^3\Pi_1(10)=-1.8330\ B_1' \text{ cm}^{-1} \quad \text{and}$$
$$^3\Pi_2(11)-{}^3\Pi_1(11)=-1.7345\ B_1' \text{ cm}^{-1}.$$

Plotting these values on our diagram and dropping the perpendiculars on the α-axis we get the corresponding values of α, namely $\alpha=-6.64$ and $\alpha=-6.82$, A being -82.2 cm^{-1} and -84.1 cm^{-1}, respectively.

Let us now look at the differences $^3\Pi_1-{}^3\Pi_0$. Averaging the a and b separations and using combination relations we get:

$$^3\Pi_1(10)-{}^3\Pi_0(10)=[Q_3(10)-R_3(10)+{}^RQ_{32}(10)-Q_2(10)]/2$$
$$+[P_2(11)+R_3(11)-{}^RQ_{32}(11)-P_3(11)]/2$$
$$=-17.135 \text{ cm}^{-1} \text{ (for the (1, 0) band).}$$

Returning to the diagram we find that $\alpha=-7.18$ and $A=-88.9$ cm^{-1}. *These values of α and A lie indeed more closely to the true ones than the values found by Loomis and Brandt.*

The similar computation of $^3\Pi_1(11)-{}^3\Pi_0(11)$ is impossible because of lack of experimental data for certain frequencies when $K=12$. The computation for lower values of K would enable us to get more precise values of A and α.

The Hill and Van Vleck equation does not take into account the perturbations. As long as the formulae used in the calculation involve the perturbed branches Q_2, P_2 and R_2, the discrepancy which still exists in the values should be accounted for by perturbations.

I wish to thank Professor K. V. Nikolsky (Moscow University) for his consultation and help.

M. KOVNER

Woronezh University, U. S. R. S.,
May 16, 1936.

[1] Loomis and Brandt, Phys. Rev. **49**, 55 (1936).
[2] Hill and Van Vleck, Phys. Rev. **32**, 259 (1928).
[3] Proc. State Optic. Inst. U. S. S. R. (in press).

Some Experiments with Photo-Neutrons

We have performed experiments with the neutrons obtained from the photo-disintegration[1] of Be and D by the γ-rays from radon. The γ-ray source was about 700 mc of radon in a 2 mm diameter spherical bulb of Gundlach glass. The neutrons were detected with a boron lined ionization chamber previously described.[2]

The source of photo-neutrons from Be was a rectangular parallelepiped of Be metal with the Rn bulb at its center (59 g of Be about $2.5\times2.5\times5.5$ cm^3). This source was placed at the center of cylinders of water of various sizes and in each case the number of neutrons detected was counted with and without a $\frac{1}{4}$ mm sheet of Cd in front of the ionization chamber. The growth in number of slow neutrons thus observed is shown in Fig. 1. In order to compare the slowing of these photo-neutrons with that of neutrons from a Rn$-$Be source of the sort used in earlier experiments on the production of slow neutrons[3] the corresponding growth curve, also in Fig. 1, was obtained under identical geometrical conditions.

From the shape of the curves two conclusions may be drawn. The increasing portion of the curve indicates that the neutrons from the photo-disintegration of Be have less energy than those from the alpha-disintegration since they are slowed down to detectable speeds in a thinner layer of water. The relative mean free paths in water of neutrons from the two sources may be estimated from the decreasing parts of the curves since beyond the peaks of the curves there should be an approximate equilibrium between the fast neutrons and the slow neutrons which are strongly absorbed by Cd. The rate of decrease observed for the slow neutrons should then be the same as that of the fast neutrons. A comparison of the curves shows that the MFP of the Rn$_\gamma-$Be photo-neutrons is about 5 cm as compared with 9 cm for the Rn$_\alpha-$Be neutrons.

Chadwick and Goldhaber[1] using a radio-thorium source have measured the maximum energy of photo-neutrons thus obtained from Be. From their data they obtained 1.6 MEV as the minimum γ-ray energy required to release the photo-neutron from Be. The 2.2 and 1.76 MEV γ-lines[4] from Ra C should therefore give neutrons of $8/9\times0.16$ and $8/9\times0.6$ MEV neutrons. As the relative efficiency of these two γ-lines in producing photo-neutrons is not known we can only say that the above MFP of 5 cm is that of the mixture of these two groups of neutrons.

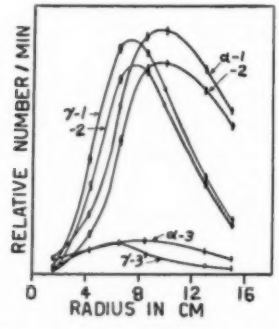

FIG. 1. Number of neutrons vs. radius (R = ht.) of water cylinders. The Rn$_\alpha-$Be curves are marked α and the Rn$_\gamma-$Be are marked γ. In each case the curves 1, 2 and 3 are, respectively, all neutrons, slow and fast neutrons.

A rough estimate of the relative numbers of neutrons per mc of Rn is obtained from the maxima of the two curves. This indicates that $\frac{1}{3}$ as many photo-neutrons as α-particle neutrons may be expected under these experimental conditions.

Similar experiments were made with the Rn bulb in the center of a 200 cc sphere of pure D_2O. In this case the yield of photo-neutrons is so low that the neutrons produced by the α-particle bombardment of the light elements in the glass of the bulb must be taken into account. These "glass" neutrons were in our experiments $\frac{1}{2}$ as numerous as the photo-neutrons from the deuterium. In order to separate the two effects in each case a count was taken with and without the D_2O around the bulb of Rn. The count with the D_2O minus that without the D_2O (all other conditions being the same) gives the count from D_2O only. The maximum of the growth curve shows that the number of photo-neutrons from the D_2O was 2 percent of the number of neutrons obtainable from an equal amount of Rn mixed with Be powder. This in turn indicates that 1 percent of the neutrons from the usual Rn$-$Be source come from the glass of the bulb. The peak of the growth curve for Rn$-$D photo-neutrons was at 7 cm ($-3\frac{1}{2}$ for the space occupied by the D_2O) in two experiments and 8 cm ($-3\frac{1}{2}$) in a third. A growth curve for the usual Rn$_\alpha-$Be source in the same D_2O and cylinders of water had its maximum at $10\frac{1}{2}$ cm ($-3\frac{1}{2}$).

Using the net thickness of H_2O through which the neutrons diffused when the number of detected neutrons was a maximum, we obtain:

$5\frac{1}{2}$ cm for Rn$_\gamma-$Be and $8\frac{1}{2}$ for Rn$_\alpha-$Be under the same conditions,

$3\frac{1}{2}$ cm for Rn$_\gamma-D_2O$ and 7 cm for Rn$_\alpha-$Be.

This is at least a good indication that the photo-neutrons obtained from D are much slower than those from Be. If the binding energy of D is 2.14 MEV[5] and the hardest strong γ-ray from Ra C is 2.198 MEV[4] these photo-neutrons are of very low energy. That the effect with D is observable suggests that there may be some γ-radiation from Ra C that is harder than the above.

We wish to acknowledge our debt to Dr. J. J. Duffy of Memorial Hospital for the loan of the Rn and to Professor H. C. Urey of Columbia University for the loan of the D_2O used in these experiments.

D. P. MITCHELL
F. RASETTI
G. A. FINK
G. B. PEGRAM

Pupin Physics Laboratories,
Columbia University,
June 19, 1936.

[1] J. Chadwick and M. Goldhaber, Proc. Roy. Soc. **A151**, 479 (1935).
[2] D. P. Mitchell, Phys. Rev. **49**, 453 (1936).
[3] J. R. Dunning, G. B. Pegram, G. A. Fink and D. P. Mitchell, Phys. Rev. **47**, 970 (1935).
[4] C. D. Ellis, Proc. Roy. Soc. **A143**, 350 (1933).
[5] H. A. Bethe and R. F. Bacher, Rev. Mod. Phys. **8**, 123 (1936).

Viscosity of Air and the Electronic Charge

As one of the possible explanations for the discrepancy between the "oil drop value" and the "x-ray value" of the electronic charge it has been suggested[1] that Millikan has used too low a value for the coefficient of viscosity of air η, which enters as a factor of the power 3/2 in calculating e by the oil drop method. In order to examine this hypothesis, the author has undertaken a new determination of η, using the rotating cylinder method. As a preliminary result was published[2] the value

$$\eta_{20^\circ} = (18200 \pm 30) \cdot 10^{-8} \quad \text{corresponding to}$$
$$\eta_{23^\circ} = (18348 \pm 30) \cdot 10^{-8}.$$

This is 0.67 percent higher than the value used by Millikan in 1916 ($18226 \cdot 10^{-8}$), and would give a value of e 1.0 percent higher than Millikan's.

Since this result was published, the apparatus has been improved so as to insure greater constancy of the temperature and of the speed of rotation of the outer cylinder. The mean of 54 determinations, carried out with the improved apparatus, is

$$\eta_{20^\circ} = (18201 \pm 27) \cdot 10^{-8} \quad \text{or} \quad \eta_{23^\circ} = (18349 \pm 27) \cdot 10^{-8}$$

in good agreement with the previous value, and with somewhat greater accuracy.

If we use Millikan's data with this value of η we would find for e

$$e = \left(\frac{18349}{18226}\right)^{\frac{1}{2}} 4.770 \cdot 10^{-10} = (4.818 \pm 0.011) \cdot 10^{-10} \text{ e.s.u.}$$

the uncertainty stated being due only to the viscosity.

It should be emphasized, that the error in η has been calculated so as to give a reasonable *limit* of error rather than a probable error, as some systematic errors have also been considered. (The probable accidental error, computed by the usual least square method from the individual deviations would be only $1.5 \cdot 10^{-8}$ or 0.008 percent.)

From this result the conclusion can be drawn, that the lower value of e obtained by the oil drop method of Millikan can very well be explained by the error in the η-value used. New measurements by Bäcklin and Flemberg[3] seem to indicate that other errors may also exist.

A detailed report has been sent for publication elsewhere.

GUNNAR KELLSTRÖM

Physics Laboratory,
University of Uppsala, Sweden,
June 20, 1936.

[1] K. Shiba, Sci. Pap. Inst. phys. chem. Res. Tokyo **19**, 97 (1932).
[2] G. Kellström, Nature **136**, 682 (1935).
[3] E. Bäcklin and H. Flemberg, Nature **137**, 655 (1936).

JULY 15, 1936 PHYSICAL REVIEW VOLUME 50

Erratum: Heat Conductivity of Tungsten and the Cooling Effects of Leads upon Filaments at Low Temperatures

IRVING LANGMUIR AND JOHN BRADSHAW TAYLOR, *General Electric Company*

(Phys. Rev. **50**, 68 (1936))

IN the last sentence of the abstract the equation was misprinted. The correct equation is:

$$\log \lambda = 0.9518 - 0.30 \log T.$$